Chen *et al. Energy Mater* 2023;3:300031
DOI: 10.20517/energymater.2023.12

Energy Materials

Review

Open Access

Check for updates

Research advances in earth-abundant-element-based electrocatalysts for oxygen evolution reaction and oxygen reduction reaction

Xiaodong Chen[1,#], Zhiyuan Zhang[2,#], Ya Chen[1,#], Runjing Xu[2,*], Chunyu Song[3], Tiefeng Yuan[2], Wenshuai Tang[4], Xin Gao[1,*], Nannan Wang[3,*], Lifeng Cui[1,*]

[1]College of Smart Energy, Shanghai Jiao Tong University, Shanghai 200240, China.
[2]School of Environmental Science and Engineering, University of Shanghai for Science and Technology, Shanghai 200093, China.
[3]College of Chemistry and Material Engineering, Chao Hu University, Hefei 238000, Anhui, China.
[4]College of Chemistry and Chemical Engineering, Henan University of Technology, Zhengzhou 450001, Henan, China.
[#]Authors contributed equally.

***Correspondence to:** Dr. Runjing Xu, School of Environmental Science and Engineering, University of Shanghai for Science and Technology, Shanghai 200093, China. E-mail: 211580109@st.usst.edu.cn; Dr. Xin Gao, College of Smart Energy, Shanghai Jiao Tong University, 665 Jianchuan Road, Minhang District, Shanghai 200240, China. E-mail: gx499708331@163.com; Prof. Nannan Wang, College of Chemistry and Material Engineering, Chao Hu University, 1 Bantang Road, Chaohu Economic Development Zone, Hefei 238000, Anhui, China. E-mail: nnw1990@126.com; Prof. Lifeng Cui, College of Smart Energy, Shanghai Jiao Tong University, 665 Jianchuan Road, Minhang District, Shanghai 200240, China. E-mail: cui_lifeng@sjtu.edu.cn

How to cite this article: Chen X, Zhang Z, Chen Y, Xu R, Song C, Yuan T, Tang W, Gao X, Wang N, Cui L. Research advances in earth-abundant-element-based electrocatalysts for oxygen evolution reaction and oxygen reduction reaction. *Energy Mater* 2023;3:300031. https://dx.doi.org/10.20517/energymater.2023.12

Received: 2 Mar 2023 **First Decision:** 26 Apr 2023 **Revised:** 15 May 2023 **Accepted:** 5 Jun 2023 **Published:** 4 Jul 2023

Academic Editor: Hao Liu **Copy Editor:** Fangling Lan **Production Editor:** Fangling Lan

Abstract

The oxygen evolution reaction (OER) and oxygen reduction reaction (ORR) are crucial half-reactions of green electrochemical energy storage and conversion technologies, such as electrochemical water-splitting devices and regenerative fuel cells. Researchers always committed to synthesizing earth-abundant-element-based nanomaterials as high-efficiency electrocatalysts for realizing their industrial applications. In this review, we briefly elaborate on the underlying mechanisms of OER and ORR during the electrochemical process. Then, we systematically sum up the recent research progress in representative metal-free carbon (C)-based electrocatalysts; metal-nitrogen-C electrocatalysts; and nonprecious-metal OER/ORR electrocatalysts, including transition-metal oxides, phosphides, nitrides/oxynitrides, chalcogenides, and carbides. Among these, some representative bifunctional electrocatalysts for the OER/ORR are mentioned. In particular, we discuss the effects of physicochemical properties-morphology, phases, crystallinity, composition, defects, heteroatom doping, and strain

engineering-on the comprehensive performance of the abovementioned electrocatalysts, with the aim of establishing the nanostructure-function relationships of the electrocatalysts. In addition, the development directions of OER and ORR electrocatalysts are determined and highlighted. The generic approach in this review expands the frontiers of and provides inspiration for developing high-efficiency OER/ORR electrocatalysts.

Keywords: Electrocatalysts, OER, ORR, nanomaterials, nanostructure-function

INTRODUCTION

The excessive spending on non-renewable fossil fuels not only worsens the global energy shortage but also hinders the carbon (C) neutrality of natural ecosystems[1-4]. To achieve a harmonious and sustainable society, it is crucial to employ renewable and eco-friendly energy sources, such as hydrogen (H_2) and tidal energy, as viable substitutes for conventional fossil fuels[5]. Despite the efficient conversion of these abundant clean energy resources into electricity, they face the challenges of intermittency and instability; moreover, electricity generation is extremely dependent on the weather conditions[6,7]. This inherent drawback results in difficulties in grid connections and generation of a large amount of unused electricity[8]. Therefore, efficient utilization of this surplus electric power under real conditions is of practical significance.

Numerous studies have affirmed that H_2 is a highly promising renewable energy resource due to several key advantages. These include its all-weather usability, wide availability, absence of pollutant emissions, and high combustion value. Hence, converting unused electricity into H_2 using an electrochemical water-splitting device and further harnessing the H_2 for electricity generation at the point of use in fuel-cell-assembled electric vehicles is of practical significance[9-15]. The oxygen evolution reaction (OER) and oxygen reduction reaction (ORR) are the rate-determining steps (RDSs) in electrochemical water-splitting devices and fuel cells, respectively, owing to the sluggish kinetics of O=O bond formation and breaking. The complex four-electron transfer reaction, which mainly determines the integrated energy conversion efficiency of the electrochemical reaction, is responsible for the sluggish kinetics[16-18]. To overcome the challenges mentioned above and enable the industrial implementation of H_2, it is essential to develop and produce electrocatalysts that are highly efficient in both OER and ORR.

Precious-metal-based nanomaterials, such as Pt, Ir, Ru, IrO_2, and RuO_2, have been recognized as benchmark electrocatalysts owing to their high-efficiency OER or ORR activity[19,20]. However, their inherent shortcomings of high cost, uneven distribution, and barren storage have severely hindered their large-scale commercial application[21]. Thus, extensive efforts have been undertaken to harness earth-abundant-element-based compounds such as transition-metal oxides (TMOs), phosphides (TMPs), nitrides/oxynitrides (TMNs/TMONs), chalcogenides, and carbides (TMCs); metal-free C nanomaterials; and metal-nitrogen (N)-C (M-N-C) nanocomposites, potentially advancing the development of OER and ORR electrocatalysts[22,23]. Kumar *et al.* conducted a study on spinel cobalt catalysts (Co_3O_4@rGO (reduced graphene oxide), Co_3S_4@rGO) to investigate their efficacy in water decomposition reactions under acidic conditions[24]. The spinel cobalt catalysts demonstrated notable improvements in performance when subjected to a current density of 10 mA·cm^{-2}. Specifically, they were able to reduce the overpotential by 239 mV and 151 mV in the H_2 evolution reaction (HER) and 380 mV and 350 mV in the OER, respectively. Additionally, these catalysts exhibited high durability and lower battery voltage, which further confirms their potential for use in water-splitting applications. In another study, Kumar *et al.* synthesized a nanostructured $ZnCo_2Se_4$ catalyst supported on reduced graphite oxide nanosheets through a straightforward hydrothermal method[25]. The catalyst displayed exceptional performance in both the OER

and the ORR. Specifically, at a current density of 10 mA·cm^{-2}, the overpotential for OER was reduced by 298 mV, while the ORR achieved a half-wave potential of 0.802 V in a 0.1 M KOH solution. Based on these findings, it appears that the $ZnCo_2Se_4$ catalyst, which is supported on reduced graphite oxide nanosheets, has the potential to be a highly effective candidate for the evolution of efficient and durable water splitting systems, which are crucial for sustainable energy production. Accordingly, a detailed investigation and summary of these materials as efficient electrocatalysts would be of great significance.

In this review, we focus on the integrated catalytic performance of the aforementioned earth-abundant-element-based nanomaterials as OER and ORR electrocatalysts or bifunctional electrocatalysts, which have demonstrated excellent electrocatalytic performances. The atomic-level mechanisms of OER and ORR are comprehensively discussed to better understand the design principles of electrocatalysts. In particular, the physicochemical properties of these electrocatalysts-morphology, phases, crystallinity, composition, defects, heteroatom doping, and strain engineering-which are mainly responsible for their electrocatalytic activities, are systematically elucidated to establish their structure-activity relationships. In addition, this paper discusses and underscores the current challenges and future development directions for electrocatalysts. This review offers general guidelines for the state-of-the-art architecture of electrocatalysts and demonstrates the potential of widespread practical adoption of electrochemical water-splitting devices.

OER AND ORR ELECTROCATALYSTS

OER mechanism

H_2 is widely recognized as a sustainable, C-neutral, and abundant energy carrier that has the potential to address current energy challenges due to several key advantages. These include its ability to store high energy density during energy storage and release energy with C-free emissions[26]. The water-splitting reaction involves two half-reactions: OER and HER. The efficiency of the overall reaction is mainly determined by the rates of these two half-reactions[27]. The thermodynamic equilibrium potential required to drive the entire reaction theoretically is 1.23 V *vs.* reversible hydrogen electrode RHE. However, in practice, the required potential (E_{app}) is higher than the equilibrium potential, as illustrated in Figure 1[28]. For many metal-based electrocatalysts, HER is a relatively straightforward reaction that occurs readily at low overpotentials[29]. In contrast, the OER is a more intricate process that involves the transfer of four electrons ($4e^-$) and exhibits slow oxygen evolution kinetics. This process requires the removal of four protons from a water molecule to form an oxygen molecule, which necessitates a high overpotential and ultimately inhibits the reaction[30]. Consequently, the efficiency of the process decreases drastically, hindering the industrial-scale production of H_2 via water splitting. As a result, the OER is a critical half-reaction in the electrochemical process of water splitting[31].

Developing efficient catalysts for water splitting requires a thorough understanding of the OER mechanism [Figure 2A]. Although there are inconsistencies in the literature regarding the exact mechanism of the OER, the general consensus is that the adsorption of the intermediates, O* and OH*, on the metal electrocatalysts determine the corresponding OER performance. The typical overall reaction scheme for the OER in an acidic environment is as follows:

$$2H_2O \rightarrow O_2 + 2H_2 \quad (1)$$

Additionally, the OER proceeds via the following $4e^-$ reaction pathways[32,33]:

$$* + H_2O \rightarrow OH^* + H^+ + e^- \quad (1a)$$

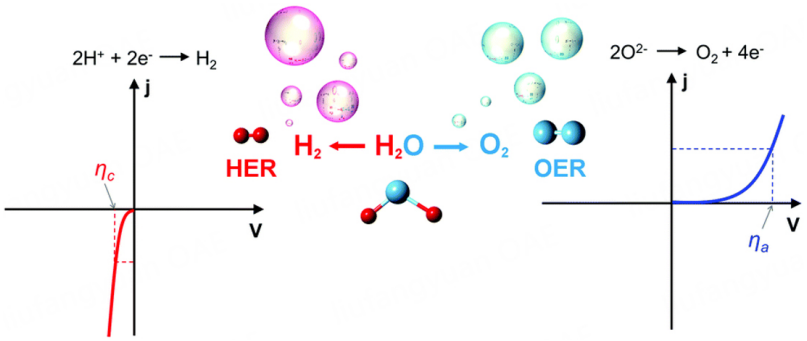

Figure 1. Polarization curves for HER (left) and OER (right). The η_c and η_a are the overpotentials for the cathode and anode at the same current (j), respectively. Reproduced with permission. Copyright 2017, Royal Society of Chemistry[28].

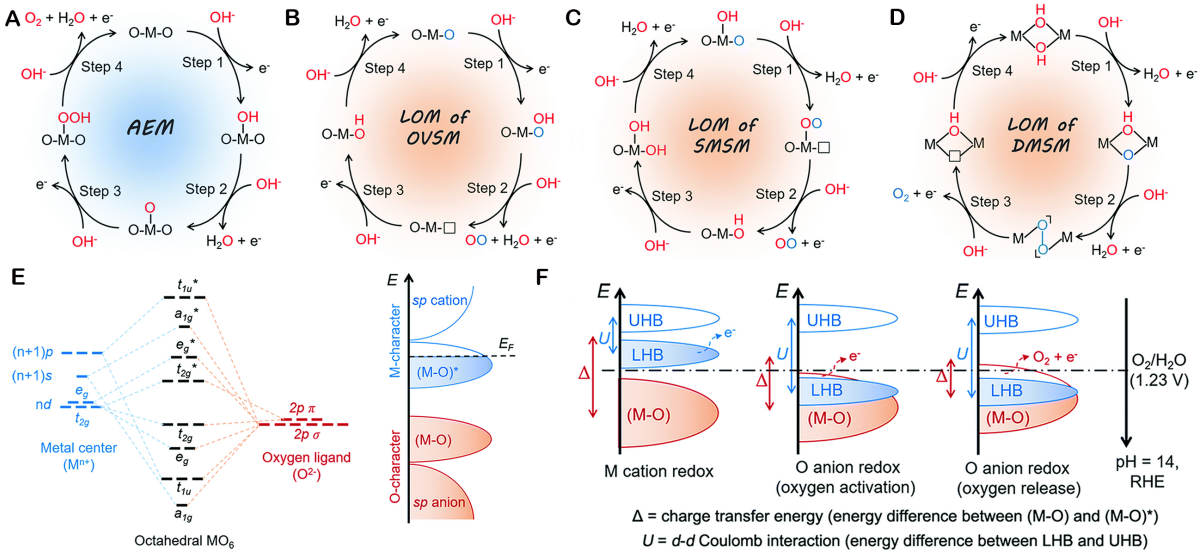

Figure 2. Different reaction pathways for OER. (A) Schematic illustration of the proposed AEM pathway of OER in alkaline media on an active metal site. The lattice oxygen and oxygen from the electrolyte are marked in black and red colors, respectively. (B) Oxygen-vacancy-site mechanism (OVSM), (C) single-metal-site mechanism (SMSM), and (D) dual-metal-site mechanism (DMSM). The chemically inert lattice oxygen, active lattice oxygen involving OER, and oxygen from the electrolyte are marked in black, blue, and red colors, respectively. (E) The schematic band structure of octahedral-symmetric TMO_6 in TMOs under the rationalization of molecular orbital theory. (F) The schematic representations of cation/anion redox chemistry guided by d-d Coulomb interaction (U) and charge transfer energy (Δ), which manifest conventional metal cation oxidation (left), oxygen anion oxidation (middle) and direct oxygen anion release (right) for OER, respectively. Δ is the energy difference between bonding (M-O) and antibonding (M-O)* bands, and U is the energy difference between UHB and LHB, respectively. Copyright 2021, Royal Society of Chemistry[35].

$$OH^* \rightarrow O^* + H^+ + e^- \quad (1b)$$

$$O^* + H_2O \rightarrow OOH^* + H^+ + e^- \quad (1c)$$

$$OOH^* \rightarrow * + O_2 + e^- \quad (1d)$$

where * refers to an atom in a particular model.

Under alkaline conditions, the OER generally proceeds via the following 4e$^-$ reaction pathways[34]:

$$OH^- \rightarrow OH^* + e^- \quad (1e)$$

$$OH^* + OH^- \rightarrow O^* + H_2O + e^- \quad (1f)$$

$$O^* + OH^- \rightarrow OOH^* + e^- \quad (1g)$$

$$OOH^* + OH^- \rightarrow * + O_2 + H_2O + e^- \quad (1h)$$

where * refers to an atom in a particular model.

In addition, as the mechanism of the OER is further studied, the high OER catalytic performance of oxygen-rich surface catalysts cannot be further explained using the adsorption energy model (AEM). Therefore, researchers have proposed an advanced mechanism to explain the catalytic action of this catalyst, where lattice oxygen with high metal-oxygen covalent bond characteristics in solid-state oxides/hydroxides undergoes oxidation at OER potential and further participates in OER reaction to generate oxygen gas. This new mechanism can break the limitations of conventional adsorption-desorption mechanisms and better explain the high activity of solid-state catalysts, known as lattice oxygen redox chemistry.

Zhang *et al.* conducted an in-depth investigation of the lattice oxygen-mediated mechanism (LOM) [Figure 2B-D][35]. In the context of OER activities, the metal center, typically represented by the motif of octahedral symmetric TMO6, plays a crucial role. As shown in Figure 2E, molecular orbital theory can be used to rationalize the orbital interactions and banding diagrams. Using oxides as an example, orbital coupling results in the formation of an (M-O) bonding band (O-2p band) reflecting the oxygen ligand properties and an (M-O)* antibonding band (M-nd band) reflecting the metal center properties. The energy difference between these two bands can be referred to as the charge transfer energy (Δ). The parameter Δ represents the level of hybridization between transition-metal (TM)-nd and O-2p orbitals. A decrease in Δ implies increased hybridization that promotes TM-O covalency, whereas an increase in Δ indicates the opposite effect. In addition, from the perspective of solid-state physics, the electrons in the (M-O)* antibonding band, which represent the metal in the band, become further localized due to strong d-d Coulomb interactions (U). The strength of these interactions depends on the valence state and orbital volume of the metal center. This on-site electron repulsion causes the (M-O)* band to split into an empty upper Hubbard band (UHB) and a filled lower Hubbard band (LHB), a phenomenon known as Mott-Hubbard splitting [Figure 2F]. In this case, thermodynamically, the electrons in the oxygen ligand will preferentially lose, resulting in lattice oxygen oxidation. Moreover, if the O-2p band shifts upward due to high covalency, the oxidized lattice oxygen will directly participate in the generation of oxygen gas when the energy is higher than that of the water oxidation reaction itself. Therefore, the energy band structure and relative positions of metal centers and oxygen ligands in materials can serve as effective descriptors to theoretically quantify the possibility of lattice oxygen oxidation.

Noble-metal-based OER electrocatalysts

The OER activity of electrochemically oxidized metals is in the order of Ru > Ir > Rh > Pt> Au, which was established on the basis of overpotentials at a geometric current density of 5 mA·cm^{-2} [Figure 3A]. Nevertheless, when considering the stability, the following trend is observed: Pt > Rh > Ir > Au ≥ Ru. The comparison of the activity and stability trends infers that, although these parameters are not inversely correlated, less-active OER electrocatalysts are generally more stable. However, Au deviates from this trend;

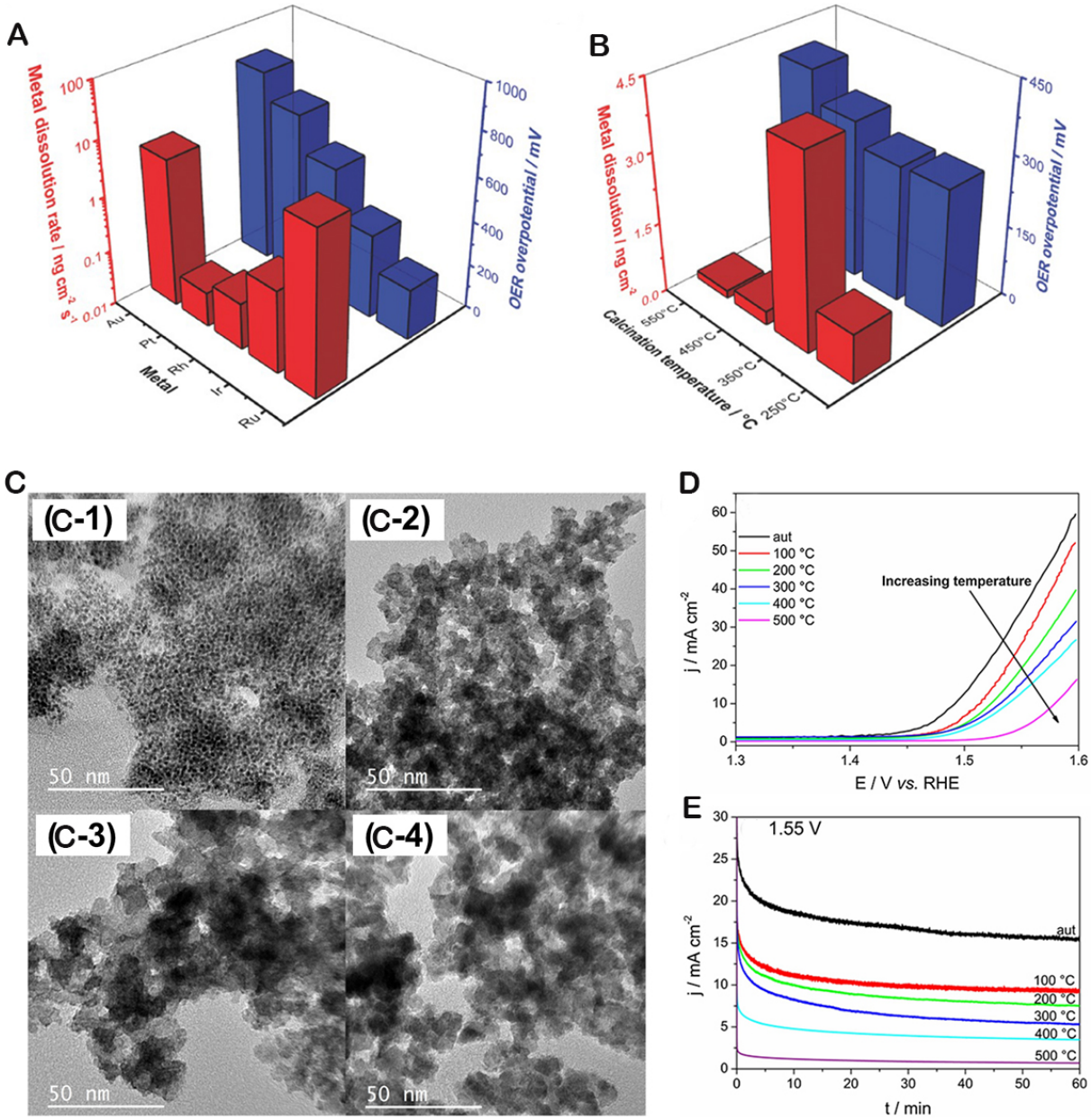

Figure 3. (A) OER performance in the form of overpotential and metal dissolution rates at 5 mA cm^{-2} geometric current density of different metal electrodes (Au, Pt, Rh, Ir, and Ru) in 0.1 M H_2SO_4; (B) OER performance of thin-film Ir oxide model catalysts in the form of overpotential and Ir dissolution as a function of the calcination temperature (constant Ir loading). Overpotentials and integral Ir dissolution within 10 min were measured at a geometric current density of 2 mA cm^{-2}. Reproduced with permission. Copyright 2017, Wiley Online Library[36]; (C) TEM images of the electrocatalysts: (C-1) aut-IrO_x, (C-2) IrO_x-300 °C, (C-3) IrO_2-400 °C, and (C-4) IrO_2 - 500 °C; (D) OER polarization curves at 5 mV·s^{-1} and 1,600 rpm for the IrO_x catalysts; (E) Chronoamperometric curves recorded at 1.55 V for the IrO_x catalysts. Reproduced with permission. Copyright 2017, Elsevier[39].

its instability is approximately the same as that of the most active electrocatalysts (Ru, Ir), but its OER activity is the lowest[36,37].

In addition to noble-metal categories, the synthesis conditions are a key factor in determining their OER performance. Studies on thin-film Ir oxide model catalysts have demonstrated a strong relationship between the OER performance and calcination temperature, as shown in Figure 3B[36]. What is more, thermally

prepared oxides generally have higher stability but lower activity than electrochemically prepared oxides[37,38]. For the Ir oxide nanoparticle (NP) electrocatalyst prepared by da Silva *et al.* using a hydrothermal method[39], the voltammetry curve obtained by the test is similar to that of the hydrated Ir oxide prepared using an electrochemical method, and the OER performance of IrO_x decreases with increasing calcination temperature, but the stability exhibits the opposite trend [Figure 3C-E]. Moreover, the thermal oxides of Ru and Ir are two-three orders of magnitude more stable than their electrochemical analogs[38]. Povia *et al.* employed a modified Adams' fusion method to synthesize Ir oxide nanodisks[40]. A portion of the resulting sample was further oxidized by a second heat treatment in air to modify the surface. Electrochemical characterization through rotating disk electrode (RDE) voltammetry showed that the surface-specific OER activity of the as-synthesized electrocatalyst was twice as high as that of the heat-treated counterpart, but it experienced a more substantial loss in activity. Generally, the OER performance of Ir oxides is highly dependent on the preparation conditions.

The general synthesis route for RuO_x is the thermal decomposition strategy of the Ru-based precursor[41]. It is approved that thermally-oxidized crystalline RuO is significantly more stable but slightly less active than electrochemically-formed RuO[42]. These results are consistent with those of Cherevko *et al.* for RuO_2 thin films[38]. Besides, Ru exhibits moderate activity after oxidation in O_2 plasma[43]. In addition, the size of Ru NPs affects the OER activity, and the maximum activity corresponds to Ru NPs sized 3-5 nm[42]. For RuO_2 crystals prepared using the sol-gel method, Macounová *et al.* showed that the OER activity decreases as the crystal size increases[44]. Furthermore, OER activity also depends on the orientation of the crystal plane. Chang *et al.* found out that the OER activity of $SrRuO_3$ single-crystal electrodes in alkaline electrolytes increases in the order of (001) < (110) < (111) plane, which is the opposite of the stability of these crystal planes[45]. Adenle *et al.* also confirmed this finding, demonstrating that selective loading of Pd NPs onto the (110) plane of Bi_4TaO_8Cl (BTOC) significantly enhances the OER activity[46]. In addition, Danilovic *et al.* showed that Ru(001) and Ir(111) single-crystal electrodes have fewer defects and, consequently, poorer activity than their corresponding polycrystalline electrodes[37].

In conclusion, the OER performance of monometallic Ru and Ir oxides is greatly influenced by their chemical and surface properties. As a result, these materials have significant potential for optimization through admixture with other components, such as other metal cations. However, the sensitivity of Ru and Ir oxides to the synthesis conditions presents difficulties in using them as standard materials. Thus, selection and characterization of Ir and Ru oxides are necessary for their usage as standard materials for OER studies.

Non-noble-metal-based OER electrocatalysts

While noble metals, such as Ru and Ir, are highly effective OER electrocatalysts, their scarcity and high-cost limit their commercial use. To overcome this, researchers have extensively studied the design, synthesis, and characterization of low-cost, highly active, and stable transition-metal-based OER electrocatalysts under oxidizing conditions, making overall water splitting more practical. Furthermore, it should be noted that these noble-metal oxides are not the most effective OER electrocatalysts under alkaline conditions, as some first-row transition-metal-based compounds have surpassed their performance[47,48].

Metal-free C-based electrocatalysts

The expenditure of OER electrocatalysts is the first consideration for practical applications. C-based nanomaterials are generally easily available and can be used as OER electrocatalysts at a low cost and earth abundance, thereby significantly decreasing economic consumption. Furthermore, C-based nanomaterials possess high electrical conductivity, flexibility, and durability[49]. However, pristine C materials, such as graphite and activated C (AC), are not promising candidates for OER due to their relatively low catalytic

activity[50,51]. Nevertheless, recent studies have demonstrated that the OER activity of C-based nanomaterials can be enhanced by modifying them with functional groups or heteroatoms, which can improve the adsorption of OER intermediates[52,53]. Zhang *et al.* developed a straightforward method for producing carboxyl-rich multiwalled C nanotubes (COOH-MWCNTs) with high stability and OER electrocatalytic activity in acidic solutions[54]. These COOH-MWCNTs exhibited an overpotential of 265 mV at a current density of 10 $mA \cdot cm^{-2}$ and a Tafel slope of 82 $mV \cdot dec^{-1}$, representing the best OER performance of metal-free electrocatalysts and a performance comparable to that of RuO_2 and IrO_2. The catalytic mechanism involves the loss of an electron from the COOH-MWCNT electrocatalyst at the beginning of the OER process, which triggers the oxidation of H_2O molecules via OH formation. An electron is then recaptured from the H_2O molecule to form oxidized H_2O and restore the initial state of the COOH-MWCNT electrocatalyst. This new OER mechanism provides insights into the critical roles of organic functional groups in electrocatalytic processes. Additionally, studies have demonstrated that doping C substrates with N, P, S, O, or B could optimize their electronic structure and further facilitate electrocatalytically active sites with excellent OER performance[52,55-57]. For example, Hu *et al.* prepared ultrafine pentlandite NPs fixed by a porous N- and S-doped C network (P-NSC/$Ni_4Fe_5S_8$-1000)[58]. Owing to the synergy between pyridinic N (p-N), S-doped C, and highly active Fe sites, P-NSC/$Ni_4Fe_5S_8$-1000 has emerged as an efficient and stable OER electrocatalyst under acidic conditions [Figure 4]. Kang *et al.* prepared ultrathin B-N codoped porous nanocarbon (BN-PCN) sheets using a carbonization-etching method[59]. Owing to its unique structural characteristics, BN-PCN exhibits high electrocatalytic OER activity. In particular, Ma *et al.* developed a descriptor based on the p_z orbital of the active site to explain the catalytic performance of bi and tridoped graphene electrocatalysts for ORR and OER[52]. This descriptor is universal and can account for multiple doping and predict the contributions of defects, edges, and defect-edge combinations. Ali *et al.* synthesized MWCNTs for OER in alkaline media by growing graphene *in situ* on Ni-silica nanocomposites at 650 °C using chemical vapor deposition[60]. After removing the silica, the resulting nanomaterial exhibited an OER performance comparable to that of commercial Ir-supported C. This is due to the defective nature of MWCNTs that contain surface discontinuities on the rolled graphene layers of C nanotubes (CNTs) and the MWCNT-graphene interface, which may contain dangling bonds that function as active sites for the OER. The MWCNT-graphene hybrid C nanostructure material gives an overpotential of 310 mV at a current density of 10 $mA \cdot cm^{-2}$ in a 1 M KOH solution at a scan rate of 5 $mV \cdot s^{-1}$, whereas the commercial Ir/C exhibits an overpotential of 305 mV under similar conditions. Although this presents a new concept for modifying C-based nanomaterials by transforming catalytically inert materials into active electrocatalysts, the performance of C-based nanomaterials lags behind that of state-of-the-art electrocatalysts[61]. Additionally, low stability is another disadvantage of C-based OER electrocatalysts, as studies have shown that they can undergo surface oxidative corrosion at high potentials and generate C dioxide, significantly decreasing their catalytic activity[61,62].

Transition-metal-compound-based electrocatalysts

Similar to C-based nanomaterials, earth-abundant first-row-transition-metal oxides/hydroxides/oxyhydroxides exhibit high electrical conductivity and can be effectively enhanced in OER electrocatalytic activity through various strategies, such as heterostructure construction, alloying, elemental doping, coating, defect engineering, exfoliation, and hybridization[63,64].

Kang *et al.* synthesized a heterostructure composed of $Ni(OH)_2$ nanosheets and tungsten (W) NPs on a conductive C cloth (W@$Ni(OH)_2$/CC) to address the problem of low catalytic activity[65]. This heterostructure reflects the advantages of the metallic properties of the catalyst and reduces the length of the charge transfer path. Co phosphide has also been shown to be an effective OER catalyst. For example, Liang *et al.* constructed a CoP/TiO_x heterostructure using metal-organic framework (MOF) nanocrystals as

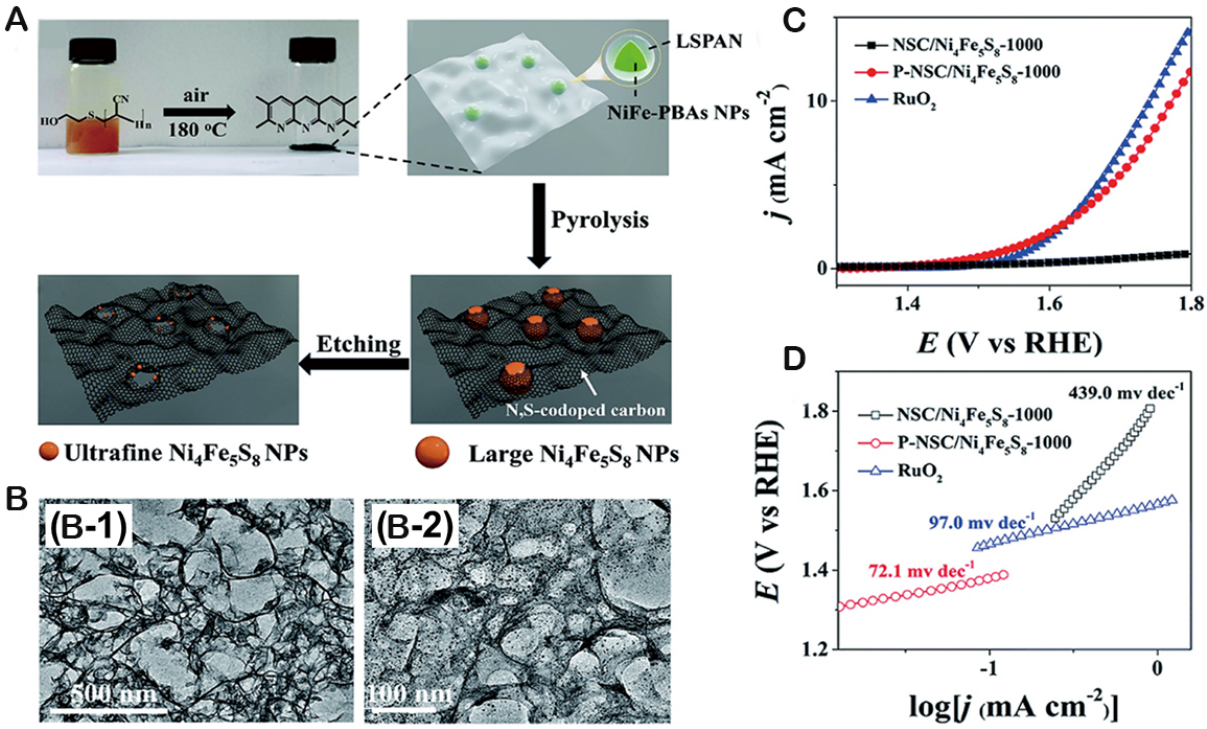

Figure 4. (A) Schematic illustration of the synthesis of P-NSC/$Ni_4Fe_5S_8$-1000; (B) TEM images of P-NSC/$Ni_4Fe_5S_8$-1000: (B-1) 500 nm and (B-2) 100 nm; (C) Steady-state polarization curves and (D) the corresponding Tafel plots of NSC/$Ni_4Fe_5S_8$-1000 (without porous structure) and P-NSC/$Ni_4Fe_5S_8$-1000 (with porous structure) and commercial RuO_2 (Alfa Aesar). Reproduced with permission. Copyright 2019, Royal Society of Chemistry[58].

templates, which significantly improved the OER performance[66]. CoP/TiO_x has a unique hollow structure, with CoP NPs evenly distributed on TiO_x. The strong interaction between CoP and TiO_x in the heterostructure and the conductivity of TiO_x due to Ti^{3+} sites endow CoP-TiO_x hybrid materials with high OER activity, comparable to that of IrO_2 or RuO_2 electrocatalysts. The CoP/TiO_x heterostructure provides a path that facilitates electron transport and optimizes the H_2O adsorption energy, thereby enhancing the OER performance. In addition to Co phosphide, multishell mixed-metal P oxides have been reported to enhance the electrocatalytic activity of the OER, as shown in Figure 5[67]. The results showed that activated manganese (Mn)-CoP oxides have excellent OER properties, with a Tafel slope of 52 mV·dec^{-1}, which is the lowest compared to Mn-Co oxide (60 mV·dec^{-1}) and RuO_2 particles. To achieve a current density of 10 mA·cm^{-2}, the overpotentials required for the activated Mn-CoP oxide, Mn-Co oxide, and RuO_2 particles are 370, 420, and 366 mV, respectively.

Alloying is a viable method to adjust the catalytic performance of single-metal electrocatalysts. Ni-Fe alloys have been extensively researched as electrocatalysts for the OER, and the significance of Fe doping has been demonstrated through proportional control[68]. Currently, Ni-Fe-based alloys are the most common OER electrocatalysts in the industry[69,70]. Zhou *et al.* reported that Fe leaching could induce the electrochemical activation of strongly coupled Ni-Fe alloys on N-doped C composites, resulting in an enhanced OER performance[71]. The leaching of the unstable FeOOH mixed layer from the $FeNi_3$ alloy surface leads to surface reconstruction and exposure of additional active sites. N-doped C, $FeNi_3$ alloy, and concomitant Fe-doped $Ni(OH)_2$ synergistically promote OER activity after full activation. High-valency Ni, p-N, and metallic N species were determined as the exact active sites, and the fully activated $Fe_{0.2}Ni_{0.8}$/NC-600 electrocatalyst is one of the best non-noble-metal OER electrocatalysts to date. It exhibits excellent OER

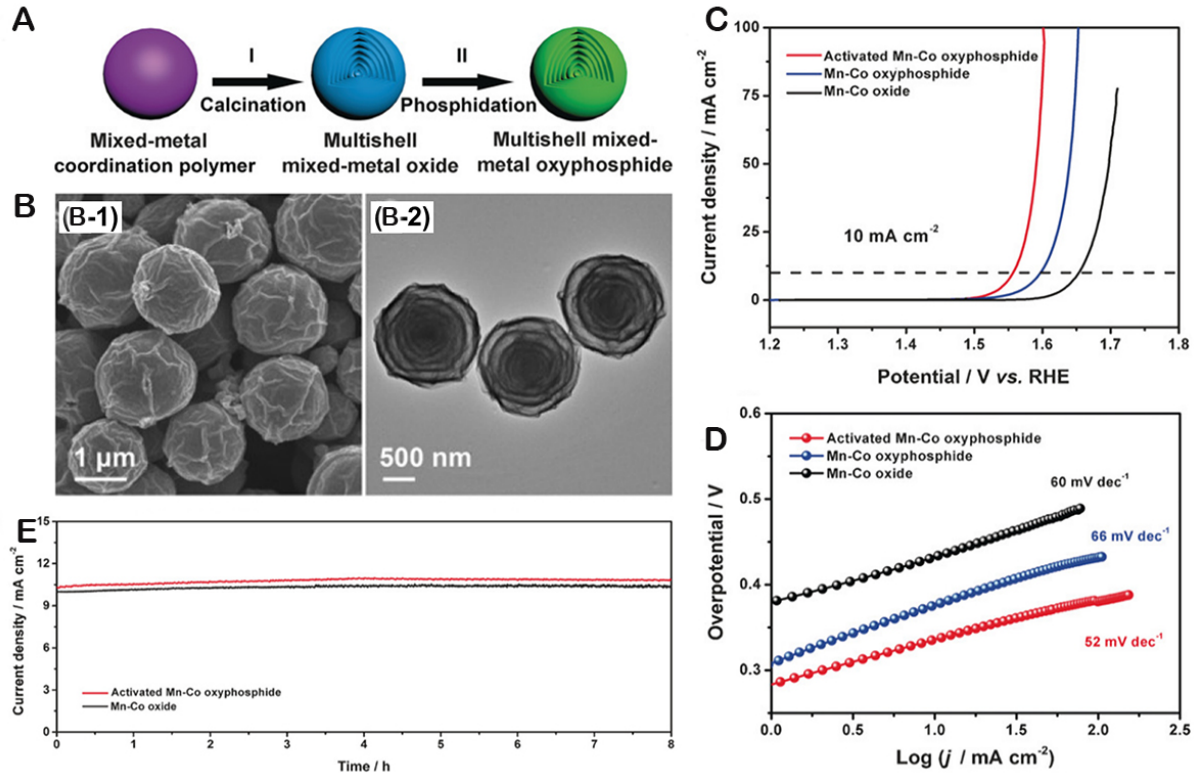

Figure 5. (A) Formation of multishell mixed-metal oxyphosphide particle; (B) Characterization of the multishell Mn-Co oxyphosphide particles: (B-1) FESEM and (B-2) TEM images; (C) LSV curves and (D) Tafel plots of activated Mn-Co oxyphosphide particles, Mn-Co oxyphosphide particles, and Mn-Co oxide particles; (E) Chronoamperometry curves of activated Mn-Co oxyphosphide particles and Mn-Co oxide particles at overpotentials of 320 mV and 420 mV, respectively. Reproduced with permission. Copyright 2017, Wiley Online Library[67].

performance with a low overpotential (η_{20} = 290 mV) and a small Tafel slope (76 mV·dec^{-1}). This study contributes to the understanding of the fundamentals of Ni-Fe alloy electrocatalysts and provides guidance for designing advanced electrocatalysts for H_2O oxidation via *in situ* electrochemical activation. Jing *et al.* adjusted the electronic structure of CN-FeO_x through hydroxyl modification to enhance the binding capacity of O-intermediates in the OER process[72]. Researchers found that increasing the Fe-Fe length in the material can improve the structural stability and activity of OER. Performance evaluation shows that the material has a low overpotential at 10 mA·cm^{-2}, close to commercial RuO_2.

Elemental doping has been shown to effectively enhance the performance of transition-metal-based compounds by tuning their electronic structure[73-75]. Therefore, many efforts have been devoted to optimizing the elemental doping species and concentrations and identifying the electrocatalytically active sites. For example, trace amounts of Fe-doped Ni hydroxide in Fe-doped Ni compounds could significantly enhance the OER electrocatalytic activity[47]. Liu *et al.* reported an amorphous NiFe-layered double hydroxide (a-NiFe-LDH) with abundant active sites that could expose additional NiFe active sites, as shown in Figure 6[75]. The OER electrocatalytic activity of a-NiFe-LDH is much higher than that of RuO_2 or pristine NiFe-LDH. Furthermore, a-NiFe-LDH has a low OER overpotential of 241 mV at 10 mV·cm^{-2} and a small Tafel slope of 55 mV·dec^{-1}.

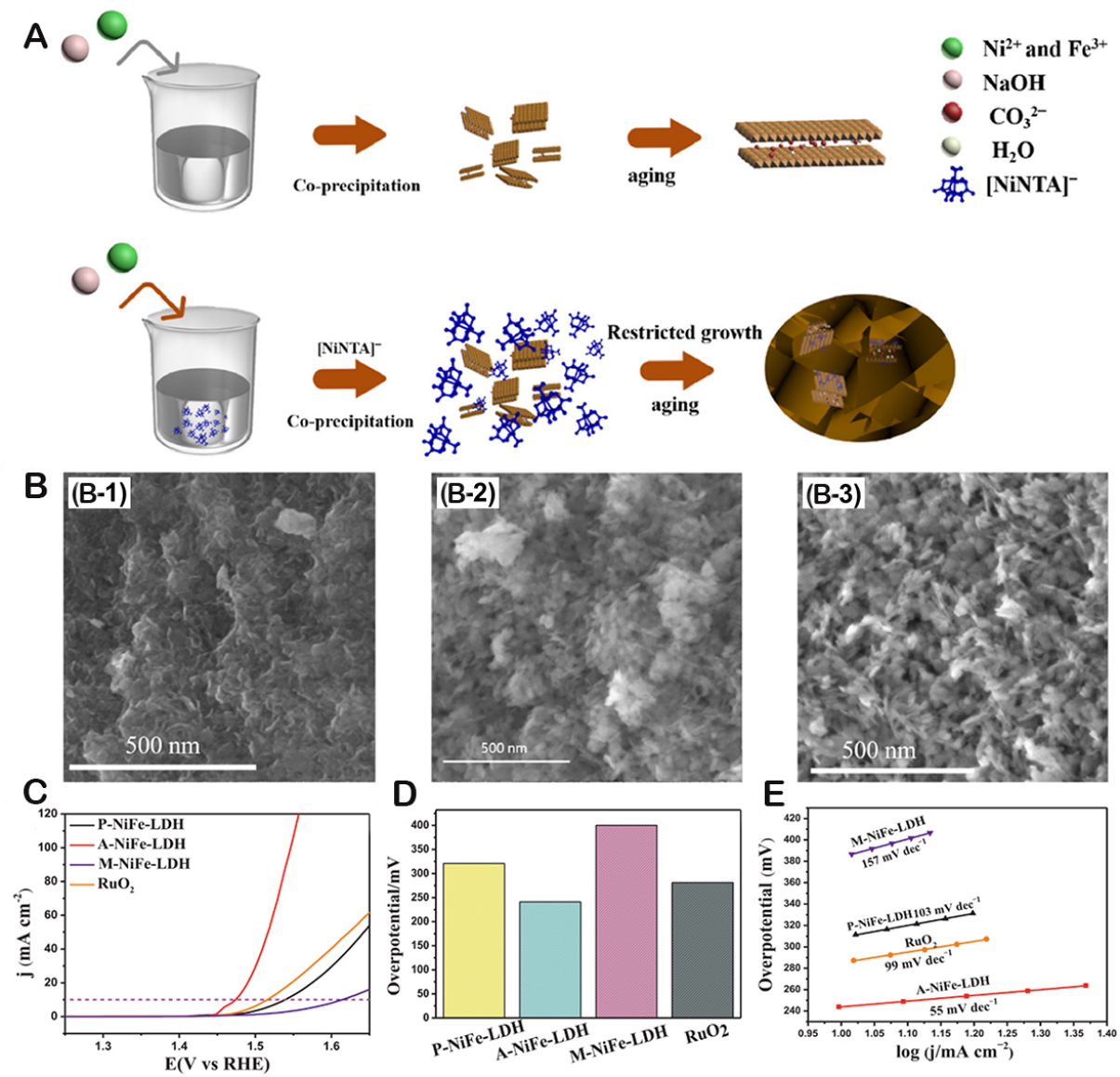

Figure 6. (A) The schematic illustration of the preparation process for P-NiFe-LDH and A-NiFe-LDH; (B) FESEM images of (B-1) A-NiFe-LDH, (B-2) P-NiFe-LDH, and (B-3) M-NiFe-LDH; (C) LSV plots of P-NiFe-LDH, A-NiFe-LDH, M-NiFe-LDH, and RuO_2; (D) The corresponding overpotential at a current density of 10 mA·cm^{-2}; (E) The corresponding Tafel plots. Reproduced with permission. Copyright 2020, Elsevier[75].

In addition to elemental doping, several new and advantageous strategies have been developed over the past few years to enhance the catalytic activity of transition-metal-based electrocatalysts. Zhang *et al.* proposed that gelled FeCoW oxyhydroxide is a ternary metal oxyhydroxide with better OER performance than Ni-Fe oxyhydroxide[76]. A simple, fast, and scalable microwave method was reported for the first time, and a series of ultrasmall transition-metal selenide NPs (~5 nm in diameter) were supported on the surface of CNTs[77]. By benchmarking the OER activity, $Ni_{0.27}Co_{0.28}Fe_{0.30}Se$@CNT was determined as the electrocatalyst with an optimized ratio and composition, exhibiting excellent OER performance and achieving a current density of 100 mA·cm^{-2} at an overpotential of 291 mV, which is 48 mV lower than that of commercial RuO_2. Furthermore, $Ni_{0.27}Co_{0.28}Fe_{0.30}Se$@CNT exhibits long-term stability of up to 50 h. Methods such as coating, defect engineering, exfoliation, and hybridization have also been explored for enhancing the catalytic

activity of transition-metal-based compounds. Wu *et al.* utilized the MOF precursor approach and polymer coating/encapsulation strategy to incorporate FeNi alloys into N-doped C with customized structures[78]. Furthermore, defect engineering has been introduced recently to enhance the catalytic performance of Co_3O_4 nanosheets by generating active sites and increasing electrical conductivity[79]. Ultrathin Ni-Co layered double hydroxide (LDH) nanosheets exhibit high OER catalytic activity owing to the presence of numerous exposed active sites[80]. These results suggest that complex engineered electrocatalysts based on transition-metal-based compounds can significantly overcome the limitations of existing electrocatalysts. However, the unstable OER potentials of transition metals under alkaline conditions should be considered, as they can lead to their conversion into hydroxides/oxyhydroxides. Therefore, the oxidized surface metals should be considered as the actual OER active sites of transition-metal electrocatalysts.

Metal-organic framework (MOF) electrocatalysts

MOFs are a promising porous material for electrocatalysis in the OER due to their high specific surface area. The evenly distributed metal nodes in the MOF framework can potentially act as active sites for electrocatalysis. However, the presence of organic ligands in MOFs can hinder the transport of electrons during the reaction process, leading to a loss of catalytic activity[81].

MOF-derived OER electrocatalysts include N-donor MOFs, carboxylate MOFs, and Prussian blue analogs (PBAs). N-donor MOFs, such as zeolitic imidazolate frameworks (ZIFs), consist of tetrahedral M(II) nodes and imidazolate-based ligands. Ding *et al.* synthesized α-$Co(OH)_2$-ZIF-L/NF-y by *in situ* surface reconstitution treatment of CoM-ZIF-L precursors, which could elevate the valence of the Co cations and promote the formation of highly active amorphous metal hydroxides[82]. The optimized α-$Co(OH)_2$-ZIF-L/NF-40 exhibited higher catalytic activity than commercial RuO_2 and many other OER catalysts. Surface reconstruction could also occur on bimetallic precursors. Lei *et al.* studied the morphology and crystalline structure reconstruction of M-ZIF-67 and produced the CoOOH-Vo catalyst, which was driven by an electric field[83]. The obtained M-ZIF-67-EA delivered low overpotentials of 175 mV at 10 $mA{\cdot}cm^{-2}$, which could be attributed to the leaching of partial ligands and the generation of CoOOH species with oxygen vacancies.

Carboxylate MOFs have versatile coordination modes and stable frameworks, making it easier to adjust their surface reconstitution process. Huang *et al.* produced CoNi-MOF nanosheet arrays (CoNi-MOFNA) via an *in situ* self-dissociation-assembly (SDA) synthetic strategy[84]. The microstructure of such MOFs was 2D nanosheets with a thickness of 8.2 nm, and during the long-term OER process, the surface of the CoNi-MOFNA was partially reconstructed. Two coordinatively unsaturated sites of Co and Ni played a significant role in catalysis. Similar excellent performance can be obtained on other carboxylate MOFs through structural transformation. For instance, $Ni_{0.9}Fe_{0.1}$-MOF achieved a low overpotential of 198 mV at 10 $mA{\cdot}cm^{-2}$[85].

PBAs are cyanide-based coordination framework materials. The introduction of CN vacancy into PBA through ionized N plasma by Yu *et al.* enhanced the OER catalytic activity[86]. The corresponding reconstruction improved the OER performance of PBA catalysts, accompanied by the formation of oxyhydroxides or hydroxides and the increase of the valence of metal ions[87,88]. Therefore, the reaction activity of MOF catalysts can be optimized through crystal structure reorganization and the optimization of organic ligands.

ORR mechanism

The ORR is an irreversible process that involves numerous fundamental reactions and proceeds through a complex mechanism. A comprehensive understanding of the ORR mechanism is essential for the development of highly efficient electrocatalysts. Although there are inconsistencies in the literature regarding the exact mechanism of the ORR, the general consensus is that the adsorption of the intermediates-O*, OOH*, and OH*-on the electrocatalysts determines the ORR performance of the metal electrocatalysts. Fundamentally, O_2 is reduced to OH^- in an alkaline environment, and the overall reaction scheme is as follows:

$$O_2 + 2H_2O(l) + 4e^- \rightarrow 4OH^- \quad (2)$$

In general, the ORR proceeds via a $4e^-$ reaction step[89]:

$$O_2 + H_2O(l) + e^- \rightarrow OOH^* + OH^- \quad (2a)$$

$$OOH^* + e^- \rightarrow O^* + OH^- \quad (2b)$$

$$O^* + H_2O(l) + e^- \rightarrow OOH^* + OH^- \quad (2c)$$

$$OH^* + e^- \rightarrow OH^- \quad (2d)$$

where * refers to an atom in a particular model.

O_2 is generally reduced to H_2O in an acidic environment, and the overall reaction scheme is as follows:

$$O_2 + 2H^+ + 4e^- \rightarrow H_2O(l) \quad (3)$$

Similarly, the ORR undergoes a $4e^-$ reaction step[90]:

$$OOH \rightarrow OOH^* \quad (3a)$$

$$OOH^* + H^+ + e^- \rightarrow O^* + H_2O(l) \quad (3b)$$

$$O^* + H^+ + e^- \rightarrow OH^* \quad (3c)$$

$$OH^* + H^+ + e^- \rightarrow H_2O(l) \quad (3d)$$

where * refers to an atom in a particular model.

Noble-metal-based ORR electrocatalysts

The ORR is a critical process in advanced fuel cell technologies and plays a determining role in their overall yield and commercial applicability. However, the ORR exhibits sluggish kinetics due to complex processes such as O_2 adsorption on the catalyst surface, activation/cleavage of O-O bonds, and product removal[91]. Therefore, high-efficiency electrocatalysts are required to meet the stringent requirements of ORR applications, and developing such catalysts remains a significant challenge. During the ORR process, the transfer of O_2 and accumulation of liquid products severely hinder the active sites[92]. To date, researchers

have conducted precise design and elaborate synthesis of Pt-based electrocatalysts for ORR, which are identified as high-efficiency ORR electrocatalysts[93]. Three research hotspots for Pt-based electrocatalysts have been identified, including (1) reducing the size of Pt NPs, increasing their dispersion and specific surface area[94]; (2) exploring the preparation of Pt NPs with specifically oriented crystal planes; and (3) adding other metallic elements to Pt catalysts through various physical and chemical methods to alloy or disperse Pt into alloys with other transition metals or oxides, respectively, thereby forming mixtures or alloys at a specific scale, such as core-shell structures[95]. Among these strategies, the precise control of nanoscale Pt structures and the tuning of morphology and composition are considered the most effective approaches for substantially improving the ORR performance and reducing the amount of expensive Pt in fuel cells[94,96].

Huang *et al.* prepared a core (Pd)/shell (Pt_3Ni(Pt-skin)) electrocatalyst using Zn underpotential deposition (UPD) onto a Ni UPD-modified Pd/C catalyst, as depicted in Figure 7[97]. The Pt_3Ni(Pt-skin) structure retains the advantages of the ultrathin layer structure and the synergy of the Ni sublayer. The synthesis process involved first electrodeposition of Ni_u onto the Pd surface of Pd20/C, followed by modification of Znu on Ni_u/Pd_{20}/C. Subsequently, Zn_u was replaced by Pt via the Galvanic process, resulting in a Pt atomic-layer cover on the Ni_u/Pd_{20}/C (PtNi/Pd_{20}/C). Repetitive Zn UPD-Galvanic deposition introduced the second and third Pt atomic layers onto PtNi/Pd_{20}/C, yielding the desired Pt_3Ni(Pt-skin)/Pd_{20}/C electrocatalyst. This electrocatalyst exhibits the best ORR performance, with a Pt specific activity of 16.7 $mA{\cdot}cm^{-2}$ and a Pt mass activity of 14.2 A mg Pt^{-1}. These values are 90 and 156 times higher, respectively than those of commercial Pt/C electrocatalysts.

Porous structures are efficient for electrocatalysis due to the presence of numerous exposed active sites on their surfaces and their smooth mass transfer capability. Various methods, including hard templating, dealloying, and surfactant-assisted synthesis, have been employed for synthesizing porous noble-metal electrocatalysts. Mesoporous silica has been extensively used as a hard template for preparing noble-metal mesoporous materials due to its low cost, highly ordered structure, and capability of facile silica removal via efficient etching processes. Chen *et al.* developed a new approach for synthesizing single-crystal-like MCM-48 nanospheres (NSs) for the templated preparation of mesoporous Pt NSs by molten salt impregnation, followed by H_2 reduction[98]. The synthesized mesoporous Pt catalysts exhibit higher activity than commercial Pt/C electrocatalysts due to their open pore structure. Dealloying is another efficient technique for preparing porous Pt nanostructures, wherein non-Pt components are selectively dissolved from the alloy by chemical or electrochemical methods. Leaching of non-Pt atoms from the surface of Pt-based alloys results in large mesoporous structures, defects, and vacancies. For instance, Li *et al.* observed that Pt/NiO core-shell nanowires synthesized in the solution can be converted into Pt-Ni alloy nanowires through thermal annealing[99]. These alloy nanowires can then be transformed into jagged Pt nanowires by electrochemical dealloying. The jagged nanowires have highly stressed, undercoordinated, and rhombus-rich surface configurations that improve ORR activity more effectively than relaxed surface configurations.

Soft templating is considered a flexible and efficient method for preparing porous nanomaterials. Attard *et al.* developed porous nanomaterials using the lyotropic liquid crystal (LLC) method to investigate Pt nanostructures[100,101]. The LLC phase was formed using polyoctylethylene glycol monohexadecyl ether ($CH_3(CH_2)_{15}(OCH_2CH_2)_8OH$) as the nonionic surfactant and hexachloroplatinic acid (H_2PtCl_6) as the Pt source. They prepared mesoporous Pt NPs[100] and films[101] using direct chemical reduction and electrochemical methods, respectively, which exhibit excellent ORR performances. Ever since the development of the LLC method, researchers have attempted to develop more environmentally friendly methods by substantially decreasing the surfactant concentration. Li *et al.* reported a micelle assembly

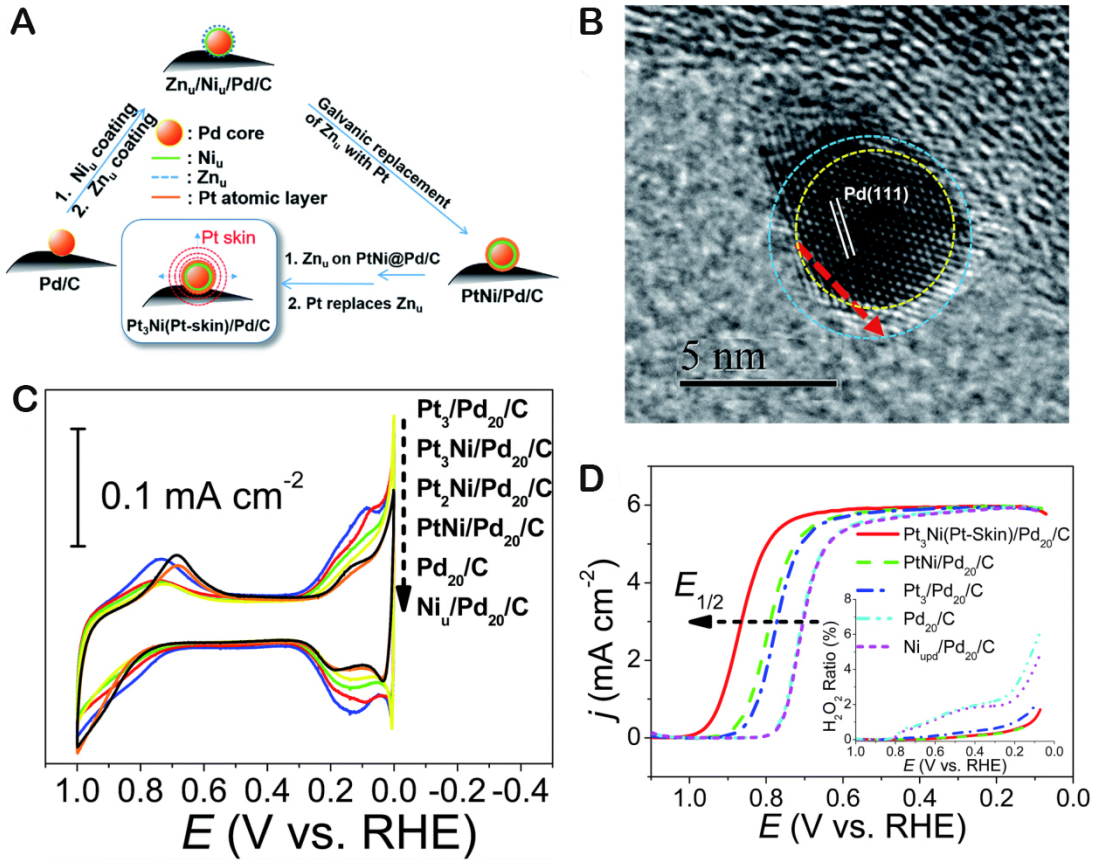

Figure 7. (A) The representative HRTEM image of a core (Pd)/shell (Pt_3Ni(Pt-skin)) nanoparticle; (B) The preparation process of Pt_3Ni(Pt-skin)/Pd_{20}/C; (C) ORR polarization curves; (D) Cyclic voltammograms. Reproduced with permission. Copyright 2018, Royal Society of Chemistry[97].

method, which requires a significantly lower surfactant concentration than the LLC method, for synthesizing mesoporous Pt nanomaterials[102].

Although numerous preparation methods have emerged, they afford excellent ORR performance. However, Pt-based noble-metal electrocatalysts have low stability and undergo structural and compositional changes under typical proton exchange membrane fuel cell operating conditions, thereby significantly degrading the performance. The degradation is attributed to the following reasons: (1) electrocatalyst dissolution, such as Pt dissolution; leading to preferential leaching of active metal elements in the Pt-based alloy NPs; and (2) electrocatalyst agglomeration.

Non-noble-metal-based ORR electrocatalysts

Non-noble-metal oxygen reduction electrocatalysts can be divided into two categories: transition-metal-based and nonmetallic electrocatalysts. Transition-metal electrocatalysts are abundant and economical and offer comparable catalytic activity to that of noble-metal electrocatalysts. Most major transition metals have great potential as ORR electrocatalysts. Therefore, researchers have been working on developing transition-metal catalysts. In addition, the research and development of nonmetallic catalysts are ongoing.

Metal-free (nonmetallic heteroatom-doped) C-based electrocatalysts

C nanomaterials generally include graphene, C nanofibers (CNFs), CNTs, ordered mesoporous carbons (OMCs), C black (CB), and graphene-related materials such as rGO[103]. Compared with metals, C-based nanomaterials have more desirable properties, such as a large specific surface area, excellent mechanical stability, high electrical conductivity, high electrochemical potential, and low cost. Therefore, C-based nanomaterials are widely used as support for ORR electrocatalysts. Doping with heteroatoms such as nonmetallic N, B, P, and S and other light nonmetallic elements can significantly improve the ORR performance of C-based nanomaterials, which have long emerged as electrocatalysts. In addition, they are effective against corrosion and poisoning and have higher durability than transition-metal-based compounds. Through heteroatomic doping of C nanostructures, the charge and spin densities of C radicals can be altered, thereby accelerating the electron transfer of electrocatalysis.

In 2009, Gong *et al.* proposed the use of N-containing CNTs as ORR catalysts[104]. The N-containing CNTs demonstrated ORR catalytic performance and long service life compared to those of Pt/C catalysts in an alkaline solution. Yan *et al.* prepared N-doped hollow C polyhedra (NHCPs) by direct pyrolysis of NaCl-templated zeolite imidazolate framework (ZIF)-8[105]. The NHCPs exhibited high ORR electrocatalytic activity due to their hollow porous structure, large surface area, high degree of graphitization, and desired N bond type. Kim *et al.* proposed a novel N-doping approach by introducing a biomimetic synthesis of monodisperse, N-rich melanin-like polymers derived from marine cuttlefish sepia biopolymer[106]. These polymers were subsequently used as highly N-doped synthetic C (MC) and biomass C (SC) spheres. The ultra-microporosity (<1 nm) of the N-doped MC and SC spheres can be fine-tuned by suitable CO_2 activation. N-doped MC and SC, with ultralarge surface areas of 2,677 and 2,506 $m^2 \cdot g^{-1}$, respectively, exhibit high ORR activity with a good $4e^-$ reduction pathway, high durability, and excellent methanol tolerance, comparable to those of commercial Pt-based electrocatalysts.

Liao *et al.* utilized malic acid, tartaric acid, and citric acid as C sources to fabricate N-doped graphene for ORR[107]. The authors found that N-doped graphene prepared from citric acid exhibits the highest electrocatalytic activity, comparable to that of commercial Pt/C electrocatalysts, and high durability due to the high p-N content in the composites, as shown in Figure 8A-D. Li *et al.* synthesized a metal-free N-doped γ-graphene catalyst and demonstrated that *in situ* p-N in N-doped γ-graphene acts as an active site for the ORR, accelerating the RDS of proton extraction, based on their theoretical calculations[108]. Wang *et al.* presented a novel approach to uncover the active sites of N-doped graphene in the oxygen reduction ORR by selectively modifying the acetyl group at the p-N and ortho-C atoms of the pyridinic ring[109]. Their research revealed that the ortho-C atom of the pyridinic ring is the active site for ORR, as evidenced by the complete inactivity towards ORR upon blocking this atom. Zhu *et al.* synthesized a highly active metal-free N-doped C catalyst (NPC-4) for ORR by KOH activation to increase the pore size and generate surface defects in ZIF-8-derived NPC nanomaterials [Figure 8E-G][110]. The authors attributed the high ORR activity of NPC-4 nanomaterials to the abundant and highly exposed active sites resulting from KOH activation. They found that the effect of numerous surface defects is more pronounced than that of the pyrrolic N and p-N functional groups. In contrast, graphitic N species in C-based materials can function as active sites for ORR in alkaline media[111,112]. Lai *et al.* produced N-graphene by annealing N-containing polymer/rGO composites (polyaniline (PANI)/rGO or polypyrrole/rGO) and demonstrated that the electrocatalytic activity depends on the graphitic N content, which determines the limiting current density[113]. Meanwhile, the p-N content increases the ORR onset potential (E_{onset}). Yasuda *et al.* attributed the $4e^-$ transfer process in the ORR in N-doped graphene catalysts to the existence of p-N, whereas graphitic N promotes a $2e^-$ transfer pathway. The authors concluded that p-N is a more effective active site for ORR than graphitic N[114].

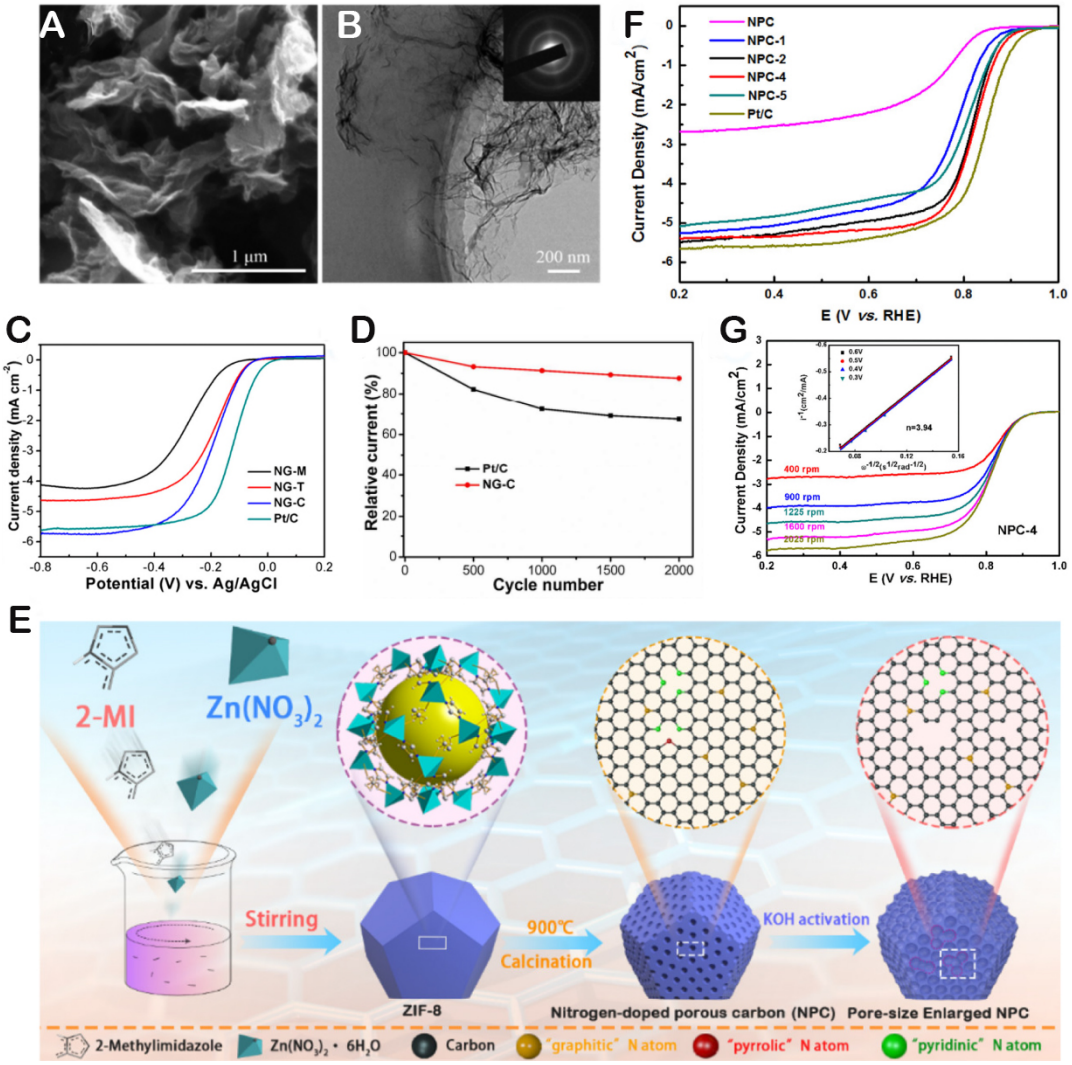

Figure 8. (A) SEM image of NG-C; (B) low-magnification TEM image and selected area electron diffraction (SAED) pattern (inset) of NG-C; (C) LSV curves of ORR on NG-M, NG-T, NG-C, and commercial Pt/C; (D) ORR forward peak maximum currents for NG-C and commercial 20 wt% Pt/C catalysts after different cycles. Reproduced with permission. Copyright 2015, ACS Publications[107]; (E) Schematic diagram of the synthesis of the pore size-enlarged NPC nanomaterials derived from ZIF-8 precursors; (F) Linear sweep voltammograms of ZIF-8-derived NPC nanomaterial, KOH-activated ZIF-8-derived NPC nanomaterials and Pt/C (20%) in O_2-saturated 0.1 M KOH solution at a scan rate of 10 mV·s^{-1} with 1,600 rpm; (G) LSV curves of NPC-4 with various rotation speeds, with the inset giving the K-L plots. Reproduced with permission. Copyright 2019, ACS Publications[110].

The P doping of C-based electrocatalysts significantly influences their ORR activity compared to that of undoped nanomaterials[115]. Wang *et al.* developed a technique for *in situ* P-doping of C dots (CDs) and simultaneous modification of graphene substrates via biomass derivatization[116]. The resulting P-doped CD/graphene (P-CD/G) nanocomposite displayed an extremely high P-doping level of C nanomaterials and ORR activity comparable to commercial Pt/C electrocatalysts. Yang *et al.* proposed four types of P-doped graphene structures, namely, PC3G, OPC3G, PC4G, and OPC4G sheets, to study the effect of the chemical bonding state of the P atoms on stability, electronic structure, and ORR catalytic activity[117]. Based on stability, electrical conductivity, Gibbs free energy barriers of the rate-determining step (ΔG_{RDS}), and the number of potential active sites of the P-doped graphene structure, OPC3G is the most efficient and stable P-doped graphene for ORR. Additionally, the C atom, which has a high negative charge, could be the most

active site for ORR. The high electrocatalytic activity and durability of the electrocatalysts are mainly attributed to P doping in the C lattice, and the amount of P incorporated into the C mainly determines the ORR activity increase and modification of the ORR pathway[118]. Wu *et al.* prepared P-doped C hollow spheres (P-CHS) through a hydrothermal method, using glucose as the C source and tetraphenylphosphonium bromide as the P source[119]. The P-CHS possesses a microporous shell structure, exhibiting a large specific surface area exceeding 500 $m^2 \cdot g^{-1}$. The electrocatalytic activity and long-term stability of the resulting P-CHS, containing 1.61 at% of P, were evaluated using rotating ring-disk electrode (RRDE) measurements in alkaline media. The microstructure and ORR activity are significantly influenced by the P content in the C. The P doping in the C lattice induces highly active catalytic sites, contributing to the high electrocatalytic activity and durability of P-CHS for ORR. Moreover, the hollow spherical structure of P-CHS facilitates the efficient mass transfer of reactants and products during the ORR. Bai *et al.* used a density functional theory (DFT) approach to investigate the ORR mechanism on P-doped divacancy graphene[120]. Their study showed that P-doped graphene with intrinsic C defects has high electrocatalytic activity for ORR. Overall, P doping in C-based electrocatalysts significantly enhances their ORR activity, and the amount of P incorporated into the C lattice plays a crucial role in determining the ORR performance.

The ORR performance can be enhanced by doping S atoms in graphene, as C-S acts as a catalytically active site, improving the ORR kinetics[121-123]. Chen *et al.* synthesized S-doped rGO (S-rGO) nanosheets using a one-pot hydrothermal method [Figure 9A][124]. The prepared S-rGO consisted of high-quality sulfide species (mainly C-S-C) and many exposed defects and edge sites on its surface. Figure 9B-D demonstrates that S-rGO has high conductivity and electrocatalytic activity for the ORR and significantly higher stability and better methanol tolerance than commercial Pt/C electrocatalysts. Wong *et al.* proposed that changes in the number of defects in a material affect its electrochemical performance and that the amount of S dopant is positively correlated with the decrease in the required overpotential[125]. Although S-graphene has a lower onset potential than commercial Pt/C electrocatalysts, it has higher durability than N-graphene and commercial Pt/C electrocatalysts. To improve the catalytic efficiency of graphene quantum dots (GQDs) for the ORR, Banerjee *et al.* explored the role of S-dopants using a first-principles DFT-based approach[126]. They found that the ORR efficiency varies with the dopant location and configuration on the S-doped GQDs at different active sites. The charge transfer from the dopant site to the active site and intermediates and the binding energy of the intermediates on the active site mainly determine the RDSs, onset potentials, and overpotentials required for the ORR. An increase in the S-dopant concentration or the presence of O_2 significantly increases the ORR efficiency of the GQDs. Similarly, B-doping in C materials can result in better catalytic performance than undoped C materials, although they exhibit moderate ORR activity[127-129]. Zhang *et al.* used Na borohydride as a reducing agent to convert CO_2 into B-doped porous C (B-PC), which was further activated by heat treatment[130]. The treated B-PC has the same ORR activity as the Pt-AC catalyst but shows better ORR selectivity. The improvement in electrocatalytic performance is attributed not to the change in C morphology but to the change in the bond between B and C atoms on the surface and the broadening of π states. Xiao *et al.* reported a method to synthesize porous graphene and B-doped porous graphene with an abundant porous structure and high B-doping level [Figure 9E][131]. The abundant pore structures and B-related active sites accelerate the ORR kinetics. Overall, doping of S and B in C-based electrocatalysts can significantly enhance their ORR activity, and the dopant concentration, location, and configuration play a crucial role in determining their electrocatalytic performance.

Single-heteroatom-doped C-based materials exhibit high electrocatalytic activity. However, bidoped nanocarbon exhibits better electrocatalytic performance[132-135]. For example, Duan *et al.* synthesized N, S-bidoped graphene, which shows higher ORR electrocatalytic activity than S- or N-doped graphene[136].

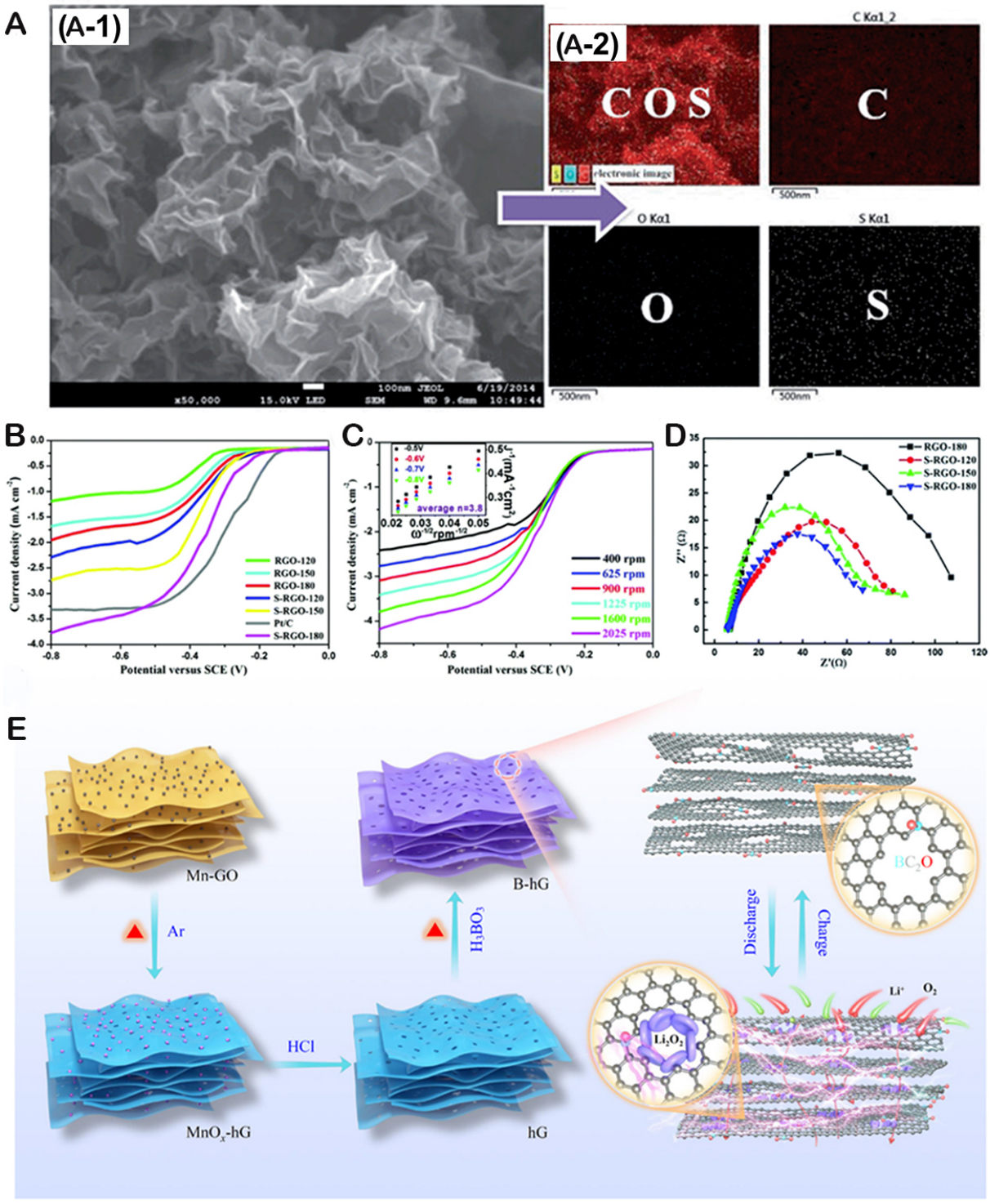

Figure 9. (A) Micrographs of S-RGO-180, (A-1) FE-SEM image of S-RGO-180 and (A-2) the corresponding C-, O-, and S-elemental mappings; (B) LSV curves of RGOs, S-RGOs, and Pt/C; (C) Rotating-disk voltammograms recorded for S-RGO-180 electrode in an O_2-saturated 0.1 M KOH solution at a different rotation rate. The inset in (C) shows the corresponding Koutecky-Levich plots (J^{-1} *vs.* $\omega^{-0.5}$) at different potentials; (D) The magnified Nyquist plots of RGO-180 and S-RGOs. Reproduced with permission. Copyright 2014, Royal Society of Chemistry[124]; (E) Schematic illustration of the synthesis process of B-hG and its charge/discharge processes as cathode for LOBs. Reproduced with permission. Copyright 2022, Elsevier[131].

Zhang *et al.* demonstrated that N, S-codoped graphene/CNT composites (N, S-GCNT) exhibit superior electrochemical ORR activity compared to graphene-doped or N, S-codoped CNTs[137]. Xue *et al.* reported that B, N-codoped graphene foams display significantly enhanced electrocatalytic ORR activity compared to foams doped with only B or N[138]. In addition, Zhao *et al.* found that the ORR activity of CNTs doped sequentially with B and N is higher than that of CNTs doped simultaneously with B and N[139]. Furthermore, the B, N-codoped graphene nanoribbons exhibit ORR activity comparable to that of the 20 wt% Pt/C electrocatalyst, owing to the synergy between N, B-codoping and active sites located at the edges of the nanoribbons[140]. N, P-bidoped C electrocatalysts present higher ORR activity than N- or P-doped composites [Figure 10A-D][141]. Furthermore, N, P-bidoped porous C synthesized via high conversion of coconut shell residues exhibit high electrocatalytic ORR activity[142]. Tridoping also leads to high ORR activity[143-145]. For instance, N/S/O-doped OMCs (N/S/O-OMCs) exhibit high ORR activity [Figure 10E and F][146]. Nanocarbons with nanoporous morphology and heteroatom (N, P, and B) codoping exhibit higher ORR activity than single- or bidoped catalysts, as evidenced by their superior current density and onset potential[147]. Li *et al.* doped F and S atoms into a graphene C matrix using N as the main dopant via a novel ternary-N-precursor-inspired strategy to promote the ORR[148]. The use of secondary and tertiary N precursors enhances the configuration of active sites, resulting in increased ORR activity. Additionally, the ORR performance of N, F, S-tridoped porous graphene is significantly improved, largely due to the presence of additional active sites and the porous structure of the material. These results highlight the importance of bi and tridoping of electrocatalysts with different heteroatoms for increasing their ORR activity. The development of ternary or multi-doped C remains a significant challenge due to various factors. These challenges include difficulties in selecting appropriate precursors, a lack of established design principles, and problems in optimizing the beneficial composition of heteroatoms.

Metal-N-C electrocatalysts

N-doped-C-containing transition-metal-based materials are currently considered the most promising non-Pt catalysts for the ORR, exhibiting high activity in both 0.1 M KOH and 0.5 M H_2SO_4 or 0.1 M $HClO_4$ solutions[95]. The high ORR activity of macrocyclic compounds with metal-N ($M-N_4$) centers was first reported in 1964, leading to research on non-Pt-based ORR electrocatalysts. Since then, transition-metal macrocyclic compounds have been of interest to many researchers. Initially, N-containing macrocyclic compounds, such as phthalocyanine, tetraphenylporphyrin, tetramethoxyporphyrin, and tetrazene, were used as N source precursors to provide $M-N_4$ structures[149]. More recently, a major breakthrough in the synthesis of M-N-C electrocatalysts has been achieved through the pyrolysis of simple and inexpensive C substrates, N precursors, and transition-metal salts in the absence of precursors with $M-N_4$ groups to obtain nanomaterials with $M-N_4$ structures.

Determining the correlation between the ORR catalytic activity and $M-N_4$ structure has proven difficult, leading to the use of various nonmacrocyclic N-containing compounds as N-source precursors. These include small inorganic molecules such as NH_3 and Na azide, small organic molecules such as acetonitrile, pyrrole, ethylenediamine, and phenanthroline, and N-containing organic polymers such as polyacrylonitrile (PAN), polypyrrole, polyethyleneimine, melamine resins, and PANI[150-154]. N-containing polymers have advantages over small organic molecules as they can form ordered templates and more stable C-based active layers, preventing the collapse of the C skeleton and severe loss of active sites during catalyst pyrolysis. They are also cheaper and more accessible than macrocyclic polymers. The choice of N source precursor significantly influences the activity and stability of the catalyst, and the selection of C support, transition metal, and pyrolysis process affects the final properties. Current research is mainly focused on Fe- or Co-containing nanomaterials as they exhibit the highest ORR activity.

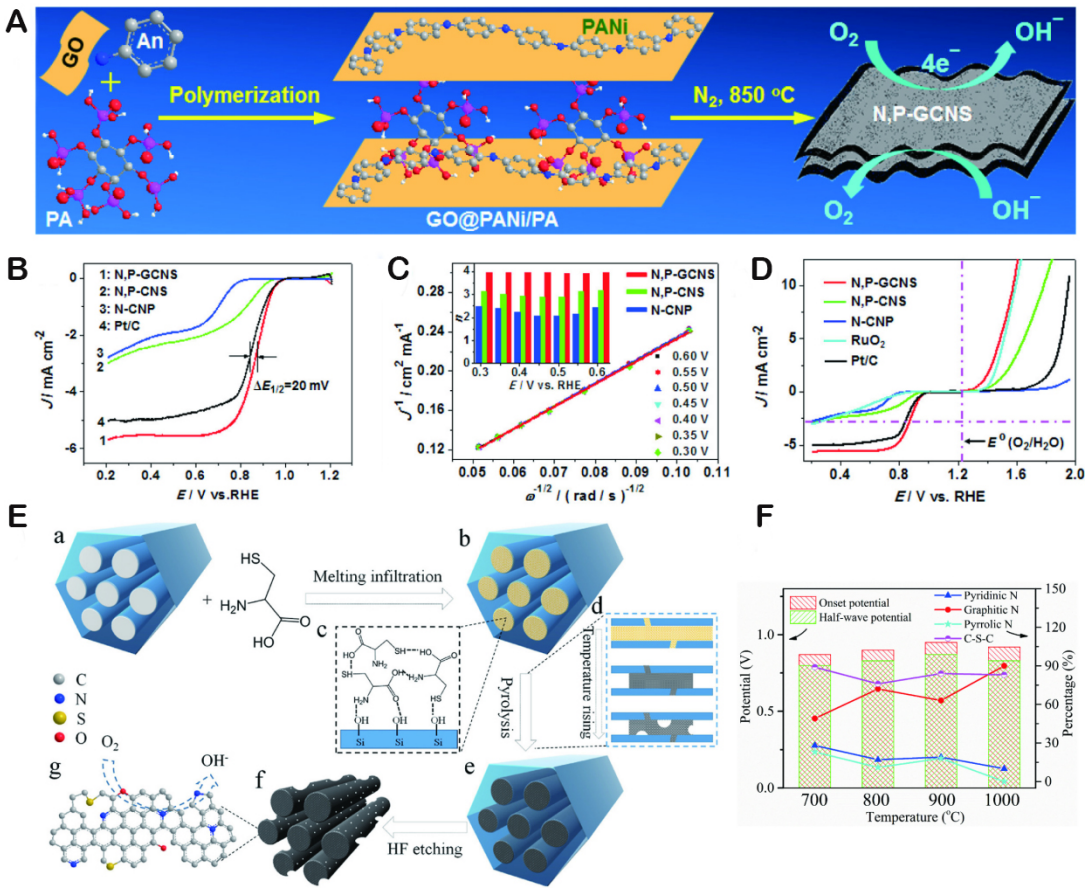

Figure 10. (A) Schematic illustration of the fabrication process and structure of the N,P-GCNS bifunctional oxygen electrocatalyst; (B) LSV curves of various catalysts at a rotation rate of 1,600 rpm; (C) K-L plots of N,P-GCNS at different potentials. (Inset) Electron transfer number (n) of various catalysts at different potentials; (D) Bifunctional catalytic activity of various catalysts toward both ORR and OER. Reproduced with permission. Copyright 2015, ACS Publications[141]; (E) Schematic illustration of the synthetic process; (F) The dependences of onset and half-wave potentials, and percentages of different types of N sites on the carbonization temperatures for the N/S/O-OMCs. Reproduced with permission. Copyright 2021, Elsevier[146].

A one-pot method using dopamine as the N source and metal salts as precursors for the ORR was used to incorporate various transition metals into N-doped CNTs (M-N-C/CNT, M = Fe, Mn, Co, and Ni), as shown in Figure 11[155]. Among the four as-synthesized catalysts, Mn-N-C/CNT-800 and Co-N-C/CNT-800 exhibit much higher electrocatalytic activities than Ni-N-C/CNT-800 and Fe-N-C/CNT-800. Mn-N-C/CNT-800, in particular, has an E_{onset} approximately 75 mV lower than that of Pt/C (-35 mV) and an $E_{1/2}$ approximately 20 mV lower than that of Pt/C (-150 mV), indicating its high ORR activity. The stability test results demonstrate excellent stability, with the curve obtained after 2,000 or 5,000 cycles highly consistent with that obtained initially by linear sweep voltammetry. Moreover, the limiting current density decreases by only 5.57% in approximately 11 h, indicating its high durability. The electrocatalytic performance of M-N-C/CNT catalysts is affected by the degree of metal graphitization and the metal state, which depend on the type of transition metal.

Progress has been made in optimizing the C support and pyrolysis temperature of M-N-C electrocatalysts, depending on the preferred N source or transition-metal precursor. Single-atomic catalysts (SACs), in particular, have shown higher ORR catalytic activity and stability than commercial Pt/C electrocatalysts[156,157]. Despite these advancements, improving the catalytic activity and stability of M-N-C

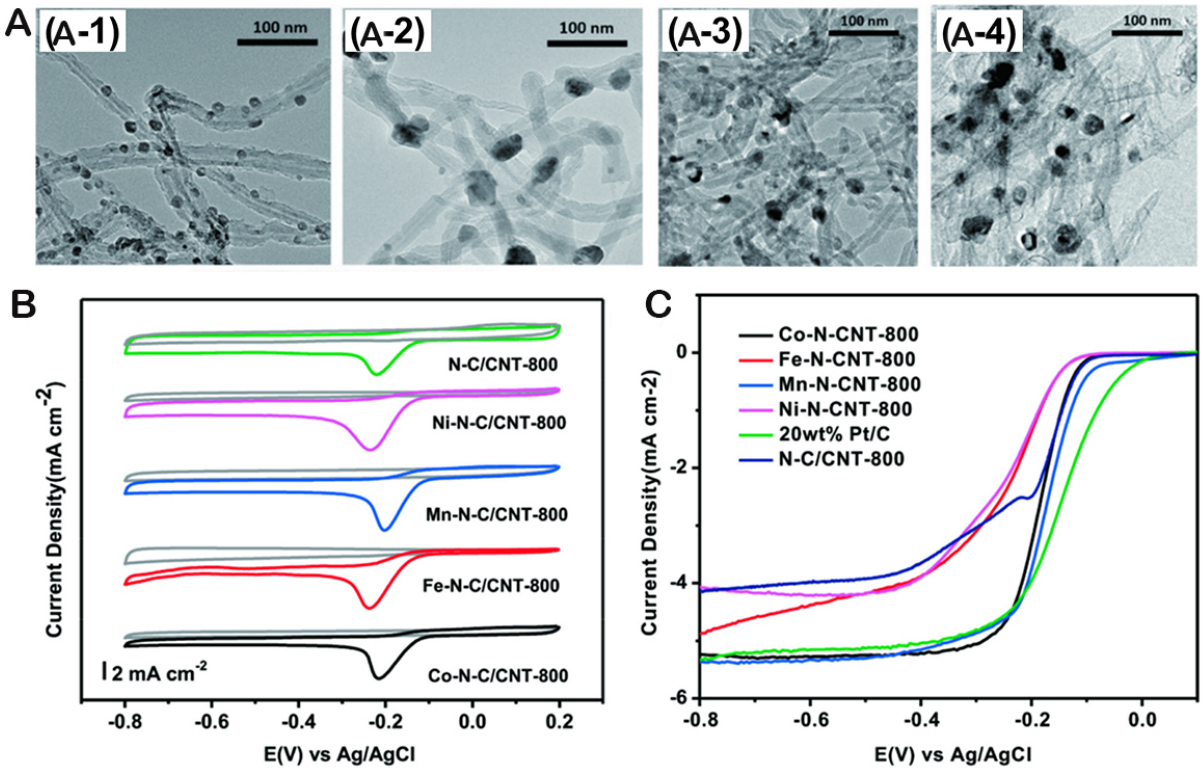

Figure 11. (A) The TEM images of M-N-C/CNT: (A-1) Co-N-C/CNT-800, (A-2) Mn-N-C/CNT-800, (A-3) Ni-N-C/CNT-800 and (A-4) Fe-N-C/CNT-800; (B) CV curves of M-N-C/CNT-800 s and N-C/CNT-800 in N_2-saturated (grey) and O_2-saturated (colored) 0.1 M KOH electrolytes; (C) LSV plots of M-N-C/CNT-800 s, N-C/CNT-800 and 20 wt% Pt/C. Reproduced with permission. Copyright 2018, Elsevier[155].

electrocatalysts remains a significant challenge. Two key factors influence the catalytic activity and stability of M-N-C electrocatalysts:

(i) The catalytic activity and spatial distribution of ORR active sites in M-N-C catalysts are determined by complex interactions between the elemental compositions and different components. However, there is no consensus on the exact nature of the catalytically active sites in M-N-C catalysts[158]. N plays a crucial role in M-N-C electrocatalysts, with its role in catalytic reactions divided into three categories. Firstly, N functional groups on the surface of C-based supports directly participate in the catalytic reaction and are responsible for the ORR activity[159]. Secondly, the N functional group coordinates the environment, and the coordination bond formed by the lone electron pair provided by the transition-metal ion serves as the catalytically active center for the ORR[157,160,161]. For example, in a Co-N-C catalyst prepared with PANI as the N source precursor, Co facilitates the entry of N into the structural matrix of C, and Fe can form an active center of Fe-N_x with N[162,163]. Researchers have harnessed the bimetallic effect by simultaneously introducing Fe and Co to increase the activity and stability of CoFe-based electrocatalysts[164-166]. Thirdly, a combination of the above two methods exists. *In situ* (isotope-labeled) Raman spectroscopy of a molecular Fe phthalocyanine model catalyst and a pyrolytic Fe-N-C catalyst has shown that besides the single-atom Fe-N_x sites, two C-N sites were identified in the pyrolyzed Fe-N-C catalyst and elucidated as separate active sites, showing distinct ORR intermediates and RDSs[166,167]. In summary, the exact nature of the catalytically active sites in M-N-C catalysts remains unclear, but N plays a crucial role in catalytic reactions and is involved in three different categories of mechanisms. Researchers have used bimetallic effects and identified separate active sites to increase the activity and stability of M-N-C electrocatalysts.

(ii) The effective active site density and oxygen transportation of electrocatalysts are determined by their specific surface area and porous structure[168,169]. Direct high-temperature heat treatment typically results in M-N-C electrocatalysts with a nonuniform active site distribution and difficulty forming a porous structure, which is not conducive to O_2 transport. The introduction of nanoporous structures could effectively resolve this challenge. A large specific surface area increases the number of catalytically active sites, while an ordered mesoporous structure increases the mass transfer rate. Xu *et al.* developed a facile dual molten salt ($ZnCl_2$ and NaCl)-mediated templating method for preparing Fe-N-C electrocatalysts with tailored porous frameworks[170]. The resulting Fe-N-C material exhibits excellent ORR performance and high stability in both alkaline and acidic media. Furthermore, the electrocatalyst has a large surface area (1,605 $m^2 \cdot g^{-1}$), which facilitates the mass transfer and exposure of the Fe-N_4 sites.

To obtain porous nanomaterials with large specific surface areas that can carry many active sites, new and efficient synthesis methods must be explored. Future research should focus on in-depth studies of the catalytic reaction mechanism and microstructure of M-N-C, which will be the key to the development of efficient electrocatalysts.

Transition-metal-oxide-, phosphide-, chalcogenide-, nitride-/oxynitride-, and carbide-based electrocatalysts

Nonprecious-metal-based ORR electrocatalysts, including TMOs, TMPs, transition-metal sulfides, TMNs/TMONs, and TMCs, have been extensively researched, along with nonmetallic and M-N-C electrocatalysts. Although the use of transition-metal-compound catalysts in acidic media poses a challenge, their performance in alkaline media is excellent[171]. The ORR kinetics is significantly improved in alkaline media compared to acidic media. Rational structural design can endow transition-metal-compound electrocatalysts with high activity comparable to that of Pt-based electrocatalysts.

(i) Transition-metal oxides: TMOs have garnered significant interest as electrocatalysts for the electrochemical ORR in alkaline media due to their potential applications in metal-air batteries and fuel cells. They are often naturally abundant, cost-effective, and environmentally friendly, displaying a high catalytic activity for ORR. Among various TMOs, Mn oxides (MnO_x) have gained much attention due to their low cost, abundance, and high electrocatalytic activity for both ORR and OER. The relationship between the structure and composition of TMOs and their ORR catalytic activity has been a subject of research. In the 1990s, Bockris and Otagawa studied the impact of transition metal cation properties on oxygen electrocatalysis[172]. Later publications extended the conclusion of the work of Bockris and Otagawa to the ORR and other types of TMOs. For instance, a study on TMOs with perovskite structures investigated the OER and reported the following order of ORR activity in a recent paper on the effects of crystal structure[173]: α-MnO_2 > amorphous MnO_x > β-MnO_2 > δ-MnO_2 [Figure 12A-C]. The authors also studied the relationship between ORR activity and O_2 adsorption strength using a temperature-programmed desorption method. Liu *et al.* studied the effect of Co_3O_4 NP surface orientation and found that the ORR activity follows the order of (111) > (100) > (110)[174]. Meanwhile, Tang *et al.* attributed the dependence of ORR activity on MnO_x structure and composition to the redox potential of surface Mn cations[175]. In binary and mixed MnO_x, ORR activity was found to be linked to the surface Mn(IV)/Mn(III) redox transition potential (E_f). Mn_2O_3 demonstrated the highest ORR activity among all the studied MnO_x due to its highest E_f, which arises from the unique property of the crystal structure related to waffle Fe fluorite, making it suitable for larger Mn(III) cations but not for smaller Mn(IV) cations. Other studies have also investigated the effect of the redox properties of transition-metal cations on ORR activity. For instance, in the $La_xCa_{1-x}MnO_3$ perovskite[176], the ORR activity was found to increase as the average Mn oxidation state decreased from 4.0 to 2.8. Qaseem *et al.* synthesized a hybrid nanomaterial consisting of $MnCo_2O_4$ and N-doped rGO (NGr) to serve as an ORR electrocatalyst. They found that the addition of spinel TMO NPs

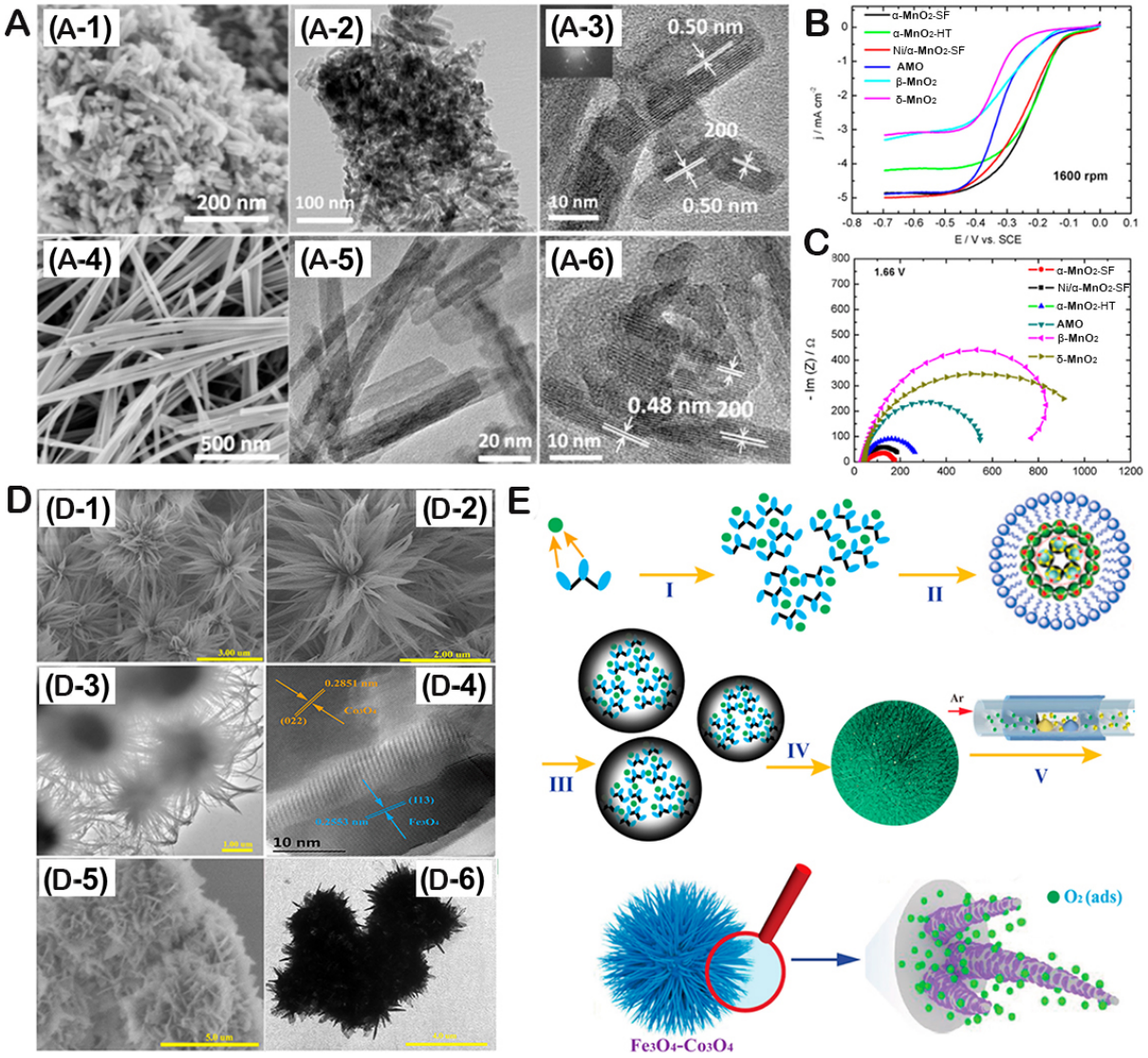

Figure 12. (A) SEM and images of materials: (A-1) SEM image of Ni/α-MnO_2-SF, (A-2 and A-3) TEM images of Ni/α-MnO_2-HT, (A-4) SEM image of α-MnO_2-SF, and (A-5 and A-6) TEM images of α-MnO_2-HT; (B) LSV curves studied on RDE electrodes in O_2-saturated 0.1 M KOH solution, at a rotation rate of 1,600 rpm with a scan rate of 5 mV·s^{-1}; (C) Nyquist plots obtained from EIS measurements in O_2 -saturated 0.1 M KOH solution on the manganese oxide modified PG carbon electrodes at an anodic polarization potential of 0.65 V (1.66 V *vs.*RHE). Reproduced with permission. Copyright 2014, ACS Publications[173]; (D) Morphology and microstructure characteristics of Actiniae-25 and Actiniae-65: (D-1 and D-2) SEM images of Actiniae-65, (D-3) TEM image of Actiniae-65, (D-4) HRTEM image of Actiniae-65, (D-5) SEM image of Actiniae-25, and (D-6) TEM image of Actiniae-25; (E) Schematic illustration of the solvothermal quasi-reverse-emulsion induced fabrication of actiniae-like hierarchical Fe_3O_4/Co_3O_4 nanoheterojunctions. Reproduced with permission. Copyright 2020, Elsevier[181].

via nucleation and cation substitution on graphene flakes led to covalent coupling with NGr, resulting in higher activity than either NPs or NGr alone[177]. The substitution of Mn also increased the ORR activity of the catalytic site of the hybrid nanomaterial compared to that of the pure CoxOy/NGr hybrid. The $MnCo_2O_4$/NGr hybrid electrocatalyst exhibited comparable current density to that of the Pt/C electrocatalyst at low overpotentials and higher current density at higher overpotentials. Additionally, the hybrid catalyst demonstrated excellent stability, retaining 96% of its initial ORR current density after continuous operation for over 5,000 s, while the Pt/C electrocatalyst retained only 78% of its initial current

density. Recently, many studies have focused on the modification engineering of transition-metal oxide catalysts (e.g., regulation of crystallinity and oxygen vacancies)[178], among which surface or interface engineering of transition-metal-oxide electrocatalysts is the most common approach[179]. Nayak *et al.* developed a surface engineering strategy for Ni- and Co-based hybrids ($NiO-Co_3O_4$) to be used as efficient and robust ORR electrocatalysts[180]. They achieved this by controlling the precursor amounts of Ni and Co during the wet chemical synthesis to easily tune the surface nanostructure of the $NiO-Co_3O_4$ nanohybrid. By optimizing the composition, they were able to create surface structures consisting of 1D nanorods and 2D nanosheets, which significantly increased the ORR electrocatalytic activity and stability of the $NiO-Co_3O_4$ nanohybrid. The excellent catalytic performance of the $NiO-Co_3O_4$ nanohybrids can be attributed to charge or mass transfer within the 1D and 2D open-surface nanostructures. Zha *et al.* investigated the interplay between nanostructure, chemical composition, and electrocatalytic ORR activity by constructing tunable anemone-like hierarchical Fe_3O_4/Co_3O_4 nanoheterojunctions with controllable porosity and structural parameters[181]. They achieved this using a solvothermal quasi-inverse-emulsion method, as depicted in Figure 12D and E. The electrocatalysts developed by Zha *et al.* possess a large specific surface area ranging from 302 to 810 $m^2 \cdot g^{-1}$, an optimized pore size distribution, and pore volume[181]. The resulting nanoheterojunctions exhibit high electrocatalytic ORR activity, long-term stability, and excellent methanol tolerance in alkaline solutions. Furthermore, the correlation analysis revealed that the electrocatalytic ORR activity of the porous nanoheterojunction is proportional to its specific surface area and is governed by the surface chemistry of the electrocatalyst.

(ii) Transition-metal phosphides: TMPs exist in many forms, among which phosphides with electrochemical catalytic properties mainly include Co phosphide[182,183], Fe phosphide[184,185], Ni phosphide[186,187], and Fe/Co/Ni binary or ternary mixed phosphides[188,189]. Hydrothermal treatment and templating are the main methods for preparing nanostructured TMP precursors, following which phosphating is performed at low temperatures using Na_2PO_2 to afford the phosphides[190]. Some phosphides can be synthesized by oil-bath heating or high-temperature annealing. The nanostructure of phosphides can be significantly altered by changing the reaction temperature, reaction time, chemical composition, template type, or support (e.g., porous C, graphene, and C cloth).

While Co phosphide is typically used as an HER electrocatalyst, Liu *et al.* prefabricated CoP@N-C for the ORR and found that the electron transfer number for CoP@N-C ranged from 3.62 to 3.94, indicating that the reaction proceeds via a complete $4e^-$ transfer ORR process[191]. The ORR catalytic activity of the CoP@N-C electrocatalyst was found to be comparable to that of the Pt/C electrocatalyst. Additionally, certain unique polymer structures were found to enhance the catalytic performance of phosphides. Wu *et al.* reported Co-porphyrin-based conjugated mesoporous polymer (CoP-CMP) as an ORR electrocatalyst with an onset potential of -0.12 V and a half-wave potential of -0.18 V, which is close to the values obtained for Pt/C electrocatalyst[192]. The electron transfer number was calculated to be 3.83-3.86, indicating the dominance of the $4e^-$ transfer ORR process. This suggests that CoP-CMP800 has the highest ORR catalytic activity and outperforms many ORR electrocatalysts reported so far. Meanwhile, Fe phosphides are also commonly used as ORR electrocatalysts. Wang *et al.* developed a facile method for fabricating myricetus-like N, P-rich C NSs embedded in Fe_2P nanocrystals (Fe_2P/NPCs) by synthesizing Myrica-like PANI-NSs through microemulsion templating, incorporating Fe into the PANI-NS during hydrothermal treatment, and obtaining Fe_xP nanocrystals and N, P-rich carbonaceous supports through pyrolysis of hydrothermally treated PANI-NS [Figure 13][193]. The FexP/NPCs synthesized in this study have a uniform particle size of about 250 nm, a large specific surface area of 523 $m^2 \cdot g^{-1}$, and a mesoporous structure with an average diameter of approximately 3.46 nm. The phase structure of FexP is determined by the Fe/P molar ratio used during hydrothermal treatment. The Fe_2P phase can be obtained when the Fe/P

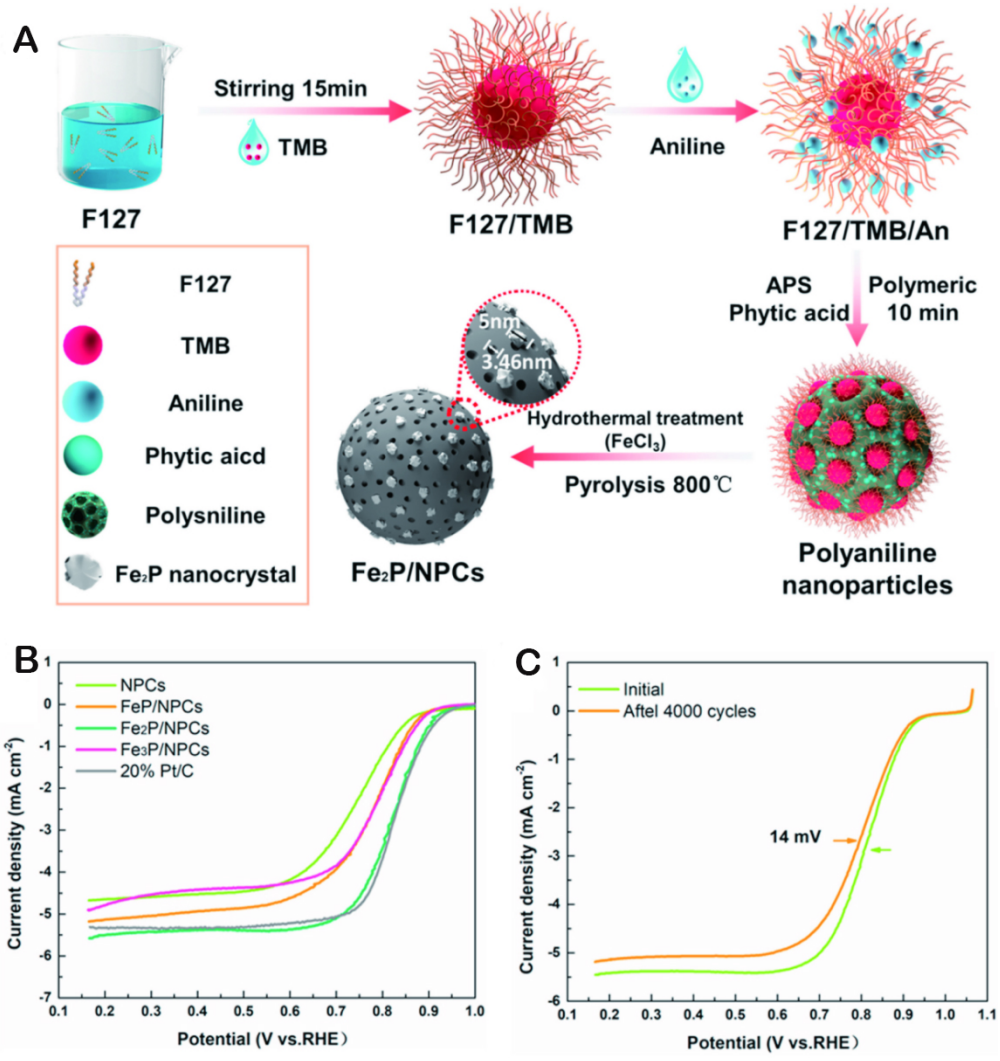

Figure 13. (A) The synthesis process of Fe_xP/NPCs as efficient electrocatalysts for ORR; (B) LSV curves of different electrocatalysts obtained at a rotation rate of 1,600 rpm; (C) LSV curves obtained before and after 4,000 CV cycles. Reproduced with permission. Copyright 2021, Elsevier[193].

ratio is around 0.2. Fe_2P/NPCs exhibit high ORR electrocatalytic activity, with a half-wave potential of 0.820 V *vs.* RHE and a diffusion-limited current density of 5.58 mA·cm^{-2}, comparable to those of commercial Pt/C electrocatalysts. Ran *et al.* also developed a honeycomb $Ni_2P/Ni_{12}P_5$ heterostructure ($Ni_2P/Ni_{12}P_5$@NF) with abundant P vacancies grown *in situ* on foamed Ni. The P vacancies can induce the delocalization of the bound electrons near the Ni-P bond, thereby adjusting the bandgap and facilitating conductivity and electrocatalytic activity enhancements[187]. Furthermore, Fe/Co/Ni binary or ternary mixed phosphides have been found to exhibit high ORR activity. Vijayakumar *et al.* developed CoP-N-doped-C@NiFeP nanoflakes (CoP-NC@NFP) from MOFs rich in multiple active sites[194]. Experimental results demonstrate that the multiple active catalytic sites of CoP-NC@NFP facilitate fast charge-transfer kinetics and excellent electrocatalytic performance for ORR.

(iii) Research on non-noble-metal chalcogenides as ORR electrocatalysts began in the 1970s. In 1974, Baresel *et al.* reported maximum current densities of 2,249 mA·m^{-2} and 1,000 mA·g^{-1} (at 600 mV) for Co-S and Co-Ni-S in acidic systems, respectively[195]. This high catalytic activity was attributed to the minimal

energy difference between the S 2p orbital and the highest occupied d orbital of the sulfide. In recent years, various transition-metal chalcogenides (M-X, where M=Co, Ni, Fe, Ru, Re, or Rh, and X=S, Se, or Te) have been utilized as ORR electrocatalysts, displaying excellent performance[171,196-198]. For instance, Zhang *et al.* developed an efficient electrocatalyst for the electrosynthesis of H_2O_2 by designing a Ti-doped Zn Co sulfide hollow superstructure (Ti-ZnCoS HSS)[199]. Ti-ZnCoS HSS was synthesized by sulfidation treatment of the MOF precursor followed by curing, forming a hollow-to-hollow superstructure (HSS) with small nanocages assembled around a large cake-like cavity [Figure 14]. The experimental and simulation results demonstrate that the multiple metallic components in Ti-ZnCoS HSS play a crucial role in altering the D-band center and their binding energy with O_2 species. The presence of abundant active sites in HSS promotes mass and electron transfer, resulting in excellent $2e^-$ transfer ORR performance at the atomic and nanometer levels. The synergy between D-band centers and superstructures in Ti-ZnCoS HSS leads to a highly selective ORR performance of 98%, with a high activity potential of 0.774 V *vs.* RHE at 1 $mA{\cdot}cm^{-2}$ and a H_2O_2 production rate of 675 mmol h^{-1} g_{cat}^{-1}. Moreover, Ti-ZnCoS HSS exhibits long-term stability under alkaline conditions. To tune ORR performance, crystal phase control is critical. For instance, co-encapsulating hexagonal (h-FeSe) and tetragonal FeSe (t-FeSe) ultrafine nanocrystals in an N-doped C matrix without agglomeration have been shown to be effective[200]. The resulting material, which contains a large number of h-FeSe nanocrystals, exhibits excellent ORR performance with a positive onset potential of 0.97 V and a high limiting current density of 5.4 $mA{\cdot}cm^{-2}$. In addition to its high catalytic activity, the material also exhibits remarkable methanol tolerance and stability. Theoretical studies have demonstrated that h-FeSe is superior to t-FeSe in terms of O_2 adsorption and *OOH intermediate dissociation of O-O bonds on the active Fe sites, making it more effective for alkaline ORR than t-FeSe. Therefore, h-FeSe is a promising alternative to t-FeSe for ORR applications. Moreover, Xiao *et al.* synthesized raisin-bread-shaped electrocatalysts composed of Fe sulfide ($Fe_{1-x}S$) and N, S-bidoped mesoporous graphite C spheres (N, S-MGCSs) via two-step pyrolysis and acid leaching[201]. This catalyst demonstrates high electrocatalytic activity for ORR in both alkaline and acidic media. Its activity is directly correlated with the content and distribution of Fe sulfide species. Notably, the electrocatalytic activity of $(Fe_{1-x}S/N, S\text{-}MGCS)_{0.2}$ surpasses that of the commercial Pt/C electrocatalyst in alkaline media. This superior catalytic performance can be attributed to the introduction of Fe sulfide nanocrystals into high-conductivity C carriers, which significantly enhances the reactivity of the catalytic active sites. Additionally, the raisin-bread-like structure improves the electron- and ion-transfer characteristics and also inhibits the self-aggregation and leaching of Fe sulfide species.

(iv) Transition-metal nitrides and oxynitrides: The synthesis of noble-metal nitrides has demonstrated that all transition metals can form nitrides[202]. These nitrides and oxynitrides possess high electrical conductivity and chemical resistance, making them attractive for various applications[203-206]. Nitride formation is particularly advantageous for modifying catalyst electronic structure, as it contracts the D-band of TMN and increases electron density near the Fermi level, giving TMNs electronic properties similar to noble metals[207]. This facilitates electron transfer to oxygen intermediates and accelerates ORR kinetics[208]. Non-noble TMNs have been reported as highly effective ORR electrocatalysts in alkaline media[208]. Air-exposed nitrides spontaneously form oxide shells several nanometers thick on conductive nitride cores, which serve as highly active catalytic structures. Among these, C-supported Co nitride (Co_3N/C) is the most active electrocatalyst, exhibiting a half-wave potential of 0.862 V and achieving a record peak power density of 700 $mW{\cdot}cm^{-2}$ in an alkaline membrane electrode assembly. However, operando X-ray absorption spectroscopy studies indicate that Co_3N/C remains stable below 1.0 V but undergoes irreversible oxidation at higher potentials. Bimetallic nitrides have also been extensively studied in this context. Tang *et al.* synthesized $Ti_{0.95}Co_{0.05}N$, a binary nitride electrocatalyst with a 3D structure that exhibits high activity and stability in ORR[209]. The 20%C-$Ti_{0.95}Co_{0.05}N$ catalyst shows comparable ORR performance to 20% Pt/C in alkaline media, with the $4e^-$ pathway dominating the reaction. The 3D structure of the catalyst provides a larger surface area and more exposed active sites, while the incorporation of Co induces a change in the

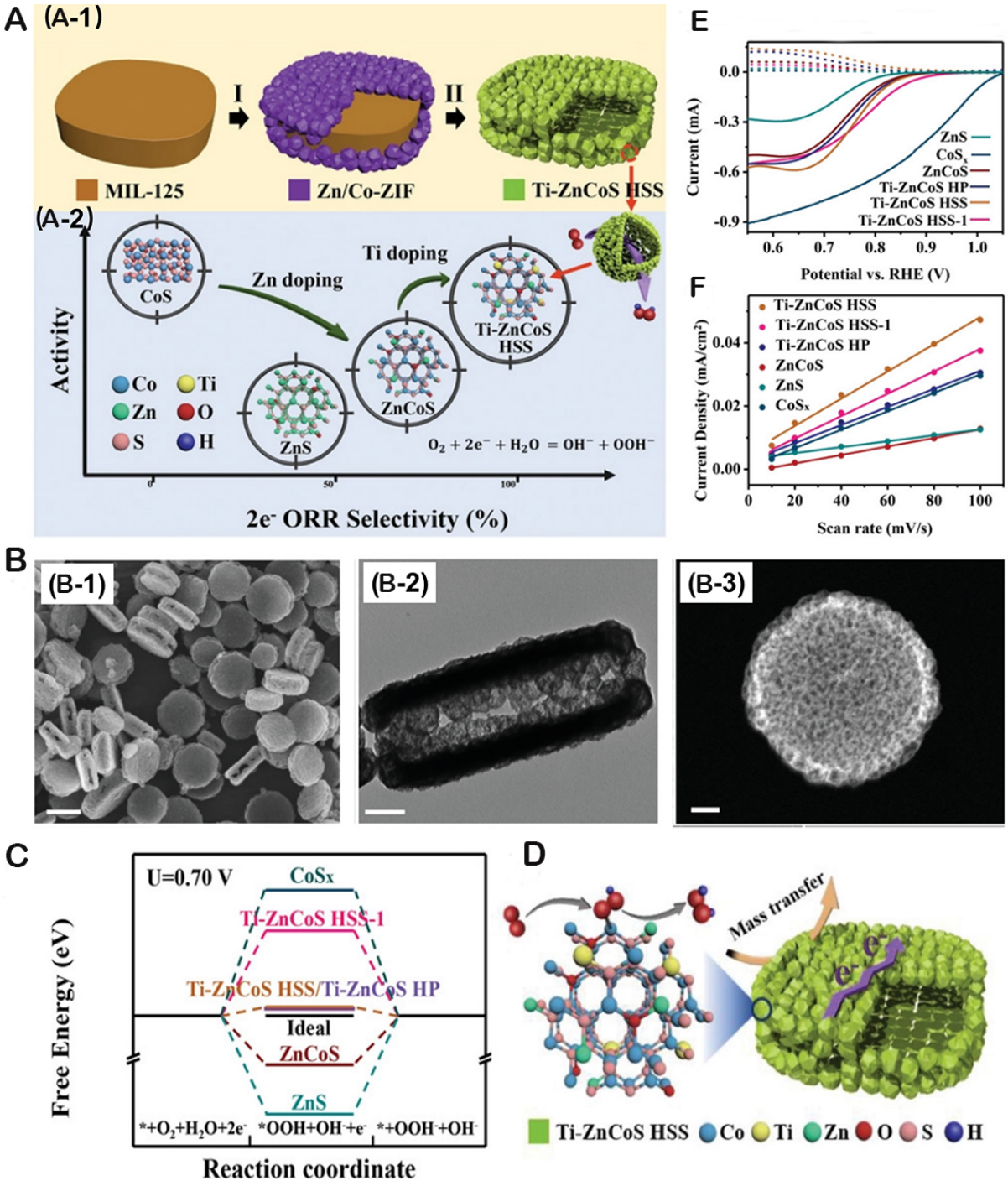

Figure 14. (A-1) A scheme of the two-step synthesis of Ti-ZnCoS HSS; (A-2) Illustration of the 2e-ORR activity-selectivity of CoSx, ZnS, ZnCoS, and Ti-ZnCoS HSS; (B) Characterization of Ti-ZnCoS HSS: (B-1) SEM, (B-2) TEM, and (B-3) HADDF-STEM; (C) Free-energy diagram for oxygen reduction to H_2O_2; (D) Schematic illustration for the 2e-ORR process of Ti-ZnCoS HSS catalyst; (E) LSV polarization curves; (F) CV current density *vs* scan rate; the linear slope is equivalent to the double-layer capacitance (C_{dl}). Reproduced with permission. Copyright 2022, Wiley Online Library[198].

electronic structure, increasing the intrinsic ORR activity of Ti nitride. Huang *et al.* demonstrated that VO_xN_y-CNTs electrocatalyst has high stability and catalytic activity in a KOH medium[210]. The porous structure facilitates full contact between the electrolyte, O_2, and electrocatalyst, while the formation of C-N

bonds increases overall conductivity and decreases overpotential. The ORR mainly follows the ideal $4e^-$ pathway, as shown by the Koutecky-Levich equation analysis. Bimetallic oxynitrides exhibit better catalytic performance than single-metal oxynitrides due to the synergy occurring on them[211]. Balamurugan *et al.* synthesized a new type of N-doped graphene ($CuMo_2ON$@NG) anchored by Cu molybdenum oxynitride using a pyrolysis method. The as-synthesized electrocatalyst exhibits trifunctional activity, the activity being higher than that of the benchmark Pt/C or IrO_2 electrocatalyst[212]. The outstanding catalytic activity of $CuMo_2ON$@NG is attributed to the synergistic electron transfer among the active $CuMo_2ON$ NPs, N-doped species, and graphitic C, as demonstrated by first-principles calculations. In the $CuMo_2ON$@NG nanohybrid, the RDS for achieving ORR activity is the creation of an O* intermediate on the $CuMo_2ON$ lattice. Several experimental investigations have indicated that adjusting the oxidation states of metals in the O-N phase can further improve the ORR activity, which has the potential to match or exceed that of Pt/C electrocatalysts.

(v) Transition-metal carbides: TMCs have been identified as potential substitutes for Pt group metals due to their high electrical conductivity[213,214]. However, their susceptibility to corrosion in acidic and oxidizing media can affect their catalytic stability. Among TMCs, TiC has received significant attention due to its high electrical conductivity and corrosion resistance[215]. Researchers have synthesized TiC/C nanofibers as ORR electrocatalysts via electrospinning[216], showing that the morphology, TiC content, and TiC-C interface of the nanofibers can be tuned by varying the preparation conditions. The TiC/C properties affect catalytic performance, with the Ti-CNFs/C samples exhibiting the best ORR performance, including an onset potential, peak potential, peak current density, and charge transfer number of 0.941 V *vs.* RHE, 0.812 V *vs.* RHE, 0.742 $mA \cdot cm^{-2}$, and 3.29, respectively. These samples also showed high catalytic durability and excellent methanol tolerance, demonstrating the potential of TiC/C nanofibers as ORR electrocatalysts. Recent studies have shown that N doping can improve the ORR performance of TiC and that the introduction of metals such as Fe and Co into TiC powder enhances its ORR performance[217]. One promising material for the ORR in alkaline environments is Fe-N-TiC. This material has been found to have the highest ORR activity among tested materials, with a reaction path of $4e^-$. N plays a role in both the formation of C-N active sites and changes to the electronic structure of the TiC surface, contributing to enhanced catalytic activity. Fe doping of Fe-N-TiC leads to further increases in ORR catalytic activity by forming Fe-N active sites. Additionally, C-based materials with Fe_3C particles have also demonstrated excellent ORR properties [Figure 15A-D]. For example, Chen *et al.* developed highly efficient electrocatalysts for the ORR in alkaline solutions by preparing N-doped C-coated Fe_3C NPs (NS) through the carbonization of Fe precursors loaded with polyacrylamide microspheres [Figure 15E-H][218]. The N-doped C and Fe_3C work synergistically as catalytically active sites, and the C shell effectively prevents leaching from the Fe_3C, resulting in excellent electrocatalytic performance. This highlights the potential for doping TMCs as a research direction for ORR electrocatalysts. In recent years, Fe carbide encapsulated in N-doped graphene (NG/Fe_3C) has emerged as a promising ORR catalyst. Patniboon *et al.* investigated the stability and catalytic activity of N-doped graphene supported on metal-Fe carbide (NG/M-Fe_3C) for the ORR using DFT calculations[219]. The NG/M-Fe_3C heterostructure was modeled by replacing Fe atoms near the NG/Fe_3C interface with metal alloy species "M" (M = Cr-Mn, Co-Zn, Nb-Mo, or Ta-W). The calculations showed that introducing M changes the work function of the N-doped graphene, which is correlated with the bond strength of the ORR intermediate. The introduction of Ni or Co atoms at the interface increases the ORR activity of NG/Fe_3C and stabilizes its heterostructure. Furthermore, increasing the concentration of Ni or Co atoms near the interface enhances the ORR activity, leading to the creation of stable heterostructures over a wide range of substitution concentrations. These findings provide approaches to improve the ORR activity of NG/Fe_3C electrocatalysts.

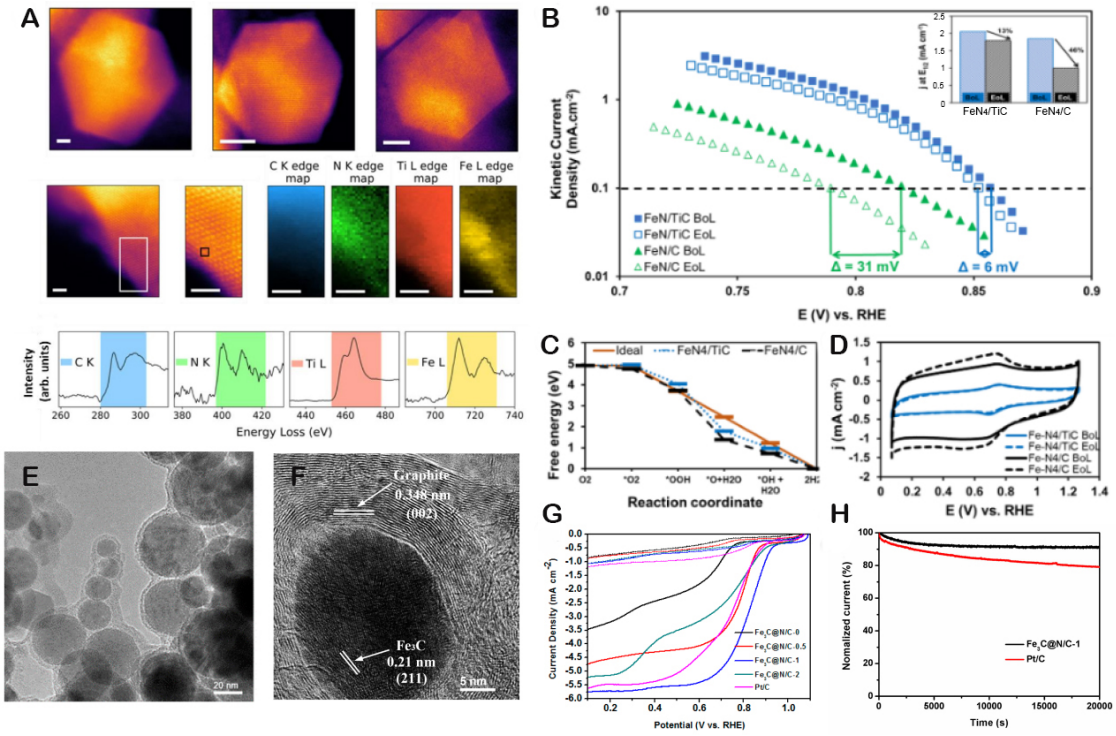

Figure 15. (A) STEM imaging and EELS spectra of FeN_4-TiC catalysts; (B) Kinetic currents extracted from linear sweep voltammograms of FeN_4-TiC and FeN_4-C catalysts at the beginning of life (BoL) and end of life (EoL); (C) DFT-calculated free energy diagram of FeN_4-TiC and FeN_4-C for ORR; (D) Cyclic voltammograms of the Fe-N-C and Fe-N-TiCcatalysts in their pristine state and after 1,000 cycles of the catalyst corrosion resistance stability protocol. Reproduced with permission. Copyright 2021, Chemistry Europe[216]; (E) TEM and (F) high-resolution TEM (HRTEM) image of Fe_3C@N/C-1; (G) Linear sweep voltammetry (LSV) curves; (H) Current-time chronoamperometric response of Fe_3C@N/C-1 catalyst and Pt/C. Reproduced with permission. Copyright 2019, MDPI[217].

OER/ORR bifunctional electrocatalysts

The ORR and OER are crucial half-reactions in energy conversion and storage systems, such as electrochemical water-splitting devices and fuel cells[220]. Thus, the development of efficient, durable, and low-cost bifunctional electrocatalysts based on earth-abundant elements is vital for the commercialization of H_2 production and utilization technologies. Such electrocatalysts would make the manufacturing of energy devices more accessible, facilitating the adoption of these new energy technologies.

Nonmetallic C-based electrocatalysts

In the field of electrocatalysts, C-based materials, such as CNTs, graphitic C nitride (g-C_3N_4), CB, graphene oxide (GO), and other metal-free C-based electrocatalysts, have shown great potential due to their high electrical conductivity and large specific surface areas. These materials promote electron transfer and mass diffusion during the electrocatalytic reaction[221,222]. Efficient and low-cost bifunctional electrocatalysts have also been developed using heteroatom-doped C materials. The introduction of heteroatoms, such as N, S, O, B, and P, can effectively adjust the charge or spin redistribution in the sp2 conjugated C matrix, leading to an increase in the bifunctional electrocatalytic activity for OER and ORR[127,223,224]. Based on research, Heteroatom-doped C materials mainly include three types: single-atom-doped, bidoped, and tridoped.

Single-atom doped: N-doped C materials have been extensively studied as electrocatalysts, with N-doped C nanomaterials being one of the earliest heteroatom-doped C materials investigated for this purpose[225,226]. In 2013, few-layer N-doped graphene materials synthesized by pyrolyzing a composite of GO and PANI were

found to have low OER activity, with a current density of less than 2.0 $mA{\cdot}cm^{-2}$ at an overpotential of 500 mV. Despite this, researchers have continued to explore this nanomaterial and have developed new methods for preparing N-doped C bifunctional electrocatalysts. For instance, Lu *et al.* used a two-step *in situ* growth method to create an air electrode using an N-doped CNT array coated with Co NPs on the surface of a C fiber cloth, resulting in a C-based electrode with high OER and ORR activities[227]. Murugesan *et al.* developed a low-cost C-based electrocatalyst by introducing highly porous C (HPC) from waste leaves[228]. To enhance its catalytic activity, HPC was subjected to treatment with urea ($CO(NH_2)_2$) and thiourea ($CS(NH_2)_2$) and doped with N and S. The OER and ORR activities of HPC, N-doped HPC, and S-doped HPC were investigated, with N-doped HPC displaying the highest bifunctional electrocatalytic activity. Moreover, Zhao *et al.* developed an electrochemically active interface to promote ORR/OER kinetics by coupling N-doped submicron C tubes (N-SMCTs) with N-doped rGO (N-rGO)[229]. The resulting N-SMCTs@N-rGO catalyst exhibited high bifunctional OER/ORR activity and durability, with an $E_{1/2}$ of 0.87 V for ORR and η_{10} of 351 mV for OER. DFT revealed a dual-site mechanism, with the C adjacent to the graphitic-N in N-SMCTs being the most active site for the OOH intermediate and the C neighboring the p-N in N-rGO being beneficial for the adsorption of O/OH* intermediates. The unique active interface with a dual-site mechanism demonstrates the potential of N-SMCTs@N-rGO to overcome the energy barrier bottleneck in traditional bifunctional electrocatalysts.

In addition to N, other types of heteroatom-doped C nanomaterials have been widely researched[230-232]. For example, Jiang *et al.* conducted a first-principles study of graphene and N-doped, B-doped, and codoped graphenes as potential electrocatalysts[233]. Among the studied samples, B-doped graphene has the lowest overpotential, which indicates that it is the best electrocatalyst for the OER and ORR. However, in the presence of Li atoms, N, B-codoping does not enhance the OER/ORR performance, suggesting that the synergy due to protons does not apply to this system. This behavior is attributed to the fact that the presence of Li atoms can change the most stable adsorption sites and the adsorption energies of the intermediates. To improve the catalytic performance of CNTs, Wang *et al.* synthesized B-doped CNTs (BC_3NTs) with different B content[234]. Raman spectroscopy revealed that the number of defects increased with increasing B content. The BC_3NT-based hybrid Li-air battery (HLAB) exhibits excellent cycling performance and catalytic performance in air, with an overpotential of 0.3 V for 200 h at a current density of 0.05 $mA{\cdot}cm^{-2}$. Furthermore, DFT-based theoretical calculations confirmed the effect of topological defects in BC_3NTs on the ORR and OER. BC_3NTs containing numerous defect rings were obtained owing to the doping of B into the CNTs. The defect generation is beneficial for battery reactions. Therefore, BC_3NTs are highly favorable cathode materials for the OER and ORR in HLABs, and the topological defect loops generated by them enhance the catalytic performances of the OER and ORR.

Moreover, P is a widely studied dopant[235]. Liu *et al.* developed efficient electrocatalysts for OER and ORR applications by modifying CDs with P and amidogen[236]. These modified CDs, synthesized from the same environmentally friendly C-based nanomaterial, exhibit similar electrocatalytic activities and higher stability compared to benchmark metal electrocatalysts. Amidogen-terminated CDs display slightly higher OER activity than IrO_2, while P-terminated CDs show ORR activity similar to that of Pt/C. Lei *et al.* synthesized large-scale 2D P-doped C nanosheets (2D-PPCNs) with tunable porosity, using P pentoxide and common carbohydrates in a stepwise multiple templating process for 2D construction, P doping, and regulated micro/mesoporous generation, as illustrated in Figure 16[237]. The impact of various porous structures on the electrocatalytic activity of 2D-PPCN-based electrocatalysts was studied. The interconnected open-pore system and large specific surface area resulted in high catalytic efficiency for both OER and ORR. This reliable technology for producing 2D porous C has the potential to be applied in various fields related to energy storage and conversion.

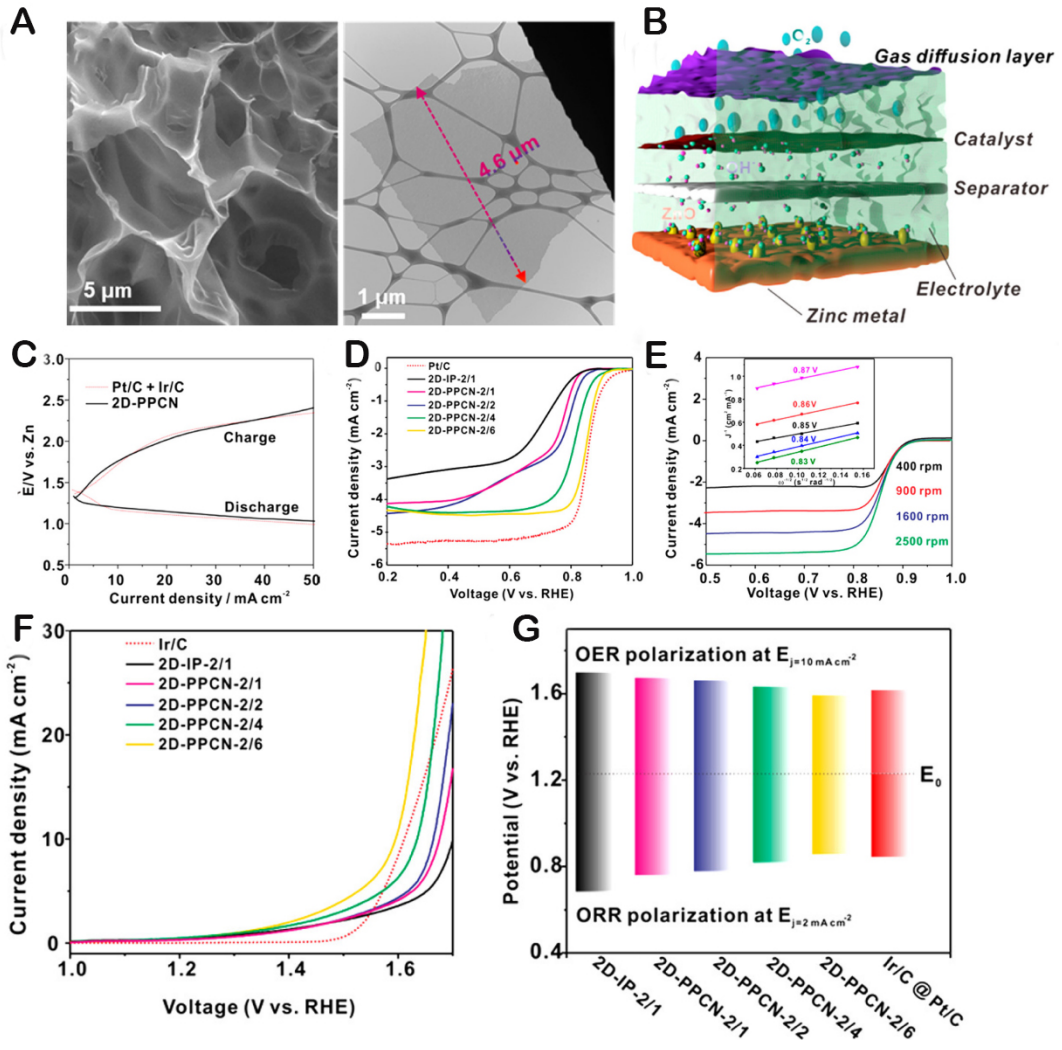

Figure 16. (A) SEM and TEM images of 2D-PPCN; (B) Schematic illustration of the zinc-air battery configuration; (C) Galvanodynamic charge/discharge polarization curves of 2D-PPCN and Pt/C+Ir/C based air electrode; (D) ORR activity at 1,600 rpm; (E) ORR polarization curves of 2D-PPCN-2/6 at various rotating speeds; (F) OER activity at 1,600 rpm; (G) Potential differences between the E_j = 2 of ORR and E_j = 10 of OER for all the catalysts. Reproduced with permission. Copyright 2018, ACS Publications[236].

Bidoped: Bidoping of C frameworks with two heteroatoms can produce a synergy, increasing the catalytic activity; hence, bidoping has become an increasingly popular method for optimizing the electrocatalytic activity. The electrocatalyst performance can be significantly improved via various types of doping, especially codoping of N with other heteroatoms such as B, P, and S[52,237-240]. In 2016, Qu *et al.* introduced an efficient and environmentally friendly method for incorporating S into C frameworks, resulting in the synthesis of N, S-codoped mesoporous C nanosheets that exhibited excellent performance, fast kinetics, and high durability as bifunctional OER and ORR electrocatalysts[238]. The study suggests that a combination of high concentrations of multiple dopants, abundant porous structures, and good electron transfer ability can significantly enhance the catalytic processes of OER and ORR.

Recently, Sun *et al.* found that the P-N bond is favorable for OER, and N dopants only affect ORR activity[241]. By tuning the heterogeneous atomic weights of C nanomaterials, they obtained high bifunctional OER/ORR activity. They synthesized the P, N-codoped graphene framework (PNGF) using GO and N/P-

containing organic precursors via a hydrothermal method, demonstrating its high OER/ORR bifunctional activity due to the presence of P-N-bond-rich oxygen electrocatalyst. The combined configuration of P and N was characterized by X-ray photoelectron spectroscopy, as shown in Figure 17A-C. The electrocatalyst was further optimized by adjusting the ammonium dihydrogen phosphate (ADP) concentration and adding an N source [PNGF(op)] during synthesis, resulting in the highest content of P-N bonds and p-N and exhibiting excellent electrocatalytic performance. PNGF(op) showed an ORR half-wave potential $E_{1/2}$ of 0.85 V, an OER overpotential E_{10} of 1.55 V, and a bifunctional potential difference of 0.70 V, outperforming Pt/C and Ir/C hybrid electrocatalysts, as shown in Figure 17D. The activity remained unchanged after 5,000 cycles, with stability higher than that of the Pt/C and Ir/C mixed electrocatalysts. Zhang *et al.* synthesized N, S-codoped graphene nanosheets (NSGs) using a one-step pyrolysis method with different N-containing precursors, namely 5-aminouracil (ANA), ammonium persulfate, and 2,5-dithiobisurea (DBA)[242]. The NSGs derived from ANA and DBA demonstrated exceptional bifunctional activity for OER and ORR, with a ΔE of 0.73 V. These NSGs were dominated by p-N and pyrrolic N dopants. The performance of NSG was validated in a rechargeable Zn-air battery (ZAB), yielding a peak power density of 146 $mW \cdot cm^{-2}$ and a specific capacity of 796 $mA \cdot h \cdot gZn^{-1}$. Notably, these values were higher than those achieved by the state-of-the-art Pt/C and IrO_2 (1:1 wt%) electrocatalyst for the same loading. These excellent properties were achieved by optimizing the OER or ORR intermediate energies through the configuration of S and different N species in the graphene nanosheets, depending on the specific S and N precursors used.

Tridoped: Codoping has been shown to introduce additional active sites into the C lattice, and researchers have proposed that adding more types of heteroatoms could further improve catalytic activity, leading to the development of tridoped C materials as bifunctional electrocatalysts[243-246]. For instance, N, S, P-tridoped graphene (NSP-Gra) exhibits a higher ORR onset potential (0.95 V *vs.* RHE) than binary N, S-codoped graphene and undoped graphene, approaching the performance of commercial Pt/C electrocatalysts[247]. This improvement in electrocatalytic performance is mainly attributed to local changes in the charge distribution and the abundant active sites generated by the heteroatom dopants. Li *et al.* synthesized a metal-free C bifunctional electrocatalyst (NFS-CNF) through direct pyrolysis electrospinning of PAN/polymeric ionic liquid nanofibers [Figure 18A][248]. The electrocatalyst exhibits uniform multiheteroatom (N, F, and S) doping and a large specific surface area (1,450.7 $m^2 \cdot g^{-1}$). As shown in Figure 18B-E, the NFS-CNF exhibits excellent catalytic performance and high durability, with the ORR and OER associated with a positive half-wave potential of 0.91 V and a low overpotential of 380 mV at a current density of 10 $mA \cdot cm^{-2}$, respectively, in an alkaline medium. Zheng *et al.* synthesized a piperazine-containing covalent triazine framework (P-CTF) using an ultrasonic-initiated route, in addition to N, F, S-tridoped C materials[249]. The polycondensation and assembly of monomers into a nanoflower-like morphology were initiated using ultrasonic energy without the use of a template. The subsequent carbonization of the P-CTF resulted in N, P, F-tridoped porous C (NPF@CNFs) with a well-retained nanoflower morphology [Figure 18F and G]. The resulting NPF@CNFs exhibited higher electrocatalytic activity and stability than commercial Pt/C and IrO_2 electrocatalysts for ORR and OER, respectively [Figure 18H-M]. In recent years, various heteroatom-doped C nanomaterials have been developed using specific tools and toxic precursors. For example, N, P, S-tridoped C NSs (NPSCteamSs) have been synthesized via polymer derivative groups, template etching, and secondary pyrolysis, endowing the NSs with hollow and mesoporous structures, numerous defects, large specific surface areas, and other advantageous properties, which make a great contribution to OER and ORR performance[250].

Transition-metal-C-based electrocatalysts

Although heteroatom-doped nonmetallic C catalytic nanomaterials have been proven as effective ORR/OER bifunctional electrocatalysts, they are prone to electrochemical corrosion under high potential

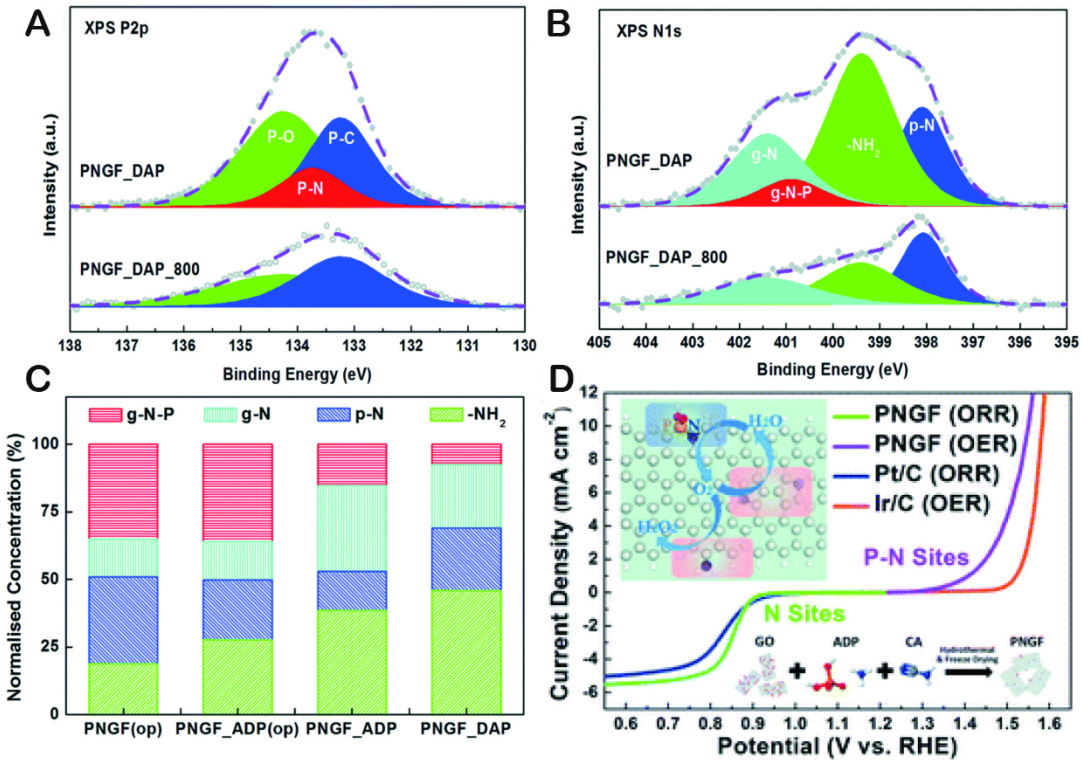

Figure 17. XPS (A) P2p and (B) N1s spectra for PNGF_DAP and PNGF_DAP_800; (C) Relative ratio of XPS N1s binding configurations for PNGF_DAP, PNGF_ADP, PNGF_ADP(op) and PNGF(op); (D) Bifunctional ORR/OER activities. Reproduced with permission. Copyright 2017, Royal Society of Chemistry[31].

conditions[251]. And their electrocatalytic activity is strictly limited. Therefore, researchers have found that hybrid electrocatalysts prepared by strongly coupling heteroatom-doped C and metal oxides can moderately solve the problem of low stability of C-based nanomaterials. Moreover, C-based nanomaterials can increase the conductivity and dispersibility of metal oxides[252,253].

(i) Transition-metal oxide/carbon composites: TMO/C composite can facilitate strong interfacial chemical interactions or electronic coupling between the two components, leading to increased OER and ORR activities[253-255]. In 2011, Liang *et al.* demonstrated that the excellent OER/ORR performance of Co_3O_4/N-graphene electrocatalyst was due to the formation of Co-N-C and Co-O-C bonds, proposing the concept of an interfacial chemical interaction between Co_3O_4 and N-doped graphene[256]. Since then, numerous efforts have focused on designing and developing metal oxide/C nanomaterials with different structures and compositions as bifunctional electrocatalysts[257-261]. For example, Li *et al.* prepared a unique bifunctional electrocatalyst using a one-dimensional bimetallic (Co, Mn) ZIF pyrolysis method. The resulting product is a fibrous material with surface-attached particles, referred to as $Co_3O_4/Mn_3O_4/CN_x$@CNFs, as shown in Figure 19A[262]. Strong coupling exists between the nanostructure and N-C bonds of each component in the material, resulting in a highly efficient catalytic performance for the ORR and OER [Figure 19B]. In particular, the ZAB assembled with $Co_3O_4/Mn_3O_4/CN_x$@CNFs demonstrated a high open-circuit voltage of 1.518 V, maximum power density of 265 mW·cm^{-2}, high cycling stability, and excellent mechanical flexibility. These properties surpass those of previously reported MOF-derived bifunctional electrocatalysts [Figure 19C]. Li *et al.* prepared a 3D flower-like composite electrocatalyst by hydrothermal synthesis, which contained $NiCo_2O_4$ and N-doped C derived from g-C_3N_4[263]. The resulting $NiCo_2O_4$-CN electrocatalyst had a hierarchical structure composed of interconnected nanosheets and exhibited multifunctional bifunctional

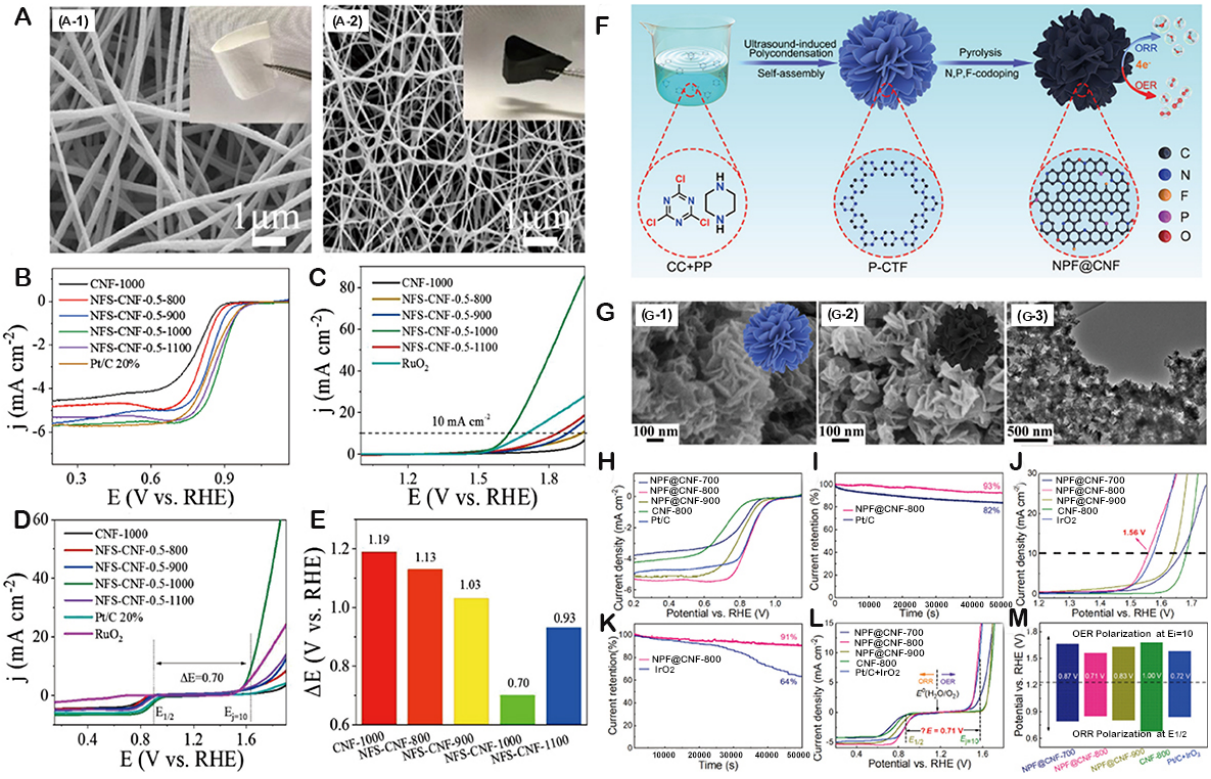

Figure 18. (A) SEM images of the (A-1) as-spun PDADMAFSI-PAN-PMMA-0.5 and (A-2) NFS-CNF-0.5-1000 nanofibers; (B) LSV curves of ORR at an RDE (1,600 rmp) in O_2-saturated 0.1 M KOH electrolyte; (C) LSV curves of OER without IR compensation; (D) LSV curves on a RDE (1,600 rpm) in 0.1 M KOH; (E) Potential gap (ΔE) between E_j=10 and $E_{1/2}$ for all the catalysts. Reproduced with permission. Copyright 2021, Elsevier[247]; (F) Procedures of Ultrasound-Triggered Assembly of P-CTF Nanoflowers for Synthesizing NPF@CNFs; (G) Characterization of P-CTF nanoflowers: (G-1) SEM image of P-CTF nanoflowers, (G-2) SEM, (G-3) TEM; (H) LSV curves in O_2-saturated 0.1 M KOH; (I) Chronoamperometric responses in O_2-saturated 0.1 M KOH; (J) OER polarization curves in 1 M KOH at 5 mV·s^{-1}; (K) Chronoamperometric responses in 1 M KOH; (L) LSV curves between the ORR and OER; (M) Potential differences between the OER current density at 10 mA·cm^{-2} and the $E_{1/2}$ of ORR. Reproduced with permission. Copyright 2021, ACS Publications[248].

electroactivity for OER and ORR. The half-wave potential for the ORR was 0.81 V, and the overpotential for the OER at a current density of 10 mA·cm^{-2} was 383 mV. The ZAB with a $NiCo_2O_4$-CN cathode demonstrated high performance, including a peak power density of 149.6 mW·cm^{-2} and a capacity of up to 738.7 mA·h·g^{-1}, along with exceptional durability. These results highlight the potential of $NiCo_2O_4$-CN for use in electrochemical energy devices.

(ii) Transition metal (or alloy)/C composites: Although TMOs are promising, they have not been developed for practical application because of their low electrical conductivity[264,265]. In comparison, transition metals and their alloys are expected to provide more advantages as bifunctional electrocatalysts due to their high electrical conductivities, in contrast to other materials[266,267]. Therefore, the combination of metals or their alloys with heteroatom-doped C affords another type of C composite, which is of great interest for bifunctional electrocatalysts[268]. An important type of electrocatalytic structure is the monometallic M-N/C, exemplified by Fe-N/C and Co-N/C[269-273]. Quantum chemical calculations indicate that the electronegativity of N (3.04) is considerably higher than that of C (2.55). Consequently, the introduction of doped N atoms can create active electrocatalytic sites due to their strong electron affinity. This, in turn, enhances the positive charge density of the adjacent C atoms[274-276].

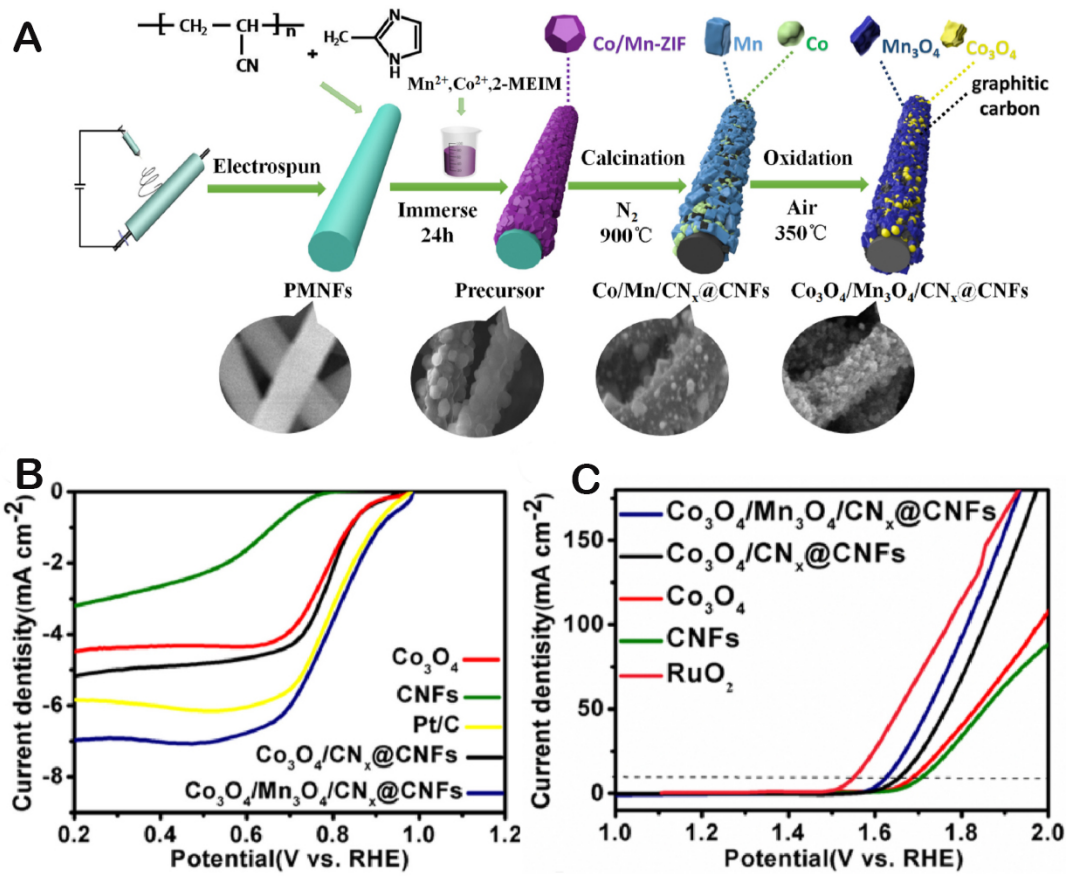

Figure 19. (A) Schematic illustration of the preparation process of Co_3O_4, Mn_3O_4 and CN_x supported on 1D carbon nanofibers (Co_3O_4/Mn_3O_4/CN_x@CNFs); (B) LSV curves of Co_3O_4, CNFs, Co_3O_4/CN_x@CNFs, Co_3O_4/Mn_3O_4/CN_x@CNFs and Pt/C for ORR; (C) LSV curves of RuO_2, CNFs, Co_3O_4, Co_3O_4/CN_x@CNFs and Co_3O_4/Mn_3O_4/CN_x@CNFs for OER in 1 M KOH at 1,600 rpm. Reproduced with permission. Copyright 2020, Elsevier[261].

For instance, Zhong *et al.* developed a single-atom Fe-N-C electrocatalyst by *in situ* carbonizing wood porous C after a simple Lewis acid pretreatment[275]. The pretreatment of wood cell walls with $FeCl_3$ not only created numerous microchannels but also introduced atomically dispersed Fe-N reactive species into the hierarchical structures. The resulting electrocatalyst, consisting of uniformly dispersed SACs on a layered structure, exhibited enhanced performance and durability for OER and ORR. Recently, Wang *et al.* developed a NaCl-template-assisted strategy for 3D honeycomb N-doped C substrates to integrate nanoscale Co species, resulting in 3D Co/N-C bifunctional, highly active OER and ORR electrocatalysts, as shown in Figure 20A-F[272]. The results demonstrated that 3D Co/N-C exhibits a positive half-wave potential of 0.84 V (*vs.* RHE) for ORR and a low overpotential of 1.56 V (*vs.* RHE) at a current density of 10 $mA{\cdot}cm^{-2}$ for OER. Tang *et al.* utilized the inherent structural defects of nanocarbons to fabricate Co/N/O ternary doped graphene meshes with single-atom dispersed Co-N_x-C active sites[277]. The electrocatalyst Co-NGM-Co possesses desirable bifunctional activities for OER and ORR in alkaline media, owing to the presence of Co-N_x-C sites, N dopants, oxygen functional groups, and topological defects. Upon assembly into a flexible solid-state ZAB, it demonstrates a high open-circuit voltage of 1.44 V, a small charge-discharge potential difference of 0.7 V at 1.0 $mA{\cdot}cm^{-2}$, and a high energy efficiency of 63% at the same current density [Figure 20G-M]. These results suggest that defect engineering is an effective and innovative strategy for developing high-performance M-N-C nanomaterials.

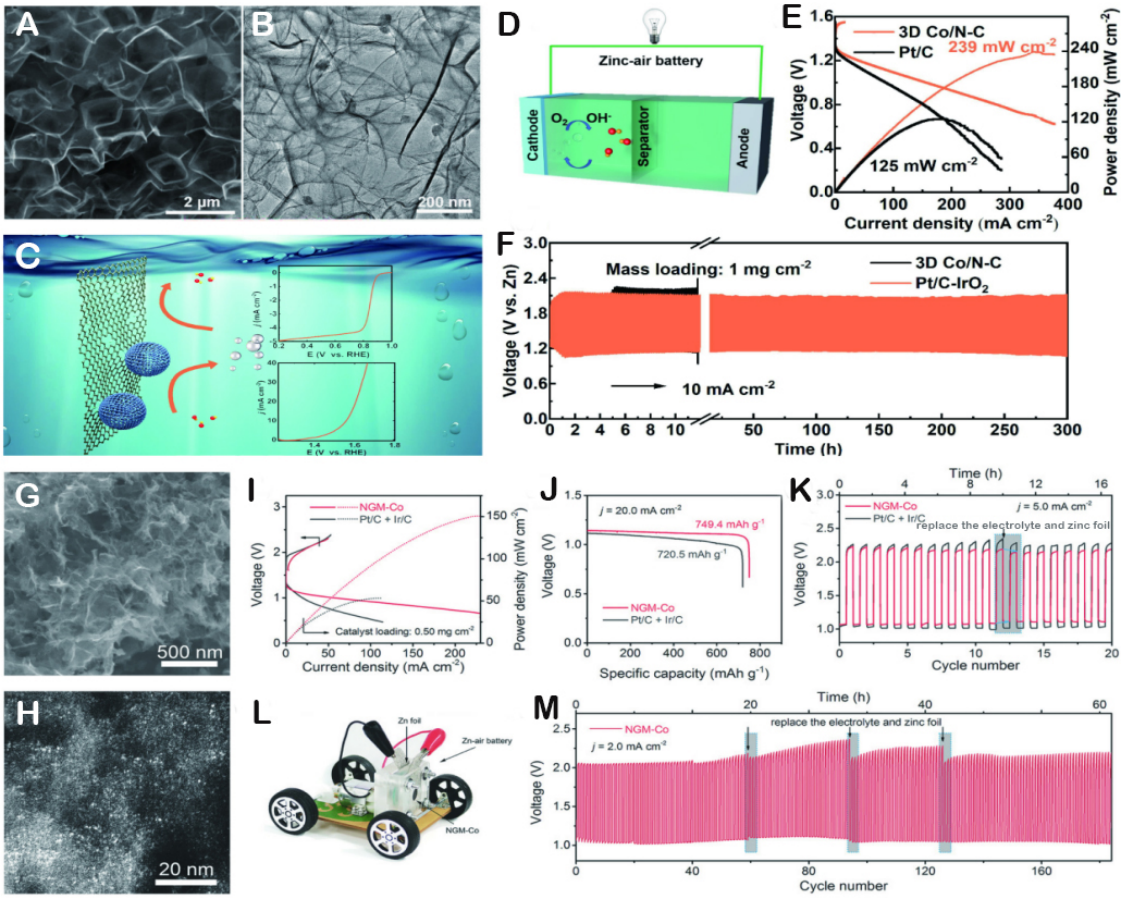

Figure 20. Morphology characterization of 3D Co/N-C. (A) SEM; (B) TEM; (C) Graphical abstract;(D) Schematic diagram of an aqueous zinc-air battery; (E) Discharge polarization lines of 3D Co/N-C and 20% Pt/C based air electrodes for the rechargeable ZABs and the correspondent power density curves of ZABs; (F) Galvanostatic discharging plots at a current density of 10 mA·cm^{-2} of 3D Co/N-C and 20% Pt/C + IrO_2. Reproduced with permission. Copyright 2022, Elsevier[271];Morphology and composition characterization of NGM-Co catalysts. (G) SEM; (H) Dark-field high-resolution TEM image; (I) Charge and discharge polarization curves of the NGM-Co and Pt/C + Ir/C catalysts; (J) Galvanostatic discharge-charge cycling curves at 5.0 mA·cm^{-2} of the rechargeable Zn-air batteries with the NGM-Co or Pt/C + Ir/C catalysts; (K) Discharge curves of Zn-air batteries assembled from the NGM-Co and Pt/C + Ir/C catalysts at 20.0 mA·cm^{-2} discharging rate; (L) Photograph of a toy car powered by one Zn-air battery based on NGM-Co catalyst; (M) Long time cycling test at 2.0 mA·cm^{-2}.Reproduced with permission. Copyright 2017, Wiley Online Library[276].

In addition, the catalytic activity of an electrocatalyst depends on its electrical conductivity; the higher the conductivity, the higher the ORR/OER activity. The bonding between two transition metals of dissimilar types can create intrinsic polarity, resulting in a unique reaction pathway that exhibits higher activity than their homometallic counterparts[278,279]. Many researchers have explored NiCo NPs anchored on C-based materials. For example, Yu *et al.* demonstrated the excellent bifunctional ORR/OER performance of a B, N-codoped C nanosheet network (BNC) encapsulating Ni-Co alloy NPs (NiCo@BNC)[280]. The potential difference between $E_{ORR1/2}$ and E_{OER10} is remarkably small, measuring only 0.61 V. This value exceeds those reported for most C nanosheets decorated with either monometallic or bimetallic alloys. The exceptional performance of the electrocatalyst can be attributed to the unique role played by NiCo, which not only protects the nanosheets from destruction but also facilitates *in situ* B, N-codoping, thereby exposing numerous active sites. Moreover, the synthesis of many-layer BNC-shell-encapsulated NiCo alloys with high electrocatalytic activity and electrical conductivity further enhances the catalytic process.

Similar findings were reported for other synergistic electrocatalysts, such as FeCo/C[281-284] and NiFe/C[78,285]. For example, Liu *et al.* employed a micro-mesopore confinement technique to produce ultrasmall FeCo bimetallic alloy NPs with a size of less than 4 nm[281]. These NPs were anchored on biomass-treated porous N-C, which was synthesized using peanut shells as precursors. The synergy between the FeCo alloy NPs and N-C resulted in the formation of FeCo-NC, which exhibited high bifunctional activity for OER and ORR in alkaline media. When utilized in ZABs, the hybrid electrocatalyst showed remarkable stability even after 1,400 cycles. At a current density of 10 $mA·cm^{-2}$, the ZABs delivered an ultrahigh energy density of 922 $W·h·kg^{-1}$. Jing *et al.* utilized waste biomass (pomelo peel, PP) as a raw material to synthesize NiFe-PBAs on its surface for *in-situ* growth[284]. The resulting material, NiFe@NC/PPC (carbonized PP), was obtained by carbonization and used as a 3D binder-free and free-standing cathode in Li-O_2 batteries. NiFe@NC/PPC possesses superior features compared to PPC and NiFe@NC/CP (NiFe@NC coated on C paper), including effective diffusion rate at the O_2/electrolyte interface and high catalytic activity for the OER/ORR. A Li-O_2 battery with NiFe@NC/PPC as the cathode exhibits a high specific capacity of 13.79 $mA·h·cm^{-2}$ and a long cycle life of 290 cycles at a current density of 0.1 $mA·cm^{-2}$. Zhong *et al.* combined FeM (M=Ni, Co) particles with NPC to create FeM/NPC[285]. The resulting material demonstrated high bifunctional activity and stability toward ORR ($E_{1/2}$ of FeCo and FeNi is 0.78 V and 0.73 V, respectively) and OER (η_{10} of FeCo and FeNi is 0.46 V and 0.5 V, respectively). This was attributed to the synergy between FeM and NPC, which provided a high electrical conductivity, N doping, porous structure, and close contact between the two components. In addition to bimetallic alloys, trimetallic alloy electrocatalysts exhibit high bifunctional activity[286]. Liu *et al.* synthesized FeCoNi nanoalloys embedded in a hierarchical N-C matrix (FeCoNi@HNC), which functioned as efficient and durable electrocatalysts for the OER and ORR in alkaline media[287]. The core-shell structure of FeCoNi@HNC was found to be highly beneficial for regulating the adsorption/desorption of oxygen intermediates on the N-rich C shell through electron penetration effects, leading to higher ORR activity than Pt/C and higher OER activity than IrO_2, as demonstrated by both experimental studies and DFT calculations. Additionally, the N-rich C shell acted as a barrier, preventing excessive oxidation and dissolution of the FeCoNi alloy NPs, thereby providing high stability in alkaline electrolytes. Prototype ZABs constructed using FeCoNi@HNCs exhibited a maximum power density of 109 $mW·cm^{-2}$ without a significant increase in the voltage gap, outperforming batteries fabricated using Pt/C and IrO_2/C electrocatalysts in terms of battery performance.

Recently, synergistic combinations of transition-metal sulfides, phosphides, and C-based materials have been proposed to improve the bifunctional electrocatalytic performance[288-290]. Gong *et al.* prepared Co_2P/CoP hybrid NPs (Co_2P/CoP@NPGC) embedded on the surface of core-shell MOFs by direct pyrolysis of P-containing MOFs precursor[291]. Liu *et al.* developed a hierarchical nanostructure, CoP-HNTs@NCL, which is composed of 1D hollow CoP nanotubes surrounded by a N-doped C layer[292]. The thickness of the NCL coating on the outer surface of the hollow CoP-HNTs is 5-8 nm. The superior OER/ORR activity and stability of CoP-HNTs@NCL-0.4 can be attributed to the synergistic effect between CoP and NCL. This enhances mass transfer through the 1D hollow structures and increases the exposure of active sites on both the inner and outer surfaces of the nanotube walls. Moreover, Tiwari *et al.* synthesized an advanced bifunctional electrocatalyst by combining W disulfide (WS_2) with CNTs using a W carbide (WC) catalyst[293]. The resulting electrocatalyst utilizes the catalytically active sites provided by the WS_2 flakes on the CNT surface, while the CNTs act as conduction channels to provide a large surface area for oxygen transport. Additionally, the newly formed WC crystal structure facilitates spin-coupled electron transfer, increasing both the stability and electrocatalytic activity of the material. Liu *et al.* prepared S-$Co_{9-x}Fe_xS_8$@rGO, a hybrid of $Co_{9-x}Fe_xS_8$/Co, Fe-N-C, by semivulcanization and calcination of GO-wrapped bimetallic CoFe-ZIF precursors[294]. As shown in Figure 21A-E, owing to the synergy between the CoFeS and Co components, high dispersity, and high conductivity, the obtained S-$Co_{9-x}Fe_xS_8$@rGO-10 electrocatalyst shows an ultrasmall overpotential of ~0.29 V at a current density of 10 $mA·cm^{-2}$ for OER and a half-wave

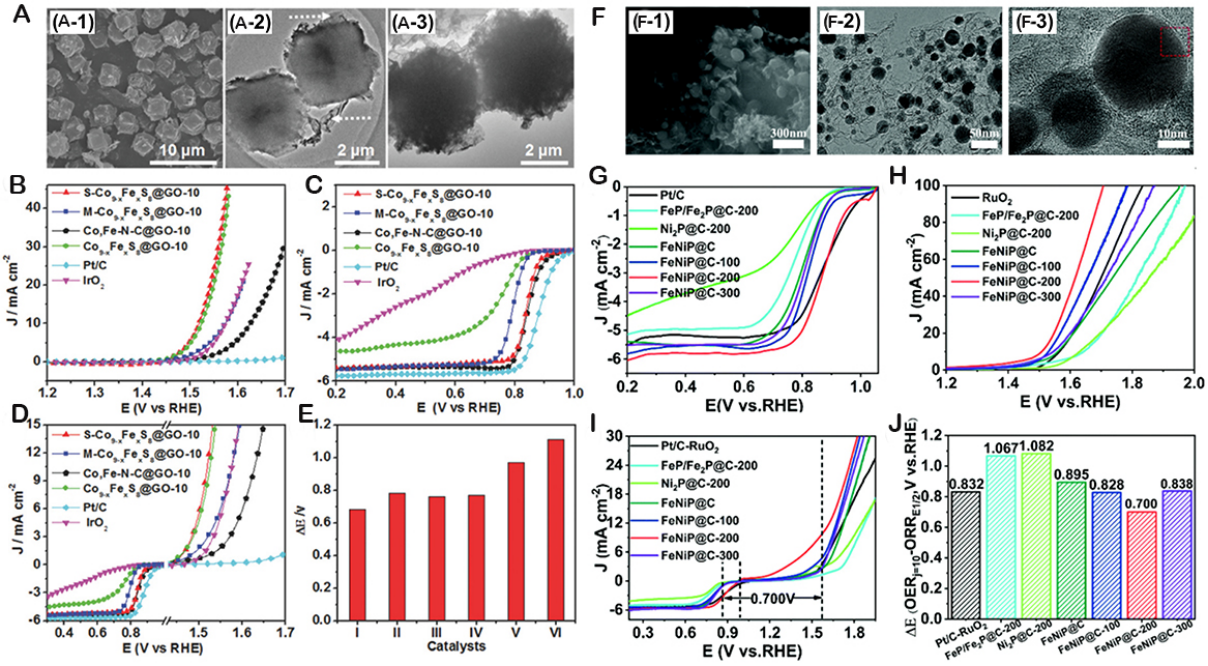

Figure 21. (A) Characterization of CoFe-ZIF@GO-10 and S-$Co_{9-x}Fe_xS_8$@rGO-10: (A-1) SEM image of CoFe-ZIF, (A-2) TEM image of CoFe-ZIF@GO-10, and (A-3) TEM image of S-$Co_{9-x}Fe_xS_8$@rGO-10; LSV curves of (B) OER, (C) ORR, (D) the overall polarization in ORR and OER region, and (E) the ΔE of S-$Co_{9-x}Fe_xS_8$@rGO-10 (I), M-$Co_{9-x}Fe_xS_8$@rGO-10 (II), Co,Fe-N-C@rGO-10 (III), $Co_{9-x}Fe_xS_8$@rGO-10 (IV), Pt/C (V), and IrO_2 (VI) in 0.1 m KOH. Reproduced with permission. Copyright 2018, Wiley Online Library[293]; (F) Characterization of FeNiP@C-200: (F-1) SEM, (F-2) TEM and (F-3) HRTEM images; (G) LSV curves of various catalysts at 1,600 rpm; (H) OER polarization curves of various catalysts at 1,600 rpm tested in 1 M KOH solution with a scan rate of 10 $mV{\cdot}s^{-1}$; (I) OER-ORR polarization curves tested in 0.1 M KOH solution; (J) ΔE ($OER_{j=10}$ - $ORR_{E=1/2}$) in 0.1 M KOH solution. Reproduced with permission. Copyright 2021, Royal Society of Chemistry[189].

potential of 0.84 V for ORR, exhibiting high oxygen electrode activity of ~0.68 V in 0.1 M KOH. Bimetallic phosphides have also been studied. Chen *et al.* prepared a novel structured bimetallic phosphide FeNiP-NP-embedded composite electrocatalyst in an N, P-bidoped C matrix[189]. It is a trifunctional electrocatalyst that can efficiently catalyze the HER, OER, and ORR. The introduction of oleylamine during the preparation process can tune the catalytic sites, resulting in the desired catalytic performance. The electrocatalyst obtained in this study demonstrates superior ORR catalytic performance in comparison to commercial Pt/C electrocatalysts, as depicted in Figure 21F-J. Additionally, its OER performance is comparable to that of RuO_2. Furthermore, the electrocatalyst exhibits exceptional HER performance. In a 0.1 M KOH solution, the ORR half-wave potential measures 0.879 V (*vs.* RHE). Conversely, the OER overpotential at a current density of 10 $mA{\cdot}cm^{-2}$ is 280 mV. The potential difference between the ORR and OER is only 0.700 V. This study establishes the groundwork for amalgamating composite electrocatalysts with bimetallic phosphides and hybrid C substrates, enabling the advancement of high-performance multifunctional electrocatalysts and their utilization in energy devices.

CONCLUSIONS AND OUTLOOK

The electrochemical OER and ORR are the core half-reactions in electrochemical water-splitting devices and regenerative fuel cells. The development of efficient non-noble-metal-based multifunctional electrocatalysts in the same electrolyte to simplify these energy devices remains a challenge. Here, we focus on the research progress in some OER/ORR electrocatalysts, such as noble- and non-noble-metal catalysts for OER (e.g., electrocatalysts based on Ru and Ir, C, and transition-metal compounds), noble-metal and non-noble-metal catalysts for ORR (e.g., electrocatalysts based on Pt, M-N-C, and TMPs), and bifunctional

catalysts (e.g., heteroatom-doped C-based materials and transition-metal-oxide/C composites). As described in the research advances, nonprecious metal, transition-metal, and nonmetallic OER and ORR electrocatalysts have been studied extensively, and they exhibit high activities, with the monofunctional activities reaching or even exceeding those of noble-metal benchmarking electrocatalysts. However, research findings indicate that certain problems are associated with such electrocatalysts:

(i) Catalytic mechanism

The micro/nano analysis limitations make it difficult to accurately comprehend the evolution mechanism of OER/ORR electrocatalysts and their corresponding mechanisms. Moreover, a fundamental understanding of some enhancement mechanisms for structural design and surface engineering in catalytic ORR/OER processes is still lacking. Heterogeneous interface characterization often concentrates on the pre-electrocatalytic state. Therefore, future studies should utilize more advanced *in situ* characterization techniques such as Transmission electron microscope (TEM), X-ray Diffraction/neutron diffraction (XRD/ND), Raman, Fourier transform infra-red (FTIR), thermogravimetric mass spectrometry (MS/TGA), X-ray absorption fine structure (XAFS), *etc*., in combination with theoretical calculations such as DFT to monitor the dynamic processes of electrocatalysts. Such an approach would yield a more comprehensive understanding of the related reaction mechanism and performance enhancement mechanism. Furthermore, the atomic-level mechanism of OER/ORR depends on the relationship between the adsorption energy of oxygen-containing intermediates and the electronic structure of electrocatalysts[295]. Greater efforts are still needed in the future to gain a deeper understanding of this mechanism.

(ii) Theoretical calculation

Undoubtedly, modeling techniques play a significant role in electrocatalyst design and activity analysis. DFT calculations based on 2D-graphene models are the basis for most electrochemical performance simulations of single-atom electrocatalysts using C-based materials[296]. Computational techniques are a powerful tool that can provide proof-of-concept patterns to verify synthesis feasibility and yield trends in electrocatalyst optimization. For example, the spin-polarized DFT calculation can accurately reflect most of the thermodynamic characteristics of the reaction of magnetic materials and describe the spin-related catalytic phenomena. Moreover, the spin polarization DFT calculation can also simulate and illustrate the spin channel by optimizing the spin structure of the electrocatalyst so as to qualitatively evaluate the electron transfer ability[297]. So far, the catalytic mechanism and the active site of ORR/OER on bifunctional electrocatalysts have not been well revealed. DFT calculations are increasingly used in such studies to gain insight into the catalytic mechanism and active site prediction. In general, based on the experimental results, theoretical calculations can simulate the OER/ORR reaction intermediates and the corresponding Gibbs free energy, calculate the active site on the material surface and finally obtain a model that corroborates the experiment[298,299]. Therefore, researchers have attempted to combine machine learning with theoretical calculations to guide the development of materials and have achieved some good results[230-302]. However, since calculations are usually "surface static", and the complexity of the surface of bifunctional electrocatalysts cannot be constructed in computational models, there is still a long way to fully elucidate the active centers and some important mechanisms[303]. Therefore, new methods suitable for revealing the active site and mechanism need to be developed. Based on more advanced modeling techniques, it will be possible to design oxygen electrocatalysts with different functions reasonably.

(iii) Construction and modification engineering (to improve exposed active sites, defective sites, and synergistic effects)

The structural engineering of OER/ORR electrocatalysts can effectively increase the specific surface area and expose more active sites, which is helpful in improving the utilization of active sites. To improve microstructural engineering strategies, we must overcome challenges such as dopant condensation and corrosion that arise from heteroatom doping and defect generation[304,305]. One approach is to explore different types and amounts of element doping to create stable functional groups as active centers. Surface engineering can also control the type and number of defects, enabling the creation of defect-rich electrocatalysts with optimal performance. Additionally, optimizing the distribution of defects and phases through lattice strain and phase transition can indirectly enhance catalyst activity and stability. While defects have been shown to improve electrocatalyst performance, creating effective defects in C nanomaterials remains a challenge. Furthermore, nanomaterials are an important research topic in electrocatalysts. On the one hand, nanomaterials can improve the active site of the catalyst and possess high surface energy, which is beneficial for enhancing catalytic efficiency. On the other hand, it is worth noting that the uneven surface composition, unclear crystal surface phases, and exposed nanocomponent surfaces make it difficult to extract intrinsic activity and stability trends. Achieving good defect control in C-based porous nanomaterials can be accomplished through rational design and development with precise control of the C micro/nanostructure. To further enhance electrocatalyst activity, the synergistic effects of multiple components should be explored. This approach combines the properties of different components to create active sites with specific structures[306]. Strategies to improve the activity of bifunctional electrocatalysts can focus on increasing intrinsic activity and apparent activity. Changing the crystal and electronic structure can increase intrinsic activity while modifying the morphology of nanostructures and utilizing synergistic effects can significantly improve apparent activity. More and more nanomaterials designed by considering micro and nanostructures have become bifunctional electrocatalysts.

(iv) structure-activity relationship

When considering new regulatory strategies for divergence, it is important to also examine the similarities among different strategies. Specifically, we should explore the relationship between chemical configuration, electronic structure, and intrinsic electrocatalytic activity. One effective approach for establishing this relationship is the use of descriptors[307]. However, determining the active contribution of the active site to the overall catalytic reaction can be challenging, particularly in the surface layer of heterogeneous electrocatalysts. There are often significant phase transitions that occur during operation, particularly at high anodic oxidation potential of OER. As a result, it can be difficult to distinguish the active site from other components of the catalyst[308]. To establish a truly meaningful structure-activity relationship, it is imperative to conduct *in-situ* and operational studies of working electrocatalysts using techniques such as Raman spectroscopy, XRD, and TEM, *etc*. In-depth research on the intrinsic factors that affect material properties could be conducted through the use of *in-situ* technology. This innovative technology provides instantaneous reaction data in real-time, with characteristics such as dynamic, intuitive, and highly sensitive. For catalyst materials, *in-situ* Raman technology could be utilized to identify the molecular structure, chemical bonding, and other chemical information of substances for qualitative analysis and quantitative detection. *In-situ* TEM offers the ability to directly observe the microstructure evolution of samples at the atomic level under the influence of force, heat, electricity, magnetism, and chemical reactions. Moreover, *in-situ* XRD technology could provide real-time information on structural phase changes during material reactions, particularly for electrode materials. By utilizing *in-situ* XRD, researchers can gain a deeper understanding of the reactions that occur during the charging and discharging process of materials. In turn, these technologies also could provide important guidance for improving materials, which could introduce descriptor methods to rationalize the OER and ORR performance of different electrocatalysts. Moreover, for heterogeneous electrocatalysts, the active sites are not homogeneous in

nature, and the combination of theoretical analysis and experimental support is beneficial to elucidate the interfacial effects[309]. However, to narrow the divide between the theoretical model and the practical electrocatalyst, it is necessary to establish a well-defined model system that can be used for theoretical calculations. This will help in bridging the gap in the structure-performance relationship.

(v) Construction of single-atomic catalysts (SACs) and diatomic catalysts (DACs)

There are emerging strategies and synthetic approaches that can precisely modulate the active sites of SACs in a reliable manner. However, although many types of SACs active sites have been predicted to have excellent catalytic activity for OER and ORR through DFT calculations, they have not yet been verified experimentally. Furthermore, only a small fraction of the current SACs may possess the desired configuration for these reactions. To enhance the intrinsic activity and durability of OER/ORR, constructing SACs using binary or polymetallic materials is a feasible strategy[308]. The OER and ORR properties of SACs are limited due to the linear scaling relationship between the adsorption energies of the reaction intermediates. The relationship between adjacent (or even different) metal atoms can sometimes result in synergistic effects that break down their effectiveness. To avoid this, it is recommended to actively explore binary and ternary SACs when searching for high-performance electrocatalysts for OER, ORR, and bifunctional ORR/OER. While SACs can significantly enhance catalyst performance, the preparation of highly dispersed SACs with high metal loading remains a key challenge. This is due to the inevitable agglomeration of metal atoms during synthesis and the limitation of low metal loading. Increasing the metal doping content by rationally designing hierarchical porous structures with appropriate pore size distribution may be an effective way to solve this problem, which can also provide good mass/electron transport. The emergence of Dual-metal-atom catalysts (DACs) has resulted in an elevated density of active sites and catalytic properties. This is owing to the synergistic interaction between different metal atoms. However, DACs are more susceptible to aggregation or alloying, which poses a significant challenge. Additionally, accurately determining the metal proportion and active sites in DACs is a daunting task, which further restricts the exploitation of synergistic effects between different metal atoms. Consequently, it is essential to develop robust metal-support interactions and more efficient synthesis techniques to prevent agglomeration. These strategies are crucial for the advancement of both Single Atom Catalysts (SACs) and DACs. In addition, multi-doping (e.g., N, P codoping; N, S codoping) and mixing of two metal atoms (such as Fe, Ni alloy) should be more advantageous for the two active centers of OER and ORR in bifunctional electrocatalysts. Therefore, designing SACs to maximize the efficiency of atom utilization will be the focus of future research on bifunctional catalysts.

Several unique applications require OER/ORR bifunctional electrocatalysts, including electrochemical water-splitting devices and fuel cells. Based on the overall reaction, OER and ORR appear to be reversible, but their energy curves are completely different; therefore, the required electrocatalysts are also different. Even for the same electrocatalysts, the potential active sites of OER and ORR have been reported inconsistently in some literature[310]. The potential "synergistic effect" and even "inhibitory effect" between different active sites should be carefully considered. Few single sites are suitable for both OER and ORR due to differences in active sites and reaction mechanisms. In order to meet the requirements of bifunctional electrocatalysts, the synergistic effect between the active centers of OER and ORR should be fully considered in the design of bifunctional electrocatalysts, and the mechanical integration of different catalytic functions into a single electrocatalyst should be avoided. It is necessary to combine the catalytic properties of OER and ORR to develop new synthesis strategies to meet the bifunctional requirements. In addition, attention should be paid to the synergistic interaction between the electrocatalyst components, and to understand the electron transport and cooperation between them, so as to promote the bifunctional catalytic performance.

On the one hand, a simple combination of compatible OER and ORR electrocatalysts is promising. On the other hand, designing common active sites for OER and ORR, the "true bifunctional active site," is both attractive and challenging. It is worth noting that recent researchers have also provided a data-driven method through machine learning and other means to capture the complex relationships of multidimensional factors, which is conducive to the development of new materials. At the same time, this technology has guidance rather than certainty, so researchers should not overly rely on machine learning and other technologies, although it could help reduce the research and development cycle of materials. Finally, the long-term stability of the OER/ORR electrocatalyst under practical conditions (oxygen bifunctional) requires further investigation. Most researchers have studied the stability of OER and ORR electrocatalysts separately, so it is necessary to perform practical stability tests under continuous ORR/OER bifunctional conditions. Therefore, the source of bifunctional catalytic activity of OER/ORR electrocatalyst and its mechanism of inactivation and toxicity must be studied and determined.

DECLARATIONS

Authors' contributions

Conceived the manuscript: Chen X, Chen Y
Wrote the manuscript: Chen X, Zhang Z
Reviewed the manuscript: Chen Y, Gao X, Yuan T, Wang N, Cui L
Contributed to the discussion of the manuscript: Chen X, Song C, Tang W, Xu R, Cui L

Availability of data and materials

Not applicable.

Financial support and sponsorship

This work was financially supported by the National Natural Science Foundation of China (Grant No. 21804008, 52102209), the International Technological Collaboration Project of Shanghai (Grant No. 17520710300), Anhui Provincial Natural Science Foundation (Grant No. 2108085QE197), Guangdong Basic and Applied Basic Research Foundation (Grant No. 2022A1515010834, 2020A1515110221), and Shanghai Post-Doctoral Excellence Program (Grant No. 2022293).

Conflicts of interest

All authors declared that there are no conflicts of interest.

Ethical approval and consent to participate

Not applicable.

Consent for publication

Not applicable.

REFERENCES

1. Jiang Y, Lu Y. Designing transition-metal-boride-based electrocatalysts for applications in electrochemical water splitting. *Nanoscale* 2020;12:9327-51. DOI PubMed
2. Chinapang P, Iwami H, Enomoto T, Akai T, Kondo M, Masaoka S. Dirhodium-based supramolecular framework catalyst for visible-light-driven hydrogen evolution. *Inorg Chem* 2021;60:12634-43. DOI PubMed
3. Tang J, Su C, Zhong Y, Shao Z. Oxide-based precious metal-free electrocatalysts for anion exchange membrane fuel cells: from material design to cell applications. *J Mater Chem A* 2021;9:3151-79. DOI

4. Chen L, Msigwa G, Yang M, et al. Strategies to achieve a carbon neutral society: a review. *Environ Chem Lett* 2022;20:2277-310. DOI PubMed PMC
5. Gonçalves JM, Martins PR, Araki K, Angnes L. Recent progress in water splitting and hybrid supercapacitors based on nickel-vanadium layered double hydroxides. *J Energy Chem* 2021;57:496-515. DOI
6. Hu Y, Ding S, Chen P, Seaby T, Hou J, Wang L. Flexible solar-rechargeable energy system. *Energy Stor Mater* 2020;32:356-76. DOI
7. Mir N, Bicer Y. Integration of electrodialysis with renewable energy sources for sustainable freshwater production: a review. *J Environ Manag* 2021;289:112496. DOI PubMed
8. Rostami M, Manshadi MD, Afshari E. Energy production and storage from a polygeneration system based on parabolic trough solar collector, proton exchange membrane fuel cell, organic Rankine cycle, and alkaline electrolyzer. *J Energy Stor* 2022;47:103635. DOI
9. Liu X, Zhang X, Li D, Zhang S, Zhang Q. Recent advances in the "on-off" approaches for on-demand liquid-phase hydrogen evolution. *J Mater Chem A* 2021;9:18164-74. DOI
10. Li X, Zhao L, Yu J, et al. Water splitting: from electrode to green energy system. *Nanomicro Lett* 2020;12:131. DOI PubMed PMC
11. Hou GL, Yang T, Li M, et al. Water splitting by C_{60}-supported vanadium single atoms. *Angew Chem Int Ed* 2021;60:27095-101. DOI
12. Safari F, Dincer I. A review and comparative evaluation of thermochemical water splitting cycles for hydrogen production. *Energy Conver Manag* 2020;205:112182. DOI
13. Dingenen F, Verbruggen SW. Tapping hydrogen fuel from the ocean: a review on photocatalytic, photoelectrochemical and electrolytic splitting of seawater. *Renew Sustain Energy Rev* 2021;142:110866. DOI
14. Liu Y, Li Y, Chen Y, et al. A CO_2/H_2 fuel cell: reducing CO_2 while generating electricity. *J Mater Chem A* 2020;8:8329-36. DOI
15. Qu T, Hu J, Dai X, et al. Electrospinning highly dispersed Ru nanoparticle-embedded carbon nanofibers boost CO_2 reduction in a H_2/CO_2 fuel cell. *ACS Appl Mater Interfaces* 2021;13:23523-31. DOI
16. Yin M, Miao H, Hu R, Sun Z, Li H. Manganese dioxides for oxygen electrocatalysis in energy conversion and storage systems over full pH range. *J Power Sources* 2021;494:229779. DOI
17. Ren M, Lei J, Zhang J, Yakobson BI, Tour JM. Tuning metal elements in open frameworks for efficient oxygen evolution and oxygen reduction reaction catalysts. *ACS Appl Mater Interfaces* 2021;13:42715-23. DOI PubMed
18. Du J, You S, Li X, et al. In situ immobilization of copper oxide thin-layer on zeolitic imidazolate framework-67-derived cobalt oxide@nitrogen-doped carbon with multi-level architecture and versatile active sites for enhancing oxygen evolution/reduction reactions. *J Power Sources* 2020;478:228707. DOI
19. Srinivas K, Lu Y, Chen Y, Zhang W, Yang D. $FeNi_3$-Fe_3O_4 heterogeneous nanoparticles anchored on 2D MOF nanosheets/1D CNT matrix as highly efficient bifunctional electrocatalysts for water splitting. *ACS Sustain Chem Eng* 2020;8:3820-31. DOI
20. Chen L, Cui L, Wang Z, He X, Zhang W, Asefa T. Co_8FeS_8/N, S-doped carbons derived from Fe-Co/S-bridged polyphthalocyanine: efficient dual-function air-electrode catalysts for rechargeable Zn-Air batteries. *ACS Sustain Chem Eng* 2020;8:13147-58. DOI
21. Rong Z, Dong C, Zhang S, Dong W, Huang F. $Co_{5.47}N$ loaded N-doped carbon as an efficient bifunctional oxygen electrocatalyst for a Zn-air battery. *Nanoscale* 2020;12:6089-95. DOI
22. Nolan H, Browne MP. Hydrogen energy currency: beyond state-of-the-art transition metal oxides for oxygen electrocatalysis. *Curr Opin Electrochem* 2020;21:55-61. DOI
23. Das C, Sinha N, Roy P. Transition metal Non-Oxides as electrocatalysts: advantages and challenges. *Small* 2022;18:e2202033. DOI
24. Kumar SR, Karthikeyan S, Ramakrishnan S, et al. Anion dependency of spinel type cobalt catalysts for efficient overall water splitting in an acid medium. *Chem Eng J* 2023;451:138471. DOI
25. Kumar RS, Prabhakaran S, Ramakrishnan S, et al. Developing outstanding bifunctional electrocatalysts for rechargeable Zn-Air batteries using high-purity spinel-type $ZnCo_2Se_4$ nanoparticles. *Small* 2023;19:e2207096. DOI
26. Tarhan C, Çil MA. A study on hydrogen, the clean energy of the future: hydrogen storage methods. *J Energy Stor* 2021;40:102676. DOI
27. Zhang J, Zhang Q, Feng X. Support and interface effects in water-splitting electrocatalysts. *Adv Mater* 2019;31:e1808167. DOI
28. Suen NT, Hung SF, Quan Q, Zhang N, Xu YJ, Chen HM. Electrocatalysis for the oxygen evolution reaction: recent development and future perspectives. *Chem Soc Rev* 2017;46:337-65. DOI PubMed
29. Callejas JF, Read CG, Roske CW, Lewis NS, Schaak RE. Synthesis, characterization, and properties of metal phosphide catalysts for the hydrogen-evolution reaction. *Chem Mater* 2016;28:6017-44. DOI
30. Shi Z, Wang X, Ge J, Liu C, Xing W. Fundamental understanding of the acidic oxygen evolution reaction: mechanism study and state-of-the-art catalysts. *Nanoscale* 2020;12:13249-75. DOI
31. Chai G, Qiu K, Qiao M, Titirici M, Shang C, Guo Z. Active sites engineering leads to exceptional ORR and OER bifunctionality in P,N Co-doped graphene frameworks. *Energy Environ Sci* 2017;10:1186-95. DOI
32. Jamesh M, Harb M. Tuning the electronic structure of the earth-abundant electrocatalysts for oxygen evolution reaction (OER) to achieve efficient alkaline water splitting-a review. *J Energy Chem* 2021;56:299-342. DOI
33. Zhang Y, Zhu X, Zhang G, Shi P, Wang A. Rational catalyst design for oxygen evolution under acidic conditions: strategies toward enhanced electrocatalytic performance. *J Mater Chem A* 2021;9:5890-914. DOI
34. Li S, Hao X, Abudula A, Guan G. Nanostructured Co-based bifunctional electrocatalysts for energy conversion and storage: current status and perspectives. *J Mater Chem A* 2019;7:18674-707. DOI

35. Zhang N, Chai Y. Lattice oxygen redox chemistry in solid-state electrocatalysts for water oxidation. *Energy Environ Sci* 2021;14:4647-71. DOI
36. Reier T, Nong HN, Teschner D, Schlögl R, Strasser P. Electrocatalytic oxygen evolution reaction in acidic environments-reaction mechanisms and catalysts. *Adv Energy Mater* 2017;7:1601275. DOI
37. Danilovic N, Subbaraman R, Chang KC, et al. Activity-stability trends for the oxygen evolution reaction on monometallic oxides in acidic environments. *J Phys Chem Lett* 2014;5:2474-8. DOI
38. Cherevko S, Geiger S, Kasian O, et al. Oxygen and hydrogen evolution reactions on Ru, RuO_2 , Ir, and IrO_2 thin film electrodes in acidic and alkaline electrolytes: a comparative study on activity and stability. *Catal Today* 2016;262:170-80. DOI
39. da Silva GC, Perini N, Ticianelli EA. Effect of temperature on the activities and stabilities of hydrothermally prepared IrOx nanocatalyst layers for the oxygen evolution reaction. *Appl Catal B* 2017;218:287-97. DOI
40. Povia M, Abbott DF, Herranz J, et al. *Operando* X-ray characterization of high surface area iridium oxides to decouple their activity losses for the oxygen evolution reaction. *Energy Environ Sci* 2019;12:3038-52. DOI
41. Chou S, Lin C, Sun B, Tso K, Chan T, Wu P. Formation of RuO_2 thin film using dopamine as a reducing, chelating, and adhesive agent simultaneously. *J Taiwan Inst Chem Eng* 2021;119:196-203. DOI
42. Paoli EA, Masini F, Frydendal R, et al. Oxygen evolution on well-characterized mass-selected Ru and RuO_2 nanoparticles. *Chem Sci* 2015;6:190-6. DOI PubMed PMC
43. Paoli EA, Masini F, Frydendal R, et al. Fine-tuning the activity of oxygen evolution catalysts: the effect of oxidation pre-treatment on size-selected Ru nanoparticles. *Catal Today* 2016;262:57-64. DOI
44. Macounová K, Jirkovský J, Makarova MV, Franc J, Krtil P. Oxygen evolution on $Ru_{1-x}Ni_xO_{2-y}$ nanocrystalline electrodes. *J Solid State Electrochem* 2009;13:959-65. DOI
45. Chang SH, Danilovic N, Chang KC, et al. Functional links between stability and reactivity of strontium ruthenate single crystals during oxygen evolution. *Nat Commun* 2014;5:4191. DOI
46. Adenle A, Shi M, Jiang W, Zeng B, Li C, Li R. Modulating surface charges of bismuth tantalum oxychloride nanoplates for promoting photogenerated charge separation. *J Mater Chem A* 2022;10:14293-9. DOI
47. Yu L, Wu L, Mcelhenny B, et al. Ultrafast room-temperature synthesis of porous S-doped Ni/Fe (oxy)hydroxide electrodes for oxygen evolution catalysis in seawater splitting. *Energy Environ Sci* 2020;13:3439-46. DOI
48. Valizadeh A, Bikas R, Nandy S, Lis T, Chae KH, Najafpour MM. Homogeneous or heterogeneous electrocatalysis: reinvestigation of a cobalt coordination compound for water oxidation. *Dalton Trans* 2021;51:220-30. DOI PubMed
49. Wang J, Kong H, Zhang J, Hao Y, Shao ZP, Ciucci F. Carbon-based electrocatalysts for sustainable energy applications. *Prog Mater Sci* 2021;116:100717. DOI
50. Hu C, Dai L. Multifunctional carbon-based metal-free electrocatalysts for simultaneous oxygen reduction, oxygen evolution, and hydrogen evolution. *Adv Mater* 2017;29:1604942. DOI PubMed
51. Pi Y, Xing X, Lu L, He Z, Ren T. Hierarchical porous activated carbon in OER with high efficiency. *RSC Adv* 2016;6:102422-7. DOI
52. Ma J, Zhi Q, Gong L, et al. A universal descriptor based on p(z)-orbitals for the catalytic activity of multi-doped carbon bifunctional catalysts for oxygen reduction and evolution. *Nanoscale* 2020;12:19375-82. DOI
53. Zoller F, Häringer S, Böhm D, Luxa J, Sofer Z, Fattakhova-Rohlfing D. Carbonaceous oxygen evolution reaction catalysts: from defect and doping-induced activity over hybrid compounds to ordered framework structures. *Small* 2021;17:e2007484. DOI PubMed
54. Zhang X, Zhang W, Dai J, et al. Carboxylated carbon nanotubes with high electrocatalytic activity for oxygen evolution in acidic conditions. *InfoMat* 2022;4:e12273. DOI
55. Wang J, Ciucci F. In-situ synthesis of bimetallic phosphide with carbon tubes as an active electrocatalyst for oxygen evolution reaction. *Appl Catal B* 2019;254:292-9. DOI
56. Gu J, Magagula S, Zhao J, Chen Z. Boosting ORR/OER activity of graphdiyne by simple heteroatom doping. *Small Methods* 2019;3:1800550. DOI
57. Kapse S, Janwari S, Waghmare UV, Thapa R. Energy parameter and electronic descriptor for carbon based catalyst predicted using QM/ML. *Appl Catal B* 2021;286:119866. DOI
58. Hu Q, Li G, Liu X, et al. Coupling pentlandite nanoparticles and dual-doped carbon networks to yield efficient and stable electrocatalysts for acid water oxidation. *J Mater Chem A* 2019;7:461-8. DOI
59. Kang Y, Wang W, Li J, Imhanria S, Hao Y, Lei Z. Ultrathin B, N Co-doped porous carbon nanosheets derived from intumescent flame retardant for rechargeable Zn-air battery. *J Power Sources* 2021;493:229665. DOI
60. Ali Z, Mehmood M, Ahmad J, Malik TS, Ahmad B. In-situ growth of novel CNTs-graphene hybrid structure on Ni-silica nanocomposites by CVD method for oxygen evolution reaction. *Ceram Int* 2020;46:19158-69. DOI
61. Pérez-rodríguez S, Sebastián D, Lázaro M, Pastor E. Stability and catalytic properties of nanostructured carbons in electrochemical environments. *J Catal* 2017;355:156-66. DOI
62. Filimonenkov IS, Bouillet C, Kéranguéven G, Simonov PA, Tsirlina GA, Savinova ER. Carbon materials as additives to the OER catalysts: RRDE study of carbon corrosion at high anodic potentials. *Electrochim Acta* 2019;321:134657. DOI
63. Li H, Han X, Zhao W, et al. Electrochemical preparation of nano/micron structure transition metal-based catalysts for the oxygen evolution reaction. *Mater Horiz* 2022;9:1788-824. DOI

64. Liu M, Li J. Cobalt phosphide hollow polyhedron as efficient bifunctional electrocatalysts for the evolution reaction of hydrogen and oxygen. *ACS Appl Mater Interfaces* 2016;8:2158-65. DOI
65. Kang T, Kim K, Kim M, Kim J. Electronic structure modulation of nickel hydroxide and tungsten nanoparticles for fast structure transformation and enhanced oxygen evolution reaction activity. *Chem Eng J* 2021;418:129403. DOI
66. Liang Z, Zhou W, Gao S, et al. Fabrication of hollow CoP/TiO_x heterostructures for enhanced oxygen evolution reaction. *Small* 2020;16:e1905075. DOI
67. Guan BY, Yu L, Lou XW. General synthesis of multishell mixed-metal oxyphosphide particles with enhanced electrocatalytic activity in the oxygen evolution reaction. *Angew Chem Int Ed* 2017;56:2386-9. DOI PubMed
68. He L, Li Z, Gao M, Sheng G. Phosphorus-accumulating organism assisted phosphorization of Ni-Fe nanocomposites for efficient oxygen evolution reaction. *ACS Sustain Chem Eng* 2020;8:11456-64. DOI
69. Gao R, Yan D. Recent development of Ni/Fe-Based micro/nanostructures toward photo/electrochemical water oxidation. *Adv Energy Mater* 2020;10:1900954. DOI
70. Shao W, Xiao M, Yang C, et al. Assembling and regulating of transition metal-based heterophase vanadates as efficient oxygen evolution catalysts. *Small* 2022;18:e2105763. DOI
71. Zhou Y, Li Y, Zhang L, et al. Fe-leaching induced surface reconstruction of Ni-Fe alloy on N-doped carbon to boost oxygen evolution reaction. *Chem Eng J* 2020;394:124977. DOI
72. Jing T, Zhang N, Zhang C, et al. Improving C-N-FeO_x oxygen evolution electrocatalysts through hydroxyl-modulated local coordination environment. *ACS Catal* 2022;12:7443-52. DOI
73. Zhao R, Li Q, Jiang X, Huang S, Fu G, Lee J. Interface engineering in transition metal-based heterostructures for oxygen electrocatalysis. *Mater Chem Front* 2021;5:1033-59. DOI
74. Guo T, Li L, Wang Z. Recent development and future perspectives of amorphous transition metal-based electrocatalysts for oxygen evolution reaction. *Adv Energy Mater* 2022;12:2200827. DOI
75. Liu J, Zhou J, Liu S, et al. Amorphous NiFe-layered double hydroxides nanosheets for oxygen evolution reaction. *Electrochim Acta* 2020;356:136827. DOI
76. Zhang B, Zheng X, Voznyy O, et al. Homogeneously dispersed multimetal oxygen-evolving catalysts. *Science* 2016;352:333-7. DOI
77. Shi Y, Zhang D, Miao H, et al. A simple, rapid and scalable synthesis approach for ultra-small size transition metal selenides with efficient water oxidation performance. *J Mater Chem A* 2021;9:24261-7. DOI
78. Wu M, Guo B, Nie A, Liu R. Tailored architectures of FeNi alloy embedded in N-doped carbon as bifunctional oxygen electrocatalyst for rechargeable zinc-air battery. *J Colloid Interface Sci* 2020;561:585-92. DOI
79. Xu L, Jiang Q, Xiao Z, et al. Plasma-engraved Co_3O_4 nanosheets with oxygen vacancies and high surface area for the oxygen evolution reaction. *Angew Chem Int Ed* 2016;55:5277-81. DOI
80. Bao J, Zhang X, Fan B, et al. Ultrathin Spinel-structured nanosheets rich in oxygen deficiencies for enhanced electrocatalytic water oxidation. *Angew Chem Int Ed* 2015;54:7399-404. DOI
81. Liu Y, Wang S, Li Z, Chu H, Zhou W. Insight into the surface-reconstruction of metal-organic framework-based nanomaterials for the electrocatalytic oxygen evolution reaction. *Coordin Chem Rev* 2023;484:215117. DOI
82. Ding J, Fan T, Shen K, Li Y. Electrochemical synthesis of amorphous metal hydroxide microarrays with rich defects from MOFs for efficient electrocatalytic water oxidation. *Appl Catal B Environ* 2021;292:120174. DOI
83. Lei Z, Jin X, Li J, et al. Tuning electrochemical transformation process of zeolitic imidazolate framework for efficient water oxidation activity. *J Energy Chem* 2022;65:505-13. DOI
84. Huang L, Gao G, Zhang H, Chen J, Fang Y, Dong S. Self-dissociation-assembly of ultrathin metal-organic framework nanosheet arrays for efficient oxygen evolution. *Nano Energy* 2020;68:104296. DOI
85. Zhao S, Tan C, He C, et al. Structural transformation of highly active metal-organic framework electrocatalysts during the oxygen evolution reaction. *Nat Energy* 2020;5:881-90. DOI
86. Yu ZY, Duan Y, Liu JD, et al. Unconventional CN vacancies suppress iron-leaching in Prussian blue analogue pre-catalyst for boosted oxygen evolution catalysis. *Nat Commun* 2019;10:2799. DOI PubMed PMC
87. Indra A, Paik U, Song T. Boosting electrochemical water oxidation with metal hydroxide carbonate templated Prussian blue analogues. *Angew Chem Int Ed* 2018;57:1241-5. DOI PubMed
88. Su X, Wang Y, Zhou J, Gu S, Li J, Zhang S. Operando spectroscopic identification of active sites in nife prussian blue analogues as electrocatalysts: activation of oxygen atoms for oxygen evolution reaction. *J Am Chem Soc* 2018;140:11286-92. DOI
89. Jiao Y, Zheng Y, Jaroniec M, Qiao SZ. Origin of the electrocatalytic oxygen reduction activity of graphene-based catalysts: a roadmap to achieve the best performance. *J Am Chem Soc* 2014;136:4394-403. DOI PubMed PMC
90. Zhang L, Xia Z. Mechanisms of oxygen reduction reaction on nitrogen-doped graphene for fuel cells. *J Phys Chem C* 2011;115:11170-6. DOI
91. Yu X, Lai S, Xin S, et al. Coupling of iron phthalocyanine at carbon defect site via π-π stacking for enhanced oxygen reduction reaction. *Appl Catal B* 2021;280:119437. DOI
92. Sui S, Wang X, Zhou X, Su Y, Riffat S, Liu C. A comprehensive review of Pt electrocatalysts for the oxygen reduction reaction: nanostructure, activity, mechanism and carbon support in PEM fuel cells. *J Mater Chem A* 2017;5:1808-25. DOI
93. Zhong H, Ly KH, Wang M, et al. A phthalocyanine-based layered two-dimensional conjugated metal-organic framework as a highly efficient electrocatalyst for the oxygen reduction reaction. *Angew Chem Int Ed* 2019;131:10787-92. DOI

94. Sandbeck DJS, Inaba M, Quinson J, et al. Particle size effect on platinum dissolution: practical considerations for fuel cells. *ACS Appl Mater Interfaces* 2020;12:25718-27. DOI
95. Long NV, Yang Y, Minh Thi C, Minh NV, Cao Y, Nogami M. The development of mixture, alloy, and core-shell nanocatalysts with nanomaterial supports for energy conversion in low-temperature fuel cells. *Nano Energy* 2013;2:636-76. DOI
96. Zhu X, Huang L, Wei M, Tsiakaras P, Shen PK. Highly stable Pt-Co nanodendrite in nanoframe with Pt skin structured catalyst for oxygen reduction electrocatalysis. *Appl Catal B* 2021;281:119460. DOI
97. Huang JF, Tseng PK. High performance layer-by-layer Pt_3Ni (Pt-skin)-modified Pd/C for the oxygen reduction reaction. *Chem Sci* 2018;9:6134-42. DOI PubMed PMC
98. Chen P, Lai N, Ho C, Hu Y, Lee J, Yang C. New synthesis of MCM-48 nanospheres and facile replication to mesoporous platinum nanospheres as highly active electrocatalysts for the oxygen reduction reaction. *Chem Mater* 2013;25:4269-77. DOI
99. Li M, Zhao Z, Cheng T, et al. Ultrafine jagged platinum nanowires enable ultrahigh mass activity for the oxygen reduction reaction. *Science* 2016;354:1414-9. DOI
100. Attard GS, Corker JM, Göltner CG, Henke S, Templer RH. liquid-crystal templates for nanostructured metals. *Angew Chem Int Ed* 1997;36:1315-7. DOI
101. Attard GS, Bartlett PN, Coleman NRB, Elliott JM, Owen JR, Wang JH. Mesoporous platinum films from lyotropic liquid crystalline phases. *Science* 1997;278:838-40. DOI
102. Li Y, Li C, Bastakoti BP, et al. Strategic synthesis of mesoporous Pt-on-Pd bimetallic spheres templated from a polymeric micelle assembly. *J Mater Chem A* 2016;4:9169-76. DOI
103. Kour R, Arya S, Young S, Gupta V, Bandhoria P, Khosla A. Review-recent advances in carbon nanomaterials as electrochemical biosensors. *J Electrochem Soc* 2020;167:037555. DOI
104. Gong K, Du F, Xia Z, Durstock M, Dai L. Nitrogen-doped carbon nanotube arrays with high electrocatalytic activity for oxygen reduction. *Science* 2009;323:760-4. DOI PubMed
105. Yan J, Zheng X, Wei C, et al. Nitrogen-doped hollow carbon polyhedron derived from salt-encapsulated ZIF-8 for efficient oxygen reduction reaction. *Carbon* 2021;171:320-8. DOI
106. Kim HS, Kim M, Kang MS, Ahn J, Sung Y, Yoo WC. Bioinspired synthesis of melaninlike nanoparticles for highly n-doped carbons utilized as enhanced CO_2 adsorbents and efficient oxygen reduction catalysts. *ACS Sustain Chem Eng* 2018;6:2324-33. DOI
107. Liao Y, Gao Y, Zhu S, et al. Facile fabrication of N-doped graphene as efficient electrocatalyst for oxygen reduction reaction. *ACS Appl Mater Interfaces* 2015;7:19619-25. DOI
108. Li Q, Chen Y, Du F, Cui X, Dai L. Bias-free synthesis of hydrogen peroxide from photo-driven oxygen reduction reaction using N-doped γ-graphyne catalyst. *Appl Catal B* 2022;304:120959. DOI
109. Wang T, Chen Z, Chen Y, et al. Identifying the active site of N-doped graphene for oxygen reduction by selective chemical modification. *ACS Energy Lett* 2018;3:986-91. DOI
110. Zhu Y, Zhang Z, Li W, et al. Highly exposed active sites of defect-enriched derived MOFs for enhanced oxygen reduction reaction. *ACS Sustain Chem Eng* 2019;7:17855-62. DOI
111. Xing T, Zheng Y, Li LH, et al. Observation of active sites for oxygen reduction reaction on nitrogen-doped multilayer graphene. *ACS Nano* 2014;8:6856-62. DOI
112. Lai Q, Zheng H, Tang Z, et al. Balance of N-doping engineering and carbon chemistry to expose edge graphitic N Sites for enhanced oxygen reduction electrocatalysis. *ACS Appl Mater Interfaces* 2021;13:61129-38. DOI
113. Lai L, Potts JR, Zhan D, et al. Exploration of the active center structure of nitrogen-doped graphene-based catalysts for oxygen reduction reaction. *Energy Environ Sci* 2012;5:7936-42. DOI
114. Yasuda S, Yu L, Kim J, Murakoshi K. Selective nitrogen doping in graphene for oxygen reduction reactions. *Chem Commun* 2013;49:9627-9. DOI PubMed
115. Li R, Wei Z, Gou X, Xu W. Phosphorus-doped graphenenanosheets as efficient metal-free oxygen reduction electrocatalysts. *RSC Adv* 2013;3:9978-84. DOI
116. Wang M, Li Y, Fang J, et al. Superior oxygen reduction reaction on phosphorus-doped carbon dot/graphene aerogel for all-solid-state flexible Al-air batteries. *Adv Energy Mater* 2020;10:1902736. DOI
117. Yang N, Zheng X, Li L, Li J, Wei Z. Influence of phosphorus configuration on electronic structure and oxygen reduction reactions of phosphorus-doped graphene. *J Phys Chem C* 2017;121:19321-8. DOI
118. Wu J, Yang Z, Sun Q, Li X, Strasser P, Yang R. Synthesis and electrocatalytic activity of phosphorus-doped carbon xerogel for oxygen reduction. *Electrochim Acta* 2014;127:53-60. DOI
119. Wu J, Jin C, Yang Z, Tian J, Yang R. Synthesis of phosphorus-doped carbon hollow spheres as efficient metal-free electrocatalysts for oxygen reduction. *Carbon* 2015;82:562-71. DOI
120. Bai X, Zhao E, Li K, et al. Theoretical insights on the reaction pathways for oxygen reduction reaction on phosphorus doped graphene. *Carbon* 2016;105:214-23. DOI
121. Lu Z, Li S, Liu C, et al. Sulfur doped graphene as a promising metal-free electrocatalyst for oxygen reduction reaction: a DFT-D study. *RSC Adv* 2017;7:20398-405. DOI
122. Li S, Ding L, Fan L. Electrochemical synthesis of sulfur-doped graphene sheets for highly efficient oxygen reduction. *Sci China Chem* 2015;58:417-24. DOI
123. Zhang L, Niu J, Li M, Xia Z. Catalytic mechanisms of sulfur-doped graphene as efficient oxygen reduction reaction catalysts for fuel

cells. *J Phys Chem C* 2014;118:3545-53. DOI

124. Chen Y, Li J, Mei T, et al. Low-temperature and one-pot synthesis of sulfurized graphene nanosheets via in situ doping and their superior electrocatalytic activity for oxygen reduction reaction. *J Mater Chem A* 2014;2:20714-22. DOI
125. Wong CH, Sofer Z, Klímová K, Pumera M. Microwave exfoliation of graphite oxides in H_2S plasma for the synthesis of sulfur-doped graphenes as oxygen reduction catalysts. *ACS Appl Mater Interfaces* 2016;8:31849-55. DOI PubMed
126. Banerjee P, Das G, Thapa R. Computationally exploring the role of S-dopant and S-linker in activating the catalytic efficiency of graphene quantum dot for ORR. *Catal Today* 2021;370:36-45. DOI
127. Sheng Z, Gao H, Bao W, Wang F, Xia X. Synthesis of boron doped graphene for oxygen reduction reaction in fuel cells. *J Mater Chem* 2012;22:390-5. DOI
128. Hsieh C, Kao C, Gandomi YA, Juang R, Chang J, Zhang R. Oxygen reduction reactions from boron-doped graphene quantum dot catalyst electrodes in acidic and alkaline electrolytes. *J Taiwan Inst Chem Eng* 2022;133:104196. DOI
129. Zhou Y, Yen CH, Fu S, et al. One-pot synthesis of B-doped three-dimensional reduced graphene oxide via supercritical fluid for oxygen reduction reaction. *Green Chem* 2015;17:3552-60. DOI
130. Zhang J, Byeon A, Lee JW. Boron-doped electrocatalysts derived from carbon dioxide. *J Mater Chem A* 2013;1:8665-71. DOI
131. Xiao F, Meng Y, Lin Z, et al. Highly boron-doped holey graphene for lithium oxygen batteries with enhanced electrochemical performance. *Carbon* 2022;189:404-12. DOI
132. Xing Z, Jin R, Chen X, et al. Self-templating construction of N, P-Co-doped carbon nanosheets for efficient eletreocatalytic oxygen reduction reaction. *Chem Eng J* 2021;410:128015. DOI
133. Ishii T, Philavanh M, Negishi J, Inukai E, Ozaki J. Preparation of chemically structure-controlled BN-doped carbons for the molecular understanding of their surface active sites for oxygen reduction reaction. *ACS Catal* 2022;12:1288-97. DOI
134. Zan Y, Zhang Z, Zhu B, Dou M, Wang F. Ultrathin two-dimensional phosphorus and nitrogen Co-doped carbon nanosheet as efficient oxygen reduction electrocatalyst. *Carbon* 2021;174:404-12. DOI
135. Zheng Y, Chen S, Zhang KAI, et al. Template-free construction of hollow mesoporous carbon spheres from a covalent triazine framework for enhanced oxygen electroreduction. *J Colloid Interface Sci* 2022;608:3168-77. DOI
136. Duan X, O'Donnell K, Sun H, Wang Y, Wang S. Sulfur and nitrogen Co-doped graphene for metal-free catalytic oxidation reactions. *Small* 2015;11:3036-44. DOI
137. Zhang J, Song X, Li P, et al. Sulfur, nitrogen Co-doped nanocomposite of graphene and carbon nanotube as an efficient bifunctional electrocatalyst for oxygen reduction and evolution reactions. *J Taiwan Inst Chem Eng* 2018;93:336-41. DOI
138. Xue Y, Yu D, Dai L, et al. Three-dimensional B,N-doped graphene foam as a metal-free catalyst for oxygen reduction reaction. *Phys Chem Chem Phys* 2013;15:12220-6. DOI
139. Zhao Y, Yang L, Chen S, et al. Can boron and nitrogen Co-doping improve oxygen reduction reaction activity of carbon nanotubes? *J Am Chem Soc* 2013;135:1201-4. DOI
140. Yazdi A, Fei H, Ye R, Wang G, Tour J, Sundararaj U. Boron/nitrogen Co-doped helically unzipped multiwalled carbon nanotubes as efficient electrocatalyst for oxygen reduction. *ACS Appl Mater Interfaces* 2015;7:7786-94. DOI PubMed
141. Li R, Wei Z, Gou X. Nitrogen and phosphorus dual-doped graphene/carbon nanosheets as bifunctional electrocatalysts for oxygen reduction and evolution. *ACS Catal* 2015;5:4133-42. DOI
142. Borghei M, Laocharoen N, Kibena-põldsepp E, et al. Porous N,P-doped carbon from coconut shells with high electrocatalytic activity for oxygen reduction: alternative to Pt-C for alkaline fuel cells. *Appl Catal B* 2017;204:394-402. DOI
143. Rong H, Zhan T, Sun Y, Wen Y, Liu X, Teng H. ZIF-8 derived nitrogen, phosphorus and sulfur tri-doped mesoporous carbon for boosting electrocatalysis to oxygen reduction in universal pH range. *Electrochim Acta* 2019;318:783-93. DOI
144. Long Y, Ye F, Shi L, et al. N, P, and S tri-doped holey carbon as an efficient electrocatalyst for oxygen reduction in whole pH range for fuel cell and zinc-air batteries. *Carbon* 2021;179:365-76. DOI
145. Chen C, Han H, Liu X, et al. Nitrogen, phosphorus, sulfur tri-doped porous carbon derived from covalent polymer with versatile performances in supercapacitor, oxygen reduction reaction and electro-fenton degradation. *Microporous Mesoporous Mater* 2021;325:111335. DOI
146. Lin Y, Hu Z, Shao Y, Chen Z, Wei X, Wu Z. Single-precursor design and solvent-free nanocasting synthesis of N/S/O-doped ordered mesoporous carbons with trimodal pores for excellent oxygen reduction. *Carbon* 2021;183:390-403. DOI
147. Zhao S, Liu J, Li C, et al. Tunable ternary (N, P, B)-doped porous nanocarbons and their catalytic properties for oxygen reduction reaction. *ACS Appl Mater Interfaces* 2014;6:22297-304. DOI
148. Li Y, Wen H, Yang J, Zhou Y, Cheng X. Boosting oxygen reduction catalysis with N, F, and S tri-doped porous graphene: tertiary N-precursors regulates the constitution of catalytic active sites. *Carbon* 2019;142:1-12. DOI
149. Liu G, Zhao C, Wang G, Zhang Y, Zhang H. Efficiently electrocatalytic oxidation of benzyl alcohol for energy- saved zinc-air battery using a multifunctional nickel-cobalt alloy electrocatalyst. *J Colloid Interface Sci* 2018;532:37-46. DOI
150. Begum H, Ahmed MS, Jung S. Template-free synthesis of polyacrylonitrile-derived porous carbon nanoballs on graphene for efficient oxygen reduction in zinc-air batteries. *J Mater Chem A* 2021;9:9644-54. DOI
151. Guo J, Liu J, Dai H, et al. Nitrogen doped carbon nanofiber derived from polypyrrole functionalized polyacrylonitrile for applications in lithium-ion batteries and oxygen reduction reaction. *J Colloid Interface Sci* 2017;507:154-61. DOI
152. Yan W, Wang L, Chen C, et al. Polystyrene microspheres-templated nitrogen-doped graphene hollow spheres as metal-free catalyst for oxygen reduction reaction. *Electrochim Acta* 2016;188:230-9. DOI

153. Zhong H, Zhang H, Liu S, Deng C, Wang M. Nitrogen-enriched carbon from melamine resins with superior oxygen reduction reaction activity. *ChemSusChem* 2013;6:807-12. DOI
154. Wang X, Zou L, Fu H, et al. Noble metal-free oxygen reduction reaction catalysts derived from prussian blue nanocrystals dispersed in polyaniline. *ACS Appl Mater Interfaces* 2016;8:8436-44. DOI
155. Gao Y, Wang L, Li G, Xiao Z, Wang Q, Zhang X. Taming transition metals on N-doped CNTs by a one-pot method for efficient oxygen reduction reaction. *Int J Hydrog Energy* 2018;43:7893-902. DOI
156. Rao P, Wu D, Wang T, et al. Single atomic cobalt electrocatalyst for efficient oxygen reduction reaction. *eScience* 2022;2:399-404. DOI
157. Jiang M, Wang F, Yang F, et al. Rationalization on high-loading iron and cobalt dual metal single atoms and mechanistic insight into the oxygen reduction reaction. *Nano Energy* 2022;93:106793. DOI
158. Yan X, Dong C, Huang Y, et al. Probing the active sites of carbon-encapsulated cobalt nanoparticles for oxygen reduction. *Small Methods* 2019;3:1800439. DOI
159. Quílez-Bermejo J, Morallón E, Cazorla-Amorós D. Polyaniline-derived N-doped ordered mesoporous carbon thin films: efficient catalysts towards oxygen reduction reaction. *Polymers* 2020;12:2382. DOI PubMed PMC
160. Schulenburg H, Stankov S, Schünemann V, et al. Catalysts for the oxygen reduction from heat-treated iron(III) tetramethoxyphenylporphyrin chloride: structure and stability of active sites. *J Phys Chem B* 2003;107:9034-41. DOI
161. Liu K, Fu J, Lin Y, et al. Insights into the activity of single-atom Fe-N-C catalysts for oxygen reduction reaction. *Nat Commun* 2022;13:2075. DOI PubMed PMC
162. Han J, Bao H, Wang J, et al. 3D N-doped ordered mesoporous carbon supported single-atom Fe-N-C catalysts with superior performance for oxygen reduction reaction and zinc-air battery. *Appl Catal B* 2021;280:119411. DOI
163. Fu X, Jiang G, Wen G, et al. Densely accessible Fe-Nx active sites decorated mesoporous-carbon-spheres for oxygen reduction towards high performance aluminum-air flow batteries. *Appl Catal B* 2021;293:120176. DOI
164. Chen Y, Li J, Zhu Y, et al. Vicinal Co atom-coordinated Fe-N-C catalysts to boost the oxygen reduction reaction. *J Mater Chem A* 2022;10:9886-91. DOI
165. Song X, Zhang S, Zhong H, et al. FeCo nanoalloys embedded in nitrogen-doped carbon nanosheets/bamboo-like carbon nanotubes for the oxygen reduction reaction. *Inorg Chem Front* 2021;8:109-21. DOI
166. Zhou X, Gao J, Hu Y, et al. Theoretically revealed and experimentally demonstrated synergistic electronic interaction of CoFe dual-metal sites on N-doped carbon for boosting both oxygen reduction and evolution reactions. *Nano Lett* 2022;22:3392-9. DOI
167. Wei J, Xia D, Wei Y, Zhu X, Li J, Gan L. Probing the oxygen reduction reaction intermediates and dynamic active site structures of molecular and pyrolyzed Fe-N-C electrocatalysts by in situ raman spectroscopy. *ACS Catal* 2022;12:7811-20. DOI
168. Xiao L, Yang Q, Wang M J, Mao ZX, Li J, Wei ZD. N-doped and Fe-, N-codoped carbon: tuning of porous structures for highly efficient oxygen reduction reaction. *J Mater Sci* 2018;53:15246-56. DOI
169. Chen N, Meng Z, Wang R, Cai S, Guo W, Tang H. Bimetal-organic framework-derived carbon nanocubes with 3D hierarchical pores as highly efficient oxygen reduction reaction electrocatalysts for microbial fuel cells. *Sci China Mater* 2021;64:2926-37. DOI
170. Xu H, Wang D, Yang P, et al. A hierarchically porous Fe-N-C synthesized by dual melt-salt-mediated template as advanced electrocatalyst for efficient oxygen reduction in zinc-air battery. *Appl Catal B* 2022;305:121040. DOI
171. Osgood H, Devaguptapu SV, Xu H, Cho J, Wu G. Transition metal (Fe, Co, Ni, and Mn) oxides for oxygen reduction and evolution bifunctional catalysts in alkaline media. *Nano Today* 2016;11:601-25. DOI
172. Bockris JO, Otagawa T. The electrocatalysis of oxygen evolution on perovskites. *J Electrochem Soc* 1984;131:290-302. DOI
173. Meng Y, Song W, Huang H, Ren Z, Chen SY, Suib SL. Structure-property relationship of bifunctional MnO_2 nanostructures: highly efficient, ultra-stable electrochemical water oxidation and oxygen reduction reaction catalysts identified in alkaline media. *J Am Chem Soc* 2014;136:11452-64. DOI
174. Liu H, Long W, Song W, Liu J, Wang F. Tuning the electronic bandgap: an efficient way to improve the electrocatalytic activity of carbon-supported Co_3O_4 nanocrystals for oxygen reduction reactions. *Chem Eur J* 2017;23:2599-609. DOI
175. Tang Q, Jiang L, Liu J, Wang S, Sun G. Effect of surface manganese valence of manganese oxides on the activity of the oxygen reduction reaction in alkaline media. *ACS Catal* 2014;4:457-63. DOI
176. Celorrio V, Calvillo L, Dann E, et al. Oxygen reduction reaction at $La_xCa_{1-x}MnO_3$ anostructures: interplay between a-site segregation and b-site valency. *Catal Sci Technol* 2016;6:7231-8. DOI
177. Qaseem A, Chen F, Qiu C, et al. Reduced graphene oxide decorated with manganese cobalt oxide as multifunctional material for mechanically rechargeable and hybrid zinc-air batteries. *Part Part Syst Charact* 2017;34:1700097. DOI
178. Tian Y, Liu X, Xu L, et al. Engineering crystallinity and oxygen vacancies of Co(II) oxide nanosheets for high performance and robust rechargeable Zn-air batteries. *Adv Funct Mater* 2021;31:2101239. DOI
179. Zhang Z, Liang X, Li J, et al. Interfacial engineering of $NiO/NiCo_2O_4$ porous nanofibers as efficient bifunctional catalysts for rechargeable zinc-air batteries. *ACS Appl Mater Interfaces* 2020;12:21661-9. DOI
180. Nayak AK, Han H. Surface engineered $NiO-Co_3O_4$ nanostructures as high-performance electrocatalysts for oxygen reduction reaction. *Ceram Int* 2020;46:25351-8. DOI
181. Zha R, Shi T, He L, Sun X, Jia Y, Zhang M. Engineering the surface active sites of actiniae-like hierarchical Fe_3O_4/Co_3O_4 nanoheterojunction for efficient oxygen reduction reaction. *Dyes Pigm* 2020;180:108439. DOI
182. Ruan QD, Liu LL, Wu DH, Feng JJ, Zhang L, Wang AJ. Cobalt phosphide nanoparticles encapsulated in manganese, nitrogen Co-

doped porous carbon nanosheets with rich nanoholes for high-efficiency oxygen reduction reaction. *J Colloid Interface Sci* 2022;627:630-9. DOI PubMed

183. Hou CC, Zou L, Wang Y, Xu Q. MOF-mediated fabrication of a porous 3D superstructure of carbon nanosheets decorated with ultrafine cobalt phosphide nanoparticles for efficient electrocatalysis and zinc-air batteries. *Angew Chem Int Ed* 2020;59:21360-6. DOI
184. Chen L, Zhang Y, Dong L, et al. Honeycomb-like 3D N-, P-codoped porous carbon anchored with ultrasmall Fe_2P nanocrystals for efficient Zn-air battery. *Carbon* 2020;158:885-92. DOI
185. Zhang P, Cai Z, You S, et al. Highly crystallized Fe_2P embedded in N-doped carbon for enhancing long-term bioelectricity generation by lowering cathode poisoning in microbial fuel cells. *ACS Sustain Chem Eng* 2020;8:10461-70. DOI
186. Ran Z, Shu C, Hou Z, et al. Phosphorus vacancies enriched Ni_2P nanosheets as efficient electrocatalyst for high-performance Li-O_2 batteries. *Electrochim Acta* 2020;337:135795. DOI
187. Ran Z, Shu C, Hou Z, et al. Modulating electronic structure of honeycomb-like $Ni_2P/Ni_{12}P_5$ heterostructure with phosphorus vacancies for highly efficient lithium-oxygen batteries. *Chem Eng J* 2021;413:127404. DOI
188. Thakur N, Kumar M, Mandal D, Nagaiah TC. Nickel iron phosphide/phosphate as an oxygen bifunctional electrocatalyst for high-power-density rechargeable Zn-air batteries. *ACS Appl Mater Interfaces* 2021;13:52487-97. DOI
189. Chen W, Chang S, Yu H, Li W, Zhang H, Zhang Z. FeNiP nanoparticle/N,P dual-doped carbon composite as a trifunctional catalyst towards high-performance zinc-air batteries and overall water electrolysis. *Nanoscale* 2021;13:17136-46. DOI
190. Bodhankar PM, Sarawade PB, Kumar P, et al. Nanostructured metal phosphide based catalysts for electrochemical water splitting: a review. *Small* 2022;18:e2107572. DOI
191. Liu W, Zhou Z, Li Z, et al. Cobalt phosphide embedded N-doped carbon nanopolyhedral as an efficient cathode electrocatalyst in microbial fuel cells. *J Environ Chem Eng* 2021;9:104582. DOI
192. Wu ZS, Chen L, Liu J, et al. High-performance electrocatalysts for oxygen reduction derived from cobalt porphyrin-based conjugated mesoporous polymers. *Adv Mater* 2014;26:1450-5. DOI
193. Wang R, Yuan Y, Zhang J, et al. Embedding Fe_2P nanocrystals in bayberry-like N, P-enriched carbon nanospheres as excellent oxygen reduction electrocatalyst for zinc-air battery. *J Power Sources* 2021;501:230006. DOI
194. Vijayakumar E, Ramakrishnan S, Sathiskumar C, et al. MOF-derived CoP-nitrogen-doped carbon@NiFeP nanoflakes as an efficient and durable electrocatalyst with multiple catalytically active sites for OER, HER, ORR and rechargeable zinc-air batteries. *Chem Eng J* 2022;428:131115. DOI
195. Baresel D, Sarholz W, Scharner P, Schmitz, J. Transition metal chalcogenides as oxygen catalysts for fuel cells. *Ber Bunsenges Phys Chem* 1974;78:608. Available from: https://www.osti.gov/etdeweb/biblio/5061040 [Last accessed on 25 June 2023]
196. Zhao S, Wang Y, Zhang Q, et al. Two-dimensional nanostructures of non-layered ternary thiospinels and their bifunctional electrocatalytic properties for oxygen reduction and evolution: the case of $CuCo_2S_4$ nanosheets. *Inorg Chem Front* 2016;3:1501-9. DOI
197. Shen M, Ruan C, Chen Y, Jiang C, Ai K, Lu L. Covalent entrapment of cobalt-iron sulfides in N-doped mesoporous carbon: extraordinary bifunctional electrocatalysts for oxygen reduction and evolution reactions. *ACS Appl Mater Interfaces* 2015;7:1207-18. DOI
198. Arunchander A, Peera SG, Sahu A. Synthesis of flower-like molybdenum sulfide/graphene hybrid as an efficient oxygen reduction electrocatalyst for anion exchange membrane fuel cells. *J Power Sources* 2017;353:104-14. DOI
199. Zhang C, Lu R, Liu C, et al. Trimetallic sulfide hollow superstructures with engineered d-band center for oxygen reduction to hydrogen peroxide in alkaline solution. *Adv Sci* 2022;9:e2104768. DOI PubMed PMC
200. Cao Y, Huang S, Peng Z, et al. Phase control of ultrafine FeSe nanocrystals in a N-doped carbon matrix for highly efficient and stable oxygen reduction reaction. *J Mater Chem A* 2021;9:3464-71. DOI
201. Xiao J, Xia Y, Hu C, Xi J, Wang S. Raisin bread-like iron sulfides/nitrogen and sulfur dual-doped mesoporous graphitic carbon spheres: a promising electrocatalyst for the oxygen reduction reaction in alkaline and acidic media. *J Mater Chem A* 2017;5:11114-23. DOI
202. Ningthoujam R, Gajbhiye N. Synthesis, electron transport properties of transition metal nitrides and applications. *Prog Mater Sci* 2015;70:50-154. DOI
203. Kreider ME, Stevens MB, Liu Y, et al. Nitride or oxynitride? Elucidating the composition-activity relationships in molybdenum nitride electrocatalysts for the oxygen reduction reaction. *Chem Mater* 2020;32:2946-60. DOI
204. Yuan Y, Wang J, Adimi S, et al. Zirconium nitride catalysts surpass platinum for oxygen reduction. *Nat Mater* 2020;19:282-6. DOI
205. Lou Y, Liu J, Liu M, Wang F. Hexagonal Fe_2N coupled with N-doped carbon: crystal-plane-dependent electrocatalytic activity for oxygen reduction. *ACS Catal* 2020;10:2443-51. DOI
206. Luo J, Qiao X, Jin J, et al. A strategy to unlock the potential of CrN as a highly active oxygen reduction reaction catalyst. *J Mater Chem A* 2020;8:8575-85. DOI
207. Ma JB, Xu LL, Liu QY, He SG. Activation of methane and ethane as mediated by the triatomic anion $HNbN^-$: electronic structure similarity with a Pt atom. *Angew Chem Int Ed* 2016;55:4947-51. DOI PubMed
208. Zeng R, Yang Y, Feng X, et al. Nonprecious transition metal nitrides as efficient oxygen reduction electrocatalysts for alkaline fuel cells. *Sci Adv* 2022;8:eabj1584. DOI PubMed PMC
209. Tang H, Luo J, Yu J, Zhao W, Song H, Liao S. Nanoconfined nitrogen-doped carbon-coated hierarchical TiCoN composites with enhanced ORR performance. *ChemElectroChem* 2018;5:2041-9. DOI

210. Huang K, Bi K, Lu YK, et al. Porous VO_xN_y nanoribbons supported on CNTs as efficient and stable non-noble electrocatalysts for the oxygen reduction reaction. *Sci Rep* 2015;5:17385. DOI PubMed PMC
211. Sharma K, Hui D, Kim NH, Lee JH. Facile synthesis of N-doped graphene supported porous cobalt molybdenum oxynitride nanodendrites for the oxygen reduction reaction. *Nanoscale* 2019;11:1205-16. DOI PubMed
212. Balamurugan J, Nguyen TT, Kim NH, Kim DH, Lee JH. Novel core-shell CuMo-oxynitride@N-doped graphene nanohybrid as multifunctional catalysts for rechargeable zinc-air batteries and water splitting. *Nano Energy* 2021;85:105987. DOI
213. Yu Y, Zhou J, Sun Z. Novel 2D transition-metal carbides: ultrahigh performance electrocatalysts for overall water splitting and oxygen reduction. *Adv Funct Mater* 2020; 30:2000570. DOI
214. Liu C, Wang X, Kong Z, et al. Electrostatic interaction in amino protonated chitosan-metal complex anion hydrogels: a simple approach to porous metal carbides/N-doped carbon aerogels for energy conversion. *ACS Appl Mater Interfaces* 2022;14:22151-60. DOI
215. Yue R, Xia M, Wang M, et al. TiN and TiC as stable and promising supports for oxygen reduction reaction: theoretical and experimental study. *Appl Surf Sci* 2019;495:143620. DOI
216. Wei Z, Ren Y, Zhao H, Wang M, Tang H. Controllable preparation and synergistically improved catalytic performance of TiC/C hybrid nanofibers via electrospinning for the oxygen reduction reaction. *Ceram Int* 2020;46:25313-9. DOI
217. Beom Cho S, He C, Sankarasubramanian S, et al. Metal-nitrogen-carbon cluster-decorated titanium carbide is a durable and inexpensive oxygen reduction reaction electrocatalyst. *ChemSusChem* 2021;14:4680-9. DOI
218. Chen M, Jiang Y, Mei P, et al. Polyacrylamide microspheres-derived Fe_3C@N-doped carbon nanospheres as efficient catalyst for oxygen reduction reaction. *Polymers* 2019;11:767. DOI PubMed PMC
219. Patniboon T, Hansen HA. N-Doped graphene supported on metal-iron carbide as a catalyst for the oxygen reduction reaction: density functional theory study. *ChemSusChem* 2020;13:996-1005. DOI PubMed
220. Huang Z, Wang J, Peng Y, Jung C, Fisher A, Wang X. Design of efficient bifunctional oxygen reduction/evolution electrocatalyst: recent advances and perspectives. *Adv Energy Mater* 2017;7:1700544. DOI
221. Zhang J, Xia Z, Dai L. Carbon-based electrocatalysts for advanced energy conversion and storage. *Sci Adv* 2015;1:e1500564. DOI PubMed PMC
222. Hu C, Dai L. Carbon-based metal-free catalysts for electrocatalysis beyond the ORR. *Angew Chem Int Ed* 2016;55:11736-58. DOI PubMed
223. Du L, Xing L, Zhang G, Sun S. Metal-organic framework derived carbon materials for electrocatalytic oxygen reactions: recent progress and future perspectives. *Carbon* 2020;156:77-92. DOI
224. Qu K, Zheng Y, Zhang X, Davey K, Dai S, Qiao SZ. Promotion of electrocatalytic hydrogen evolution reaction on nitrogen-doped carbon nanosheets with secondary heteroatoms. *ACS Nano* 2017;11:7293-300. DOI PubMed
225. Gui F, Jin Q, Xiao D, et al. High-performance zinc-air batteries based on bifunctional hierarchically porous nitrogen-doped carbon. *Small* 2022;18:e2105928. DOI
226. Lai C, Liu X, Cao C, et al. Structural regulation of N-doped carbon nanocages as high-performance bifunctional electrocatalysts for rechargeable Zn-air batteries. *Carbon* 2021;173:715-23. DOI
227. Lu Q, Zou X, Liao K, et al. Direct growth of ordered N-doped carbon nanotube arrays on carbon fiber cloth as a free-standing and binder-free air electrode for flexible quasi-solid-state rechargeable Zn-air batteries. *Carbon Energy* 2020;2:461-71. DOI
228. Murugesan C, Senthilkumar B, Barpanda P. Biowaste-derived highly porous N-doped carbon as a low-cost bifunctional electrocatalyst for hybrid sodium-air batteries. *ACS Sustain Chem Eng* 2022;10:9077-86. DOI
229. Zhao J, Li Q, Zhang Q, Liu R. Carbon tube-graphene heterostructure with different N-doping configurations induces an electrochemically active-active interface for efficient oxygen electrocatalysis. *Chem Eng J* 2022;431:133730. DOI
230. Lee J, Noh S, Pham ND, Shim JH. Top-down synthesis of S-doped graphene nanosheets by electrochemical exfoliation of graphite: metal-free bifunctional catalysts for oxygen reduction and evolution reactions. *Electrochim Acta* 2019;313:1-9. DOI
231. El-sawy AM, Mosa IM, Su D, et al. Controlling the active sites of sulfur-doped carbon nanotube-graphene nanolobes for highly efficient oxygen evolution and reduction catalysis. *Adv Energy Mater* 2016;6:1501966. DOI
232. Cheng Y, Tian Y, Fan X, Liu J, Yan C. Boron doped multi-walled carbon nanotubes as catalysts for oxygen reduction reaction and oxygen evolution reactionin in alkaline media. *Electrochim Acta* 2014;143:291-6. DOI
233. Jiang HR, Zhao TS, Shi L, Tan P, An L. First-principles study of nitrogen-, boron-doped graphene and Co-doped graphene as the potential catalysts in nonaqueous Li-O_2 batteries. *J Phys Chem C* 2016;120:6612-8. DOI
234. Wang Y, Yu M, Zhang T, Xue Z, Ma Y, Sun H. Defect-rich boron doped carbon nanotubes as an electrocatalyst for hybrid Li-air batteries. *Catal Sci Technol* 2022;12:332-8. DOI
235. Jia Y, Chen J, Yao X. Defect electrocatalytic mechanism: concept, topological structure and perspective. *Mater Chem Front* 2018;2:1250-68. DOI
236. Liu J, Zhao S, Li C, et al. Carbon nanodot surface modifications initiate highly efficient, stable catalysts for both oxygen evolution and reduction reactions. *Adv Energy Mater* 2016;6:1502039. DOI
237. Lei W, Deng Y, Li G, et al. Two-dimensional phosphorus-doped carbon nanosheets with tunable porosity for oxygen reactions in zinc-air batteries. *ACS Catal* 2018;8:2464-72. DOI
238. Qu K, Zheng Y, Dai S, Qiao SZ. Graphene oxide-polydopamine derived N, S-codoped carbon nanosheets as superior bifunctional electrocatalysts for oxygen reduction and evolution. *Nano Energy* 2016;19:373-81. DOI

239. Li Z, Yao Y, Niu Y, et al. Multi-heteroatom-doped hollow carbon tubes as robust electrocatalysts for the oxygen reduction reaction, oxygen and hydrogen evolution reaction. *Chem Eng J* 2021;418:129321. DOI
240. Zhou S, Zang J, Gao H, et al. Deflagration method synthesizing N, S Co-doped oxygen-functionalized carbons as a bifunctional catalyst for oxygen reduction and oxygen evolution reaction. *Carbon* 2021;181:234-45. DOI
241. Sun Y, Yang J, Ding X, et al. Synergetic contribution of nitrogen and fluorine species in porous carbons as metal-free and bifunctional oxygen electrocatalysts for zinc-air batteries. *Appl Catal B* 2021;297:120448. DOI
242. Zhang X, Wen X, Pan C, et al. N species tuning strategy in N, S Co-doped graphene nanosheets for electrocatalytic activity and selectivity of oxygen redox reactions. *Chem Eng J* 2022;431:133216. DOI
243. Wang Y, Gan R, Zhao S, et al. B, N, F tri-doped lignin-derived carbon nanofibers as an efficient metal-free bifunctional electrocatalyst for ORR and OER in rechargeable liquid/solid-state Zn-air batteries. *Appl Surf Sci* 2022;598:153891. DOI
244. Wu M, Wang Y, Wei Z, et al. Ternary doped porous carbon nanofibers with excellent ORR and OER performance for zinc-air batteries. *J Mater Chem A* 2018;6:10918-25. DOI
245. Zheng Y, Song H, Chen S, et al. Metal-free multi-heteroatom-doped carbon bifunctional electrocatalysts derived from a covalent triazine polymer. *Small* 2020;16:e2004342. DOI
246. Wang L, Wang Y, Wu M, et al. Nitrogen, fluorine, and boron ternary doped carbon fibers as cathode electrocatalysts for zinc-air batteries. *Small* 2018;14:e1800737. DOI
247. Wang Y, Xu N, He R, Peng L, Cai D, Qiao J. Large-scale defect-engineering tailored tri-doped graphene as a metal-free bifunctional catalyst for superior electrocatalytic oxygen reaction in rechargeable Zn-air battery. *Appl Catal B* 2021;285:119811. DOI
248. Li H, Ha TA, Jiang S, et al. N, F and S doped carbon nanofibers generated from electrospun polymerized ionic liquids for metal-free bifunctional oxygen electrocatalysis. *Electrochim Acta* 2021;377:138089. DOI
249. Zheng Y, Chen S, Zhang KAI, et al. Ultrasound-triggered assembly of covalent triazine framework for synthesizing heteroatom-doped carbon nanoflowers boosting metal-free bifunctional electrocatalysis. *ACS Appl Mater Interfaces* 2021;13:13328-37. DOI
250. Tao X, Zhang Q, Li Y, Lv X, Ma D, Wang H. N, P, S tri-doped hollow carbon nanosphere as a high-efficient bifunctional oxygen electrocatalyst for rechargeable Zn-air batteries. *Appl Surf Sci* 2019;490:47-55. DOI
251. Wu T, Han M, Zhu X, Wang G, Zhang H, Zhao H. The electrochemical corrosion of an air thermally-treated carbon fiber cloth electrocatalyst with outstanding oxygen evolution activity under alkaline conditions. *Chem Commun* 2019;55:2344-7. DOI
252. Beall CE, Fabbri E, Schmidt TJ. Perovskite oxide based electrodes for the oxygen reduction and evolution reactions: the underlying mechanism. *ACS Catal* 2021;11:3094-114. DOI
253. Morales DM, Kazakova MA, Dieckhöfer S, et al. Trimetallic Mn-Fe-Ni oxide nanoparticles supported on multi-walled carbon nanotubes as high-performance bifunctional ORR/OER electrocatalyst in alkaline media. *Adv Funct Mater* 2020;30:1905992. DOI
254. Huang Y, Zhang M, Liu P, Cheng F, Wang L. Co_3O_4 supported on N, P-doped carbon as a bifunctional electrocatalyst for oxygen reduction and evolution reactions. *Chinese J Catal* 2016;37:1249-56. DOI
255. Pandey J, Hua B, Ng W, et al. Developing hierarchically porous MnO_x/NC hybrid nanorods for oxygen reduction and evolution catalysis. *Green Chem* 2017;19:2793-7. DOI
256. Liang Y, Li Y, Wang H, et al. Co_3O_4 nanocrystals on graphene as a synergistic catalyst for oxygen reduction reaction. *Nat Mater* 2011;10:780-6. DOI
257. Wang C, Hung K, Ko T, Hosseini S, Li Y. Carbon-nanotube-grafted and nano-Co_3O_4-doped porous carbon derived from metal-organic framework as an excellent bifunctional catalyst for zinc-air battery. *J Power Sources* 2020;452:227841. DOI
258. Pham TV, Guo HP, Luo WB, Chou SL, Wang JZ, Liu HK. Carbon- and binder-free 3D porous perovskite oxide air electrode for rechargeable lithium-oxygen batteries. *J Mater Chem A* 2017;5:5283-9. DOI
259. Mechili M, Vaitsis C, Argirusis N, Pandis PK, Sourkouni G, Argirusis C. Research progress in transition metal oxide based bifunctional electrocatalysts for aqueous electrically rechargeable zinc-air batteries. *Renew Sustain Energ Rev* 2022;156:111970. DOI
260. Hazarika KK, Yamada Y, Matus EV, Kerzhentsev M, Bharali P. Enhancing the electrocatalytic activity via hybridization of Cu(I/II) oxides with Co_3O_4 towards oxygen electrode reactions. *J Power Sources* 2021;490:229511. DOI
261. Wang Z, Yang J, Tang Y, et al. Fe_3O_4/Co_3O_4 binary oxides as bifunctional electrocatalysts for rechargeable Zn-air batteries by one-pot pyrolysis of zeolitic imidazolate frameworks. *Sustain Energy Fuels* 2021;5:2985-93. DOI
262. Li L, Fu L, Wang R, et al. Cobalt, manganese zeolitic-imidazolate-framework-derived Co_3O_4/Mn_3O_4/CN_x embedded in carbon nanofibers as an efficient bifunctional electrocatalyst for flexible Zn-air batteries. *Electrochim Acta* 2020;344:136145. DOI
263. Li Y, Zhou Z, Cheng G, et al. Flower-like $NiCo_2O_4$-CN as efficient bifunctional electrocatalyst for Zn-Air battery. *Electrochim Acta* 2020;341:135997. DOI
264. Zhang Y, Chen Z, Tian J, Sun M, Yuan D, Zhang L. Nitrogen doped $CuCo_2O_4$ nanoparticles anchored on beaded-like carbon nanofibers as an efficient bifunctional oxygen catalyst toward zinc-air battery. *J Colloid Interface Sci* 2022;608:1105-15. DOI
265. Deeloed W, Priamushko T, Čížek J, Suramitr S, Kleitz F. Defect-engineered hydroxylated mesoporous spinel oxides as bifunctional electrocatalysts for oxygen reduction and evolution reactions. *ACS Appl Mater Interfaces* 2022;14:23307-21. DOI PubMed PMC
266. Cao F, Yang X, Shen C, et al. Electrospinning synthesis of transition metal alloy nanoparticles encapsulated in nitrogen-doped carbon layers as an advanced bifunctional oxygen electrode. *J Mater Chem A* 2020;8:7245-52. DOI
267. Ma X, Chai H, Cao Y, et al. An effective bifunctional electrocatalysts: controlled growth of CoFe alloy nanoparticles supported on N-doped carbon nanotubes. *J Colloid Interface Sci* 2018;514:656-63. DOI

268. Zhang W, Xu C, Zheng H, Li R, Zhou K. Oxygen-rich cobalt-nitrogen-carbon porous nanosheets for bifunctional oxygen electrocatalysis. *Adv Funct Mater* 2022;32:2200763. DOI
269. Dong F, Wu M, Chen Z, et al. Atomically dispersed transition metal-nitrogen-carbon bifunctional oxygen electrocatalysts for zinc-air batteries: recent advances and future perspectives. *Nanomicro Lett* 2021;14:36. DOI PubMed PMC
270. Zhang X, Zhang Q, Cui J, Yan J, Liu J, Wu Y. New insights into the key bifunctional role of sulfur in Fe-N-C single-atom catalysts for ORR/OER. *Nanoscale* 2022;14:3212-23. DOI
271. Shui JL, Karan NK, Balasubramanian M, Li SY, Liu DJ. Fe/N/C composite in Li-O_2 battery: studies of catalytic structure and activity toward oxygen evolution reaction. *J Am Chem Soc* 2012;134:16654-61. DOI PubMed
272. Wang R, Yang H, Lu N, et al. Precise identification of active sites of a high bifunctional performance 3D Co/N-C catalyst in zinc-air batteries. *Chem Eng J* 2022;433:134500. DOI
273. Shen M, Gao K, Xiang F, et al. Nanocellulose-assisted synthesis of ultrafine Co nanoparticles-loaded bimodal micro-mesoporous N-rich carbon as bifunctional oxygen electrode for Zn-air batteries. *J Power Sources* 2020;450:227640. DOI
274. Wang Y, Fang B, Zhang D, et al. A review of carbon-composited materials as air-electrode bifunctional electrocatalysts for metal-air batteries. *Electrochem Energ Rev* 2018;1:1-34. DOI
275. Zhong L, Jiang C, Zheng M, et al. Wood carbon based single-atom catalyst for rechargeable Zn-air batteries. *ACS Energy Lett* 2021;6:3624-33. DOI
276. Shi Z, Yang W, Gu Y, Liao T, Sun Z. Metal-nitrogen-doped carbon materials as highly efficient catalysts: progress and rational design. *Adv Sci* 2020;7:2001069. DOI
277. Tang C, Wang B, Wang HF, Zhang Q. Defect engineering toward atomic Co-N_x-C in hierarchical graphene for rechargeable flexible solid Zn-air batteries. *Adv Mater* 2017;29:1703185. DOI
278. Feng C, Guo Y, Xie Y, et al. Bamboo-like nitrogen-doped porous carbon nanofibers encapsulated nickel-cobalt alloy nanoparticles composite material derived from the electrospun fiber of a bimetal-organic framework as efficient bifunctional oxygen electrocatalysts. *Nanoscale* 2020;12:5942-52. DOI
279. Charles V, Zhang X, Yuan M, et al. CoNi nano-alloy anchored on biomass-derived N-doped carbon frameworks for enhanced oxygen reduction and evolution reactions. *Electrochim Acta* 2022;402:139555. DOI
280. Yu C, Hao S, Lei L, Zhang X. Synthesis of NiCo alloy nanoparticle-decorated B,N-doped carbon nanosheet networks via a self-template strategy for bifunctional oxygen-involving reactions. *ACS Sustain Chem Eng* 2019;7:14394-9. DOI
281. Liu J, He T, Wang Q, et al. Confining ultrasmall bimetallic alloys in porous N-carbon for use as scalable and sustainable electrocatalysts for rechargeable Zn-air batteries. *J Mater Chem A* 2019;7:12451-6. DOI
282. Li G, Tang Y, Fu T, et al. S, N Co-doped carbon nanotubes coupled with CoFe nanoparticles as an efficient bifunctional ORR/OER electrocatalyst for rechargeable Zn-air batteries. *Chem Eng J* 2022;429:132174. DOI
283. Shi F, Zhu K, Li X, Wang E, Zhu X, Yang W. Porous carbon layers wrapped CoFe alloy for ultrastable Zn-air batteries exceeding 20,000 charging-discharging cycles. *J Energy Chem* 2021;61:327-35. DOI
284. Jing S, Zhang Y, Chen F, Liang H, Yin S, Tsiakaras P. Novel and highly efficient cathodes for Li-O_2 batteries: 3D self-standing NiFe@NC-functionalized N-doped carbon nanonet derived from Prussian blue analogues/biomass composites. *Appl Catal B* 2019;245:721-32. DOI
285. Zhong H, Wang J, Zhang Q, et al. In situ coupling FeM (M = Ni, Co) with nitrogen-doped porous carbon toward highly efficient trifunctional electrocatalyst for overall water splitting and rechargeable Zn-air battery. *Adv Sustain Syst* 2017;1:1700020. DOI
286. Tang X, Cao R, Li L, et al. Engineering efficient bifunctional electrocatalysts for rechargeable zinc-air batteries by confining Fe-Co-Ni nanoalloys in nitrogen-doped carbon nanotube@nanosheet frameworks. *J Mater Chem A* 2020;8:25919-30. DOI
287. Liu J, Luo Z, Zhang X, et al. FeCoNi nanoalloys embedded in hierarchical N-rich carbon matrix with enhanced oxygen electrocatalysis for rechargeable Zn-air batteries. *J Mater Chem A* 2021;9:27701-8. DOI
288. Kumar M, Raj CR. Heteroatom-doped carbon-encapsulated FeP nanostructure: a multifunctional electrocatalyst for zinc-air battery and water electrolyzer. *ACS Appl Mater Interfaces* 2022;14:15176-86. DOI PubMed
289. Sun C, Ding J, Wang H, et al. Cobalt sulfides constructed heterogeneous interfaces decorated on N,S-codoped carbon nanosheets as a highly efficient bifunctional oxygen electrocatalyst. *J Mater Chem A* 2021;9:13926-35. DOI
290. Xu F, Wang J, Zhang Y, et al. Structure-engineered bifunctional oxygen electrocatalysts with Ni_3S_2 quantum dot embedded S/N-doped carbon nanosheets for rechargeable Zn-air batteries. *Chem Eng J* 2022;432:134256. DOI
291. Gong W, Zhang H, Yang L, Yang Y, Wang J, Liang H. Core@ shell MOFs derived Co_2P/CoP@NPGC as a highly-active bifunctional electrocatalyst for ORR/OER. *J Ind Eng Chem* 2022;106:492-502. DOI
292. Liu B, Wang R, Yao Y, et al. Hollow-structured CoP nanotubes wrapped by N-doped carbon layer with interfacial charges polarization for efficiently boosting oxygen reduction/evolution reactions. *Chem Eng J* 2022;431:133238. DOI
293. Tiwari AP, Kim D, Kim Y, Lee H. Bifunctional oxygen electrocatalysis through chemical bonding of transition metal chalcogenides on conductive carbons. *Adv Energy Mater* 2017;7:1602217. DOI
294. Liu T, Yang F, Cheng G, Luo W. Reduced graphene oxide-wrapped $Co_{9-x}Fe_xS_8$/Co/Co,Fe-N-C composite as bifunctional electrocatalyst for oxygen reduction and evolution. *Small* 2018;14:1703748. DOI
295. Liu X, Zhang G, Wang L, Fu H. Structural design strategy and active site regulation of high-efficient bifunctional oxygen reaction electrocatalysts for Zn-air battery. *Small* 2021;17:e2006766. DOI
296. Liu J, Zhang H, Qiu M, et al. A review of non-precious metal single atom confined nanomaterials in different structural dimensions

(1D-3D) as highly active oxygen redox reaction electrocatalysts. *J Mater Chem A* 2020;8:2222-45. DOI

297. Sun Y, Sun S, Yang H, Xi S, Gracia J, Xu ZJ. Spin-related electron transfer and orbital interactions in oxygen electrocatalysis. *Adv Mater* 2020;32:e2003297. DOI
298. Zhu Q, Fan J, Tao Y, et al. Photo-coupled electrocatalytic oxygen reduction to hydrogen peroxide using metal-free CNT-threaded oxidized g-C_3N_4. *Energy Mater* 2022;2:200029. DOI
299. Liang Z, Kong N, Yang C, et al. Highly curved nanostructure-coated Co, N-doped carbon materials for oxygen electrocatalysis. *Angew Chem Int Ed* 2021;60:12759-64. DOI
300. Jiang X, Wang Y, Jia B, Qu X, Qin M. Using machine learning to predict oxygen evolution activity for transition metal hydroxide electrocatalysts. *ACS Appl Mater Interfaces* 2022;14:41141-8. DOI
301. Wu L, Guo T, Li T. Machine learning-accelerated prediction of overpotential of oxygen evolution reaction of single-atom catalysts. *iScience* 2021;24:102398. DOI PubMed PMC
302. Wang X, Xiao B, Li Y, et al. First-principles based machine learning study of oxygen evolution reactions of perovskite oxides using a surface center-environment feature model. *Appl Surfe Sci* 2020;531:147323. DOI
303. Zhu Y, Zhang B. Nanocarbon-based metal-free and non-precious metal bifunctional electrocatalysts for oxygen reduction and oxygen evolution reactions. *J Energy Chem* 2021;58:610-28. DOI
304. Xu H, Yang J, Ge R, et al. Carbon-based bifunctional electrocatalysts for oxygen reduction and oxygen evolution reactions: optimization strategies and mechanistic analysis. *J Energy Chem* 2022;71:234-65. DOI
305. Pei Z, Tan H, Gu J, et al. A polymeric hydrogel electrocatalyst for direct water oxidation. *Nat Commun* 2023;14:818. DOI PubMed PMC
306. Liu H, Liu Q, Wang Y, et al. Bifunctional carbon-based cathode catalysts for zinc-air battery: a review. *Chin Chem Lett* 2022;33:683-92. DOI
307. Zhao CX, Liu JN, Wang J, Ren D, Li BQ, Zhang Q. Recent advances of noble-metal-free bifunctional oxygen reduction and evolution electrocatalysts. *Chem Soc Rev* 2021;50:7745-78. DOI
308. Peng L, Shang L, Zhang T, Waterhouse GIN. Recent advances in the development of single-atom catalysts for oxygen electrocatalysis and zinc-air batteries. *Adv Energy Mater* 2020;10:2003018. DOI
309. Luo M, Sun W, Xu BB, Pan H, Jiang Y. Interface engineering of air electrocatalysts for rechargeable zinc-air batteries. *Adv Energy Mater* 2021;11:2002762. DOI
310. Du L, Xing L, Zhang G, Dubois M, Sun S. Strategies for engineering high-performance PGM-free catalysts toward oxygen reduction and evolution reactions. *Small Methods* 2020;4:2000016. DOI